INFORMATION TO USERS

This manuscript has been reproduced from the microfilm master. UMI films the text directly from the original or copy submitted. Thus, some thesis and dissertation copies are in typewriter face, while others may be from any type of computer printer.

The quality of this reproduction is dependent upon the quality of the copy submitted. Broken or indistinct print, colored or poor quality illustrations and photographs, print bleedthrough, substandard margins, and improper alignment can adversely affect reproduction.

In the unlikely event that the author did not send UMI a complete manuscript and there are missing pages, these will be noted. Also, if unauthorized copyright material had to be removed, a note will indicate the deletion.

Oversize materials (e.g., maps, drawings, charts) are reproduced by sectioning the original, beginning at the upper left-hand corner and continuing from left to right in equal sections with small overlaps.

ProQuest Information and Learning
300 North Zeeb Road, Ann Arbor, MI 48106-1346 USA
800-521-0600

University of Alberta

The thermal infrared spectroscopy of opal-A between 0.5-25 micrometers

by

Michelle Coreena Goryniuk 

A thesis submitted to the Faculty of Graduate Studies and Research in partial fulfillment of the

requirements for Master of Science

Department of *Earth and Atmospheric Sciences*

Edmonton, Alberta

Spring 2005

Abstract

Opal-A is the main component of siliceous sinters in many terrestrial systems, and it commonly preserves silicified microorganisms. Opal-A from the Taupo Volcanic Zone (North Island, New Zealand) yielded reflectance (wavelengths between 0.5-25 μm) and absorbance spectra (wavelengths between 2.5-14 μm) consistent with the presence of isolated and hydrogen-bound water and silanol. Two classes (1 and 2/2A) reflectance spectra were detected between the wavelengths of 6-13 μm. The Class-1 spectrum is similar to existing opal-A and opal-CT spectra, and it was collected from well-consolidated samples that had low porosity. The Class-2/2A spectrum is unique when compared to the opal-A and opal-CT spectra, and it was collected from poorly consolidated samples that had high porosity. The Class-2/2A spectrum was also collected from opal-A crushed to a grain size of < 74 μm. Since fine grains dominate planetary surfaces, the Class-2/2A spectrum may be useful in the detection of hydrothermal systems on planetary surfaces.

Acknowledgements

This project would never have been successful without the support of my supervisors, Benoit Rivard and Brian Jones, who have contributed their rocks, time, and resources. I must also thank the staff and students who have passed through the Earth Observations Systems Laboratory (EOSL) at the University of Alberta between 1999-2005 for their technical and moral support. Many thanks go to Jilu Feng and Ralf Tappert. Jilu Feng took the first measurements of the opal-A samples in 1997 and taught me how to take my own measurements. Ralf Tappert provided suggestions and comments on this thesis and the associated paper.

TABLE OF CONTENTS

LIST OF TABLES

LIST OF FIGURES

Chapter 1. Introduction

1.1 Introduction

Opal-A is a hydrated amorphous silicon oxide ($SiO_4 \bullet nH_2O$) that forms in hot springs by direct precipitation from silica supersaturated water, or through the metabolic processes of microbes such as diatoms and radiolarians. Hot springs develop anywhere in the crust where water coexists with a heat source. Their existence on Mars is suggested by McSween (2002) who proposed that liquid water or ice in the subsurface could have been heated by magmatic activity. If water did reach the surface, then it is possible that opal-A was precipitated. If continuously supplied with water, these environments could have supported microbial life. The identification of opal-A on the surface of Mars would have strong implications for the search for life on other planets.

1.2 Planetary geology

At the present time, the composition of Mars is being mapped without direct physical contact. One of the primary instruments used to analyze the geology of Mars from orbit is an infrared spectrometer, which collects information about composition and is very sensitive to the presence of water. The geological maps of Mars (Head et al., 1999) are consistent with periods of volcanic activity and fluid flow on the surface, but hot springs have not yet been detected. Either they did not form on Mars, or because of their size and composition they are not being accurately identified. If opal-A does exist on Mars, two factors may hinder its identification. First, opal-A is spectrally similar to other silica polymorphs, such as opal-CT and opal-C; second, the

current spectral libraries do not contain the full range of opal-A spectral signatures that are observed in nature.

1.3 The silica polymorphs

The silica polymorphs all have the chemical formula of SiO_2, and they are subdivided based on long-range molecular order. There are eight crystalline silica polymorphs (α-quartz, β-quartz/chalcedony, α-tridymite, β-tridymite, α-cristobalite, β-cristobalite, coesite, and stishovite). Also, there are three non-crystalline silica polymorphs, which are referred to as opaline silicas or opals; in order of increasing cystallinity they are opal-A, opal-CT, and opal-C (Lynne and Campbell, 2004). The non-crystalline silica polymorphs are hydrated, and they are primarily distinguished by means of X-Ray Diffraction (XRD) techniques.

Differentiating the types of opal was first reported by Jones and Segnit (1971) wherein opaline materials were classified according to the nature of their XRD patterns. Opal-A presents a broad hump or diffuse band, opal-CT a lussatite X-ray pattern or cristobalite-tridymite arrangement, and opal-C a normal cristobalite pattern with 8 peaks.

The opal-A class was further divided by Langer and Flörke (1974) into two forms: opal-A_N and opal-A_G. Opal-A_N has a glass-like network structure and refers to silica glass formed in volcanic settings (Flörke, 1972). Opal A_G has a gel-like structure and includes precious and potch opal, which are precipitated from aqueous solutions. The former has an ordered stacking pattern which gives it a gem quality appearance, and the latter has an unordered stacking pattern making it appear dull.

Potch opals can further be classified based on their formational setting: siliceous sinter or geyserite is formed in hot springs, and diatomites are shales rich in biogenic opal-A from diatoms and radiolaria.

1.4 The remote sensing of Mars

Missions organized primarily by the National Aeronautical Space Agency (NASA) have focused on four broad scientific goals: to determine if life ever arose on Mars, to characterize the climate of Mars, to characterize the geology of Mars, and to prepare for human exploration of Mars.

In 1996, NASA began a detailed global mapping initiative of the surface of Mars with Mars Global Surveyor (MGS). That orbital probe included a Thermal Emission Spectrometer (TES) that detected two primary surface compositions: basaltic rocks in the older, southern highlands, and more andesitic rocks in the younger, northern plains (Bandfield et al., 2000). Wyatt and McSween (2001) proposed that the andesite spectra for the northern plains could be explained by a mixture of igneous and alteration minerals. MGS data was used to identify potential landing sites for the 2003 Mars Exploration Rovers (MER), and the orbiter is now serving as a data-relay station for current and future landers and orbital probes.

MGS was succeeded in 2001 by Mars Odyssey and the Thermal Emission Imaging System (THEMIS). THEMIS has collected visible and infrared data (100 x 100 m pixel size) to map the distribution of minerals on the surface of Mars. Combined with the results of MGS, these images were used to identify potential landing sites for the Mars Exploration Rovers (MER) that landed in 2003-2004.

The European initiative, Mars Express, entered the orbit of Mars in late 2003, and it is the European Space Agency's first mission to another planet. Mars Express is equipped with OMEGA, which is an infrared mineralogical mapping spectrometer that will contribute to understanding the role of water in the formation of the Martian landscape.

The Mars Exploration Rover mission includes the rovers named Spirit and Opportunity. Both rovers are equipped with Mini-TES, which is a smaller version of the TES included on the MGS spacecraft. The rovers have collected thermal emission spectra from the Martian surface with a field of view of 8-20 milli-radians.

Future missions are planned for launch every two years until 2009 and will become increasingly intensive and technically complex. The Compact Reconnaissance Imaging Spectrometer for Mars (CRISM) is to be launched with the 2005 Reconnaissance Orbiter. It will map with a resolution as small as $18m^2$, providing a preliminary site selection for Phoenix, which is to be launched in 2007.

To prepare for the next stage of planetary investigation, a long-range, long-duration science laboratory will be launched as early as 2009. This rover will pave the way for subsequent missions, which are focused on the return of samples.

1.5 Intent and organization of the thesis

This thesis presents the reflectance and absorbance spectra of hydrothermally precipitated opal-A. Analysis of eight hand samples and eight pieces of core from the Taupo Volcanic Zone on the North Island of New Zealand revealed that opal-A has two classes of reflectance spectra between 6-13 μm (Class-1 and Class-2/2A).

Background information regarding infrared spectroscopy is presented in chapter two, with the results of the study being provided in chapter three. The discussion is presented in chapter four, and the conclusions are summarized in chapter five. Following are the bibliography, and two appendices. Appendix A is the corresponding paper that was published in Geophysical Research Letters in December 2004, and appendix B contains the reflectance spectra collected from the hand samples and core.

Chapter 2. Infrared Spectroscopy

2.1 The evolution of infrared spectroscopy

It was identified early on that infrared spectroscopy could be used to complete petrologic studies of the moon and Mars (Lyon, 1964; Conel, 1969). Since then, thousands of infrared spectra from minerals and rocks have been collected and analyzed (e.g. Milkey, 1960; Lyon, 1967; Hunt and Salisbury, 1970; Hunt et al., 1973; Moenke, 1974; Salisbury et al., 1991). Research by Brown and Gibbs (1969) and Gibbs (1982) provided the theoretical background to support the empirical observations. Interest in planetary geology grew, and now infrared spectroscopy is being used to map the geology of the Martian surface (Bandfield et al., 2000; Christensen et al., 2000; Hamilton et al., 2001; Wyatt and McSween, 2001).

The analysis of non-crystalline silicates began with the studies of Keller and Pickett (1949) and McDonald (1958), who collected some of the first absorption spectra from hyalite, opal, diatomite, and opaline chert. The most up to date and thorough compilation of non-crystalline silica spectra is presented in Michalski et al. (2003).

2.2 The electromagnetic spectrum

The infrared portion of the electromagnetic spectrum is located between 0.6-1000 μm (16,666-10 cm^{-1}) (Fig. 2-1), and is divided into the Near-IR (0.6-2.5 μm), the Mid-IR (2.5-25 μm), and the Far-IR (25-1000 μm) in Clark (2004). The Near-IR region, also referred to as the visible near-infrared (VNIR), has been used to characterize and quantize materials in chemical and geologic studies (Hunt, 1977).

The Mid-IR region, also referred to as the thermal infrared (TIR), is widely used to identify minerals and rocks (Salisbury et al., 1991). The Far-IR region is principally used in the analysis of interstellar dust and is often applied to the identification of materials in other solar systems and galaxies (Flynn et al., 2002).

2.3 Infrared interactions with matter

Spectral features in the infrared can be categorized as electronic, vibrational, or rotational in origin. Electronic processes include crystal field effects, charge transfer bands, characteristic color centers, and conduction band transitions (Hunt and Salisbury, 1970). Electronic processes can produce spectral features in the spectra of silicates, but play no role in the analysis of opals.

Vibrational processes dominate infrared spectra and produce a number of spectral features. For a group to be active in the infrared it must possess a dynamic dipole that changes its orientation or dimension when electromagnetic radiation of a specific frequency is absorbed. Differences in electronegativities of bonded atoms are the basis for the establishment of dipoles which govern these vibrations. Functional groups, such as SiO_4^{-4}, H_2O, and OH^-, will vibrate when a specific frequency of energy is absorbed. Neighboring atoms can affect the electronegativity of an atom and will change the vibrational frequencies.

Each group has fundamental vibrational modes, which are a function of inter-atomic distances, bond angles, bond forces, and the relative mass of the constituent atoms (Hunt and Salisbury, 1970). The number of fundamental vibrational modes is

determined by the number of atoms (N) (Eq. 1).

$$\text{Number of Fundamental Vibrational Modes} = (3 \times N) - 6 \quad \text{(Eq. 1)}$$

Fundamental vibrational modes are notated by the symbol ν_x, where x equals 1, 2, 3, etc. Each mode is expressed in wavenumbers (cm^{-1}) or wavelengths (μm). The modes may be annotated by the terms symmetrical stretch, asymmetrical stretch, bend, or others, which refer to the movement of the group.

Overtones are bands that occur at twice or some multiple integral value (i.e. $2\nu_1$, $3\nu_1$, $2\nu_2$), and they are produced when a fundamental mode is excited by two or more quanta of energy. A combination mode produces bands at approximately the sum of fundamental or overtone frequencies (i.e. $\nu_1+\nu_2$, $\nu_2+\nu_3$, $2\nu_1+\nu_2$, $3\nu_1+\nu_2+2\nu_3$).

2.3.1 The water molecule

The isolated liquid water molecule has three fundamental vibrational modes. The symmetric OH stretch (ν_1 or ν_{OH}) is located at 3.10 μm, the HOH bend (ν_2) is located at 6.08 μm, and the asymmetric OH stretch (ν_3) is located at 2.90 μm (Fig. 2-2). In the region of 1-2 μm, overtones and combinational modes of the water molecule are observed at 0.94, 1.15, 1.38, 1.45, and 1.88 μm (Table 2-1) (Hunt, 1977).

It is common for water to exist in a network and interact with other groups (Hunt, 1977; Aines and Rossman, 1984). These networks alter the vibrational frequencies of the water molecules (Table 2-2) (Bellamy, 1975). Stoichiometric water-bearing minerals contain water as individual or clusters of molecules at specific

sites essential to its structure (i.e. gypsum). Water may also be present in various quantities in specific locations not essential to the crystal structure (i.e. zeolites). In clay minerals, various amounts of hydroxyl are present. Also, water may be trapped in fluid inclusions in the crystal structure (i.e. quartz).

The shapes of the absorption features associated with water or hydroxyl are indicative of the environments in which the water or hydroxyl exists (Aines and Rossman, 1984). Water located in a well-ordered site produces sharp absorption features, whereas water in an unordered site, or where more than one type of site is occupied, produces broad absorption features (Hunt and Salisbury, 1970; Aines and Rossman, 1984). The intensity of the bands is related to the amount of water that is in the sample, but a relatively small amount of water can produce a prominent spectral feature because the relationship is not linear (Salisbury and Walter, 1989).

2.3.2 The hydroxyl group

The hydroxyl group is an efficient absorber of infrared radiation. Therefore, infrared spectroscopy can be used to identify if hydroxyl is bound to hydrogen to form water, or cations such as magnesium, iron, or silicon, or if it is participating in hydrogen bonding (cf. Aines and Rossman, 1984; Dijkstra et al., 2002).

Silanol (Si-OH) is formed when hydroxyl is bound to silicon. The fundamental OH stretch of isolated silanol occurs between 2.6-2.7 μm (Table 2-3) (McDonald, 1958; Hunt, 1977), whereas hydrogen-bound silanol absorbs between 2.7-3.1 μm (Keller and Pickett, 1949; Langer and Flörke, 1974; Dijkstra et al., 2002).

In summary, silanol groups participating in strong hydrogen bonds vibrate at longer wavelengths.

The combination band involving the OH fundamental stretch is observed as a pair of features between 2.2-2.4 μm (Hunt, 1977). Hydroxyl bound to cations with dioctahedral coordination, such as aluminum and silicon, produce a spectral feature at 2.2 μm, whereas hydroxyl bound to cations with trioctahedral coordination, such as magnesium, produce a spectral feature at 2.3 μm (Hunt et al., 1973). Overtones of the OH fundamental stretch occur near 1.4 μm, and the Si-OH fundamental bend occurs between 10.47-11.98 μm (Table 2-3) (Bellamy, 1975; Socrates, 1980).

2.3.3 The silica group

The SiO_4^{4-} group is characterized by strong bonds and a rigid geometry (Pauling, 1980; Gibbs, 1982). The two fundamental vibrational modes of the isolated silica group that are active in the infrared are the Si-O asymmetric stretch (ν_3) at 10.4 μm, and the Si-O bend (ν_4) at 18.0 μm (Fig. 2-3) (Nakamoto, 1970; Basile et al., 1973). Two additional fundamental vibrational modes are not active in the infrared because they lack the asymmetry required to produce a dipole.

2.4 The spectral features of minerals

Infrared reflectance and absorbance spectra can be used to identify minerals and calculate their modal abundances in rocks. The useful reflectance spectral features are the fundamental Si-O asymmetrical stretch and bending modes, the

Christiansen feature, the transmission feature, the transparency feature, and the overtone and combination modes. The Christensen feature and the transparency feature do not have counterparts in absorption spectra.

It is impossible to assign the spectral features of minerals to specific vibrational modes using calculations because of substitutions and the often complex framework (Milkey, 1960). Broad terms such as "Si-O asymmetric stretch" and "Si-O bend", therefore, are used to describe the movement along the silicon-oxygen axis (Salisbury et al., 1991).

Spectral features relating to the fundamental Si-O asymmetric stretch (v_3) are observed between 8-12 μm, with the most prominent peaks being situated between 9-10 μm (Milkey, 1960). The spectral features of tectosilicates, layer, and chain silicates are found between 9-11 μm, and those of the nesosilicates are found between 10-12 μm (Moenke, 1974). With decreasing polymerization, the spectral features relating to the fundamental Si-O asymmetric stretch shift to higher wavelengths (White and Minser, 1984; Walter and Salisbury, 1989). The spectral features relating to the fundamental Si-O bend (v_4) are observed between 15-25 μm.

The Christensen feature is a reflectance minimum which is located prior to each fundamental vibrational mode. Usually located between 7.5-9 μm, the Christensen feature is located at the frequency at which the real part of the refractive index is equal to that of the surroundings; little or no scattering occurs at this frequency, and little radiation is returned to the detector (Salisbury and Walter, 1989; Cooper et al., 2002). The position of the Christensen feature is also related to the

degree of silica polymerization, with lower polymerized structures having a Christensen feature at higher wavelengths (Conel, 1969; Aronsen et al., 1971; Logan et al., 1973; Salisbury and Walter, 1989).

The transparency feature is a reflectance maximum observed between the wavelengths of 10.5-12 μm in spectra from fine grains (Salisbury et al., 1991). Like the fundamental Si-O asymmetric stretch and the Christensen feature, the transparency feature shifts to longer wavelengths with decreasing polymerization of the structure (Salisbury and Walter, 1989; Cooper et al., 2002). Although useful for identifying the mineralogy of fine-grained samples in a laboratory setting, the transparency feature might not be useful in the remote sensing of airless space targets because this feature may not be detectable at low ambient temperatures (Logan et al., 1973).

Overtones and combination modes of the silica group are located between 4-6 μm. They are more intense and more numerous in the reflectance spectra of fine-grained material than in the absorbance spectra from the same material (Salisbury et al., 1987; Salisbury et al., 1991).

2.5 Infrared spectra

2.5.1 Transmittance and absorbance spectra

Transmittance and absorbance spectra are calculated by measuring the amount of infrared energy that travels through a sample having a known thickness. Energy that travels through the sample and then is measured by the detector is referred to as

transmitted energy. From the value of transmittance, absorption can be calculated (Eq. 2).

$$\text{Absorption} = 1 - \text{Transmittance} \qquad \text{(Eq. 2)}$$

Absorption and transmittance spectra depend solely upon the absorption coefficient of the material, which is directly related to composition (Salisbury et al., 1991). Absorption and transmittance spectra are extremely useful in the analysis of rocks and minerals, however they can only be collected in laboratory settings.

2.5.2 Emission and reflectance spectra

Emission and reflectance spectra are calculated by measuring the amount of infrared radiation emitted or reflected from a surface. When a passive energy source is used, such as the sun, the energy that is returned to the detector is referred to as emitted energy. When an active energy source is used, such as a globar light source, the energy that is returned to the detector is referred to as reflected energy. The relationship between emitted and reflected energy is defined by Kirchhoff's law (Eq. 3) (Salisbury et al., 1994).

$$\text{Emission} = 1 - \text{Reflectance} \qquad \text{(Eq. 3)}$$

Emission and reflectance spectra depend on the absorption coefficient and the refractive index of the material (Salisbury and Wald, 1992, and references therein). The absorption coefficient is directly related to composition, and the refractive index changes in response to physical and textural properties. Emission and reflectance spectra are more difficult to interpret than absorbance and transmittance spectra because of the large effect that the refractive index has on the spectra of fine-grained

materials (i.e. < 74 μm). Emission and reflectance and spectra can be collected in laboratory settings, but they can also be collected from platforms on airplanes and satellites.

2.5.2.1 The refractive index

Considering that much of the material on the surface of other planets is composed of fine-grained material (i.e. < 74 μm) (Christensen and Moore, 1992), it is important to understand how fine grains scatter and absorb infrared energy. Empirical observations show that the position, intensity, and shape of reflectance and emission spectral features change as a function of the refractive index, which is governed by the physical properties of a sample (i.e. grain size, porosity, degree of packing) (Conel, 1969; Aronson et al., 1966; Mustard and Hays, 1997). Salisbury et al. (1991) provided a theoretical explanation for the changes observed in the emission and reflectance spectra of fine grained material, but scattering theories are complex and are not good predictors of the type of spectra a fine-grained material will produce (Clark and Roush, 1984).

When infrared energy directed at a particulate material is returned to the detector, the energy has either been reflected by the surface of the grains, which is called surface scattering, or it has been refracted through the grain and then reflected by the surface of another grain, which is called volume scattering (Salisbury et al., 1987, and references therein).

On the shorter wavelength side of the Christensen feature, the reflectance spectrum is dominated by volume scattering, and the spectral features are observed as

troughs (Salisbury et al., 1991) (Fig. 2-4). With a decrease in grain size, there is more volume scattering and more energy is reflected to the detector; as a result, the amplitude of the spectrum increases in the spectra from material having smaller grain sizes. The reflectance spectrum is dominated by surface scattering on the longer wavelength side of the Christensen feature, and most spectral feature are observed as peaks (Salisbury et al., 1991). As grain size decreases, less energy is reflected to the detector, and the amplitude of the spectrum decreases in this portion of the spectrum.

The arrangement of grains has also been shown to have a large effect on emission and reflectance spectra. When grains are randomly separated by a distance on the order of a wavelength, they scatter as individual grains (Salisbury and Wald, 1992). When grains are packed together, so that they are separated by less than a wavelength, the scatter as if they were a large grains (Feynman, 1963). Also, small grains clinging to large grains will produce spectra consistent with a fine-grained material.

2.5.3 Spectral libraries

Spectral libraries are useful in the analysis of terrestrial materials, but using spectral libraries to investigate extraterrestrial materials can be problematic. It is often assumed that the rocks and minerals on other planets are similar to those on Earth. If this assumption is reasonable, there are too many minerals and rocks of different compositions for all the variations on Earth to be represented in the spectral library. Furthermore, for each specimen, spectra would have to be collected for every grain size. Examples of the spectra of various terrestrial minerals and rocks can be found in

the following spectral libraries.

- The ASTER spectral library found at http://speclib.jpl.nasa.gov/. It includes data from the Johns Hopkins University (JHU) Spectral Library, the Jet Propulsion Laboratory (JPL) Spectral Library, and the United States Geological Survey (USGS - Reston) Spectral Library
- The USGS Digital Spectral Library found at http://speclab.cr.usgs.gov/spectral-lib.html
- The Arizona State University (ASU) Thermal Emission Spectral Library found at http://tes.asu.edu/speclib/

2.6 Tables

Table 2-1 An example of the overtones and combination absorption frequencies for the isolated H_2O molecule between 1-2 μm. From Hunt (1977).

Overtone or Combination	Wavelength (μm)
$2\nu_1 + \nu_3$	~0.942
$\nu_1 + \nu_2 + \nu_3$	~1.135
$\nu_1 + \nu_3$	~1.37
$2\nu_1 + \nu_3$	1.454
$\nu_2 + \nu_3$	~1.875

Table 2-2 The fundamental frequencies of the OH asymmetric stretch for the polymeric species of water. From Bellamy (1975).

Polymeric Species	Wavelength (μm)
Monomer	2.68, 2.76
Dimer	2.71, 2.82
Trimer	2.85, 2.98
Tetramer	3.01

Table 2-3 The fundamental vibrational frequencies of the OH stretch and Si-OH bend of the silanol group. From Bellamy (1975) and Socrates (1980).

Silanol Group	Wavelength (μm)
Si-OH (O-H stretch)	2.60-3.10
Si-OH (Si-OH bend)	10.47-11.98

2.7 Figures

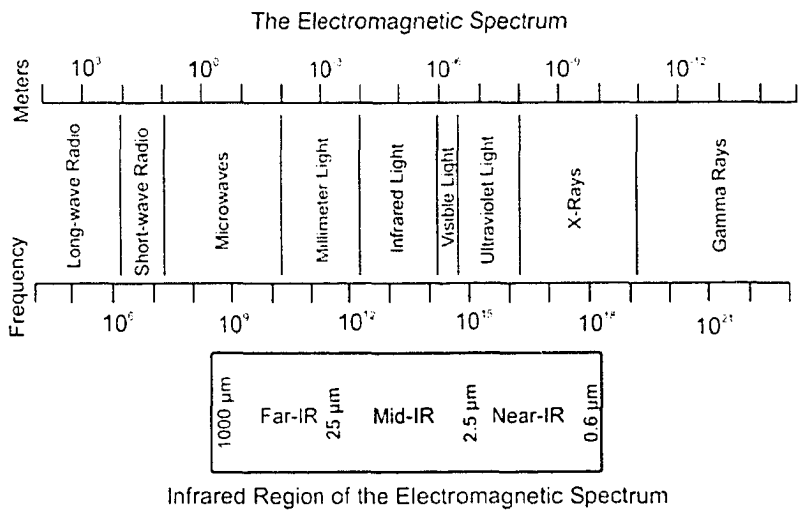

Figure 2-1 The electromagnetic spectrum highlighting the infrared region. From Clark (2004).

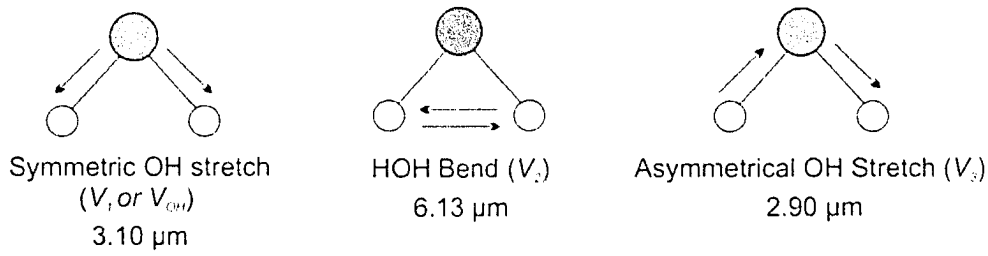

Figure 2-2 The fundamental frequencies of water.

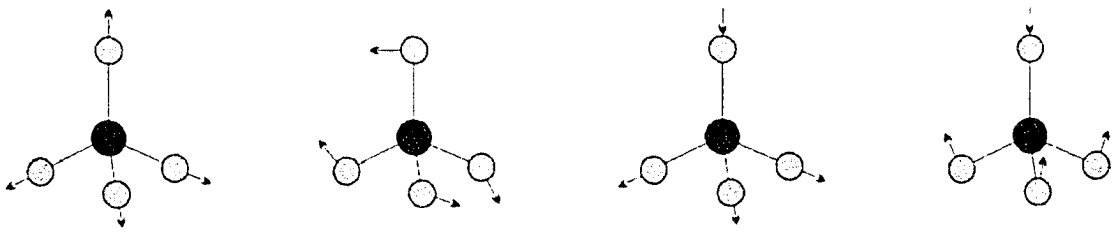

Figure 2-3 The fundamental frequencies of the silicate ion. From Nakamoto (1970) and Basile et al. (1973).

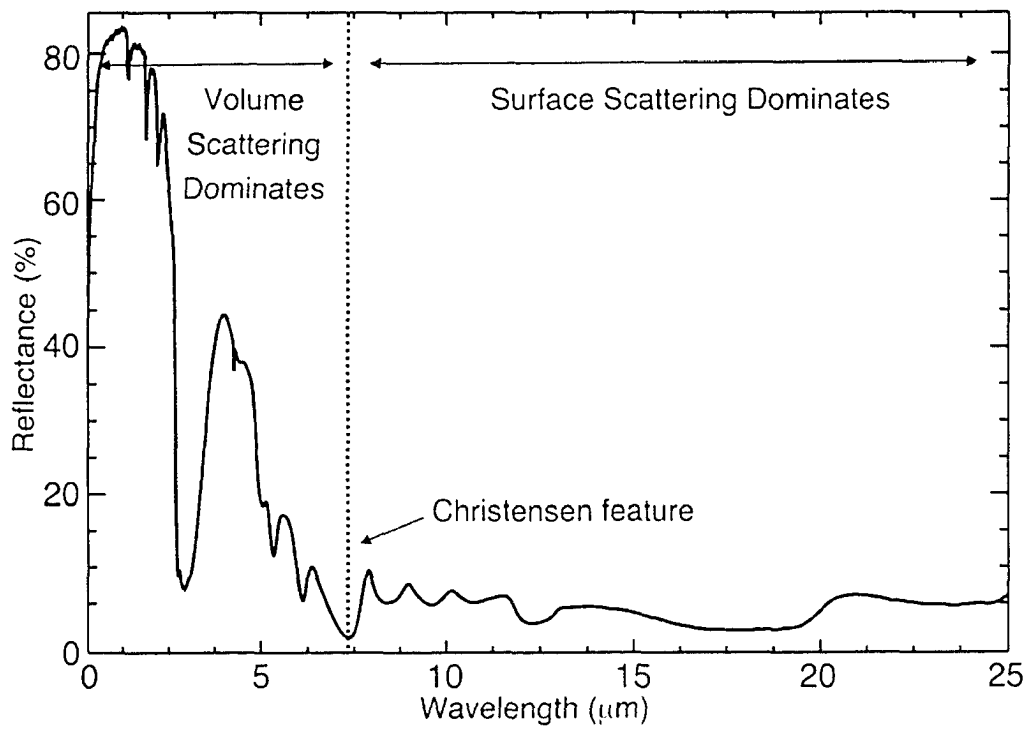

Figure 2-4 The location of the Christensen feature for opal-A. At shorter wavelengths than the Christensen feature the spectrum is dominated by volume scattering, at longer wavelengths than the Christensen feature the spectrum is dominated by surface scattering.

Chapter 3. Methods and Instrumentation

3.1 Site description

3.1.1 Ohaaki Pool

Samples of siliceous sinter were collected from the discharge apron around Ohaaki Pool (~ 45 m long and ~ 15 wide), which is located in the Taupo Volcanic Zone on the North Island of New Zealand (Fig. 3-1) (Jones et al., 1998). Sinters were precipitated from alkaline Na-HCO_3-Cl dilute spring waters at 95°C (Mahon and Finlayson, 1972). The area is characterized by shallow-dipping Quaternary volcanic deposits and lacustrine sediments that over-lie Mesozoic sediments. The hydrology of the Broadlands-Ohaaki system is now controlled by an alternating sequence of nearly horizontal permeable and less permeable units that are crossed by vertical fractures and normal faults that act as feeder channels (Browne and Ellis, 1970).

The sinters incorporated a broad array of fabrics that were controlled by filamentous and coccoid microbes that acted as templates for amorphous silica (opal-A) precipitation (Jones et al., 1998). Bacteria including *Calothrix*, *Phormidium*, and *Synechococcus* formed columnar stromatolites around the edge of the pool, oncoids in the discharge channel, intercalated stratiform stromatolites, "*Conophyton*", and coccoid microbial mats (Jones et al., 1998). The microbes were replaced and encrusted by amorphous silica while alive, or shortly after death. Consequently, the fabrics in the siliceous sinters around Ohaaki Pool are controlled by the growth patterns and composition of the microbial community. Samples NZ152, NZ313, NZ341, and the core were collected from discharge apron of Ohaaki Pool. Mineralogy was confirmed by X-Ray diffraction (Jones et al., 1998).

3.1.2 Champagne Pool

Champagne Pool is an anoxic spring located at Waiotapu (Fig. 3-1) (See Jones et al., 2001). The sinter is mainly composed of opal-A, which preserves the texture of stromatolites. The water is rich in arsenic and antimony sulphides which gives the samples a distinctive orange colour. The deposits also contain high concentrations of Au (115 ppm) and Ag (370 ppm). Sample NZ413 was collected from the rim of Champagne Pool.

3.1.3 Waikite Geyser

Located on the southern side of Rotorua in the Whakarewarewa geothermal system, the Waikite Geyser has a discharge apron that is ~ 90 m long on its N-S axis and ~60 m wide on its E-W axis. When it was active, the geyser precipitated opaline sinter with microbes acting as templates for much of the silica precipitation. Microbes were replaced and/or encrusted with silica (Jones and Renaut, 2003). Samples NZ507, NZ509, NZ518, and NZ530 were collected from the discharge apron of the Waikite Geyser.

3.2 Sample description

Eight hand samples and eight pieces of core were selected for this study. The group A sample set consists of four hand samples (NZ152, NZ313, NZ341, and NZ413), the group B sample set consists of an additional four hand samples (NZ507, NZ509, NZ518, and NZ530), and the core samples set contains eight pieces of core

(OP5-A, OP5A-A, OP5B-A, OP5B-C, OP7-A, OP8-C, OP14-B, and OP15-E). Reflectance spectra were collected first from the group A sample set. Additional reflectance spectra were then collected from the core. After these spectra were collected, the group B sample set was added to the project. Two slightly different instruments were used to collect the reflectance spectra from the group A and B hand samples and core, and therefore the results are presented separately.

3.2.1 Hand sample description

The hand samples exhibited large variations in color, porosity, degree of consolidation, and sedimentary textures. They were dull in luster and ranged in color from white to orange and dark gray. The samples showed variable amounts of porosity and degrees of consolidation, which in many cases were related. For example, poorly consolidated samples had high porosity, and well consolidated samples had low porosity. The sedimentary textures observed on the surfaces of the hand samples and in the profiles of the hand samples were indicative of the morphologies of the microbes that mediated the construction of the sinters (Jones et al., 1998). Many of the upper surfaces of the hand samples were natural and unfractured, whereas most of the lower surfaces were broken. The samples selected for this study were chosen based on their physical properties.

3.2.1.1 Group A samples set

NZ152

This sample is well consolidated and shows little porosity; the base is planar, and it is white and orange in color. This sample is 1-2 cm thick and the side profile reveals light colored laminations. The upper surface is dark grey with small spherical concretions. This sample was formed in a pool and shows a very high microbial influence with the dominant microorganism being *Phormidium* (Jones et al., 1998).

NZ313

Light-yellow in color and prone to fracture, the base and upper surface of this sample show high porosity and a low degree of consolidation. The side profiles reveal laminations with less porosity than the surfaces, which may be related to seasonal variation (Jones and Renaut, 2004). Scanning electron micrographs show silica and sheaths around microbes, with pore spaces between microbes and within the sheaths. The predominant organism is *Calothrix* (Jones et al., 1998).

NZ341

This sample is similar to NZ313 except that it is white in color. It is prone to fracture and all surfaces have a high amount of porosity and a low degree of consolidation.

NZ413

Collected from the wall and floor of a man-made canal, this sample has a distinct orange color. The base is near planar and well consolidated with low porosity, whereas the upper surface is bulbous and composed of a powdered and high porosity material. This sample is not layered because it was formed at a consistant water temperature (Jones et al., 1998).

3.2.1.2 Group B sample set

NZ507

The base of this sample is composed of a white and very porous, poorly consolidated material. The side view of this sample shows laminations (1-5 mm) of resistant, thin and well-consolidated dark layers, and thick and poorly consolidated white layers. This texture is also seen in the profiles of samples NZ509, NZ518, and NZ530. The upper surface is dark-grey in color and has planar-circular structures; it is formed of dense and well-consolidated material with low porosity. The surface textures are the result of bacterial colonies.

NZ509

On the base of this sample is a resistant brown crust. Where this material is broken off, there is a very porous and poorly consolidated white material. The side profile of the sample shows alternating laminations of a resistant grey material and a more porous white material. The upper surface of this sample is dark grey, with bulbous structures (3 mm to 3 cm in width), which are the result of bacterial colonies.

NZ518

The base of this sample is black and white in color. The material is well-consolidated, however there are large holes (0.5-1 cm wide). The sample is composed predominantly of white material, with black material filling in the pores and holes. The profile shows undulating laminations of consolidated and unconsolidated material. The upper surface is smooth and grayish brown, very consolidated with no visible porosity.

NZ530

The base of this sample is very consolidated with low porosity, and it is encrusted with grey and black material. Where the crust has been removed, there is a porous low-consolidated white material. The profile shows alternating layers that are white and cream in color. These laminations are texturally different when compared to the other samples in this group. The top surface of this sample is composed of a white material that is not porous but has a medium degree of consolidation.

3.2.2 Core description

The pieces of core were chosen based on their length (which had to be greater than 10 cm to facilitate the collection of reflectance measurements), and their proximity to the Ohaaki Pool fence (Fig. 3-1D). The cores are characterized by pervasive horizontal laminations (1-5 mm), which are the result of seasonal variations in growth (Jones et al., 1998). With the exception of one sample, which had 2 centimeters of poorly consolidated material on one end, all of the cores were well-

consolidated. The core sample set consists of eight pieces of core (OP5-A, OP5A-A, OP5B-A, OP5B-C, OP7-A, OP8-C, OP14-B, and OP15-E).

3.3 Reflectance measurements from hand samples and core

3.3.1 Sample preparation and acquisition of spectra

Depending on the texture of the surface, the reflectance spectra were collected in two manners. For most hand samples, measurements were collected along linear transects with one measurement every ~4 mm. For samples with uneven surfaces, measurements were collected at discrete locations. Measurements from the core were collected from flat surface along the inside of the longitudinally cut core.

3.3.2 Instrumentation

3.3.2.1 Bomen MB100 FTIR and Bomen MB102 FTIR

Bidirectional reflectance measurements between the wavelengths of 2.5-22 μm were collected from the group A and group B sample sets using a Bomen MB102 Fourier Transform Infrared (FTIR) spectrometer and a Bomen MB100 FTIR, respectively. Using a globar light source and a viewing angle of 35°, measurements were collected at a resolution of 16 cm^{-1}, with a field of view of approximately 4 x 4 mm. Thirty-two or 64 scans were averaged at each spot.

3.3.2.2 ASD-Field Spec

The group A hand samples were analyzed using the ASD field spec, which has a spectral range of 350-2500 nm, and a resolution of 1.4 nm between 359-1050

nm, and of 2 nm between 1000-2500 nm after resampling. There are three detectors: one 512 element Si photodiode array 350-1000 nm, and two separate thermo electrically cooled InGaAs photodiodes 1000-2500 nm.

3.4 Reflectance measurements from crushed material

3.4.1 Sample preparation and acquisition of spectra

Samples NZ152, NZ313, NZ341, and OP7-A were crushed manually and sieved into three different particle size factions (0-74 μm, 74-250 μm, and 250-500 μm). These samples were chosen for crushing because their hand sample spectra presented the full range of diversity observed in the entire data set. These particle size fractions were chosen for this study because similar ranges are used in previous literature (e.g. Salisbury and Eastes, 1985; Salisbury and Walter, 1989; Salisbury and Wald, 1992; Wald and Salisbury, 1995).

3.4.2 Instrumentation

3.4.2.1 Nicolet Nexus 870 FT-IR Spectrometer

Biconical reflectance spectra from loose crushed material were collected using a Nicolet Nexus 870 FT-IR Spectrometer between 1.8-26 μm at the Reflectance Experiment Laboratory (RELAB), which is located at Brown University, Rhode Island. Measurements were collected at a spectral resolution of 4 cm^{-1}, relative to a gold standard using globar as a light source.

3.4.2.2 UV-VIS-NIR Bidirectional Spectrometer

Additional spectra between 0.32-1.8 μm were collected from crushed material using a UV-VIS-NIR Bidirectional Spectrometer at RELAB. The spectrometer had a sampling interval of 5 nm and an incidence/emergence angles of 30° and 0°. A quartz halogen lamp was used as a light source, and halon was used as a reference standard. Corrections were based on the NBS calibration and were applied automatically.

3.5 Absorbance measurements from crushed material

3.5.1 Sample preparation and acquisition of spectra

Absorbance measurements were collected from loosely packed crushed material (< 74 μm) of samples NZ152 and NZ313. These samples were selected because there were identified as having very different reflectance spectra.

3.5.2 Instrumentation

3.5.2.1 Nicolet Magna 750 FTIR with an MCT-B detector

The spectra were acquired from 4000 to 400 wavenumbers (cm^{-1}) using 32 scans at 4 wavenumbers (cm^{-1}) resolution using Nicolet Omnic software. The instrument was used in transmission mode.

3.6 Selection and recording of spectral features

Peaks and troughs in the reflectance and absorbance spectra that relate to the fundamental vibrational modes and the overtones/combinations of molecules are referred to as spectral features. The position of a spectral feature is indicated by

wavelength (μm), and was selected using a cursor on the monitor display. Intensity is a measure of the quantity of energy returned to the detector, and was recorded as either a percentage of reflectance or absorbance. The shapes of the features were described using words such as symmetrical, asymmetrical, broad, narrow, or sharp.

3.7 Figures

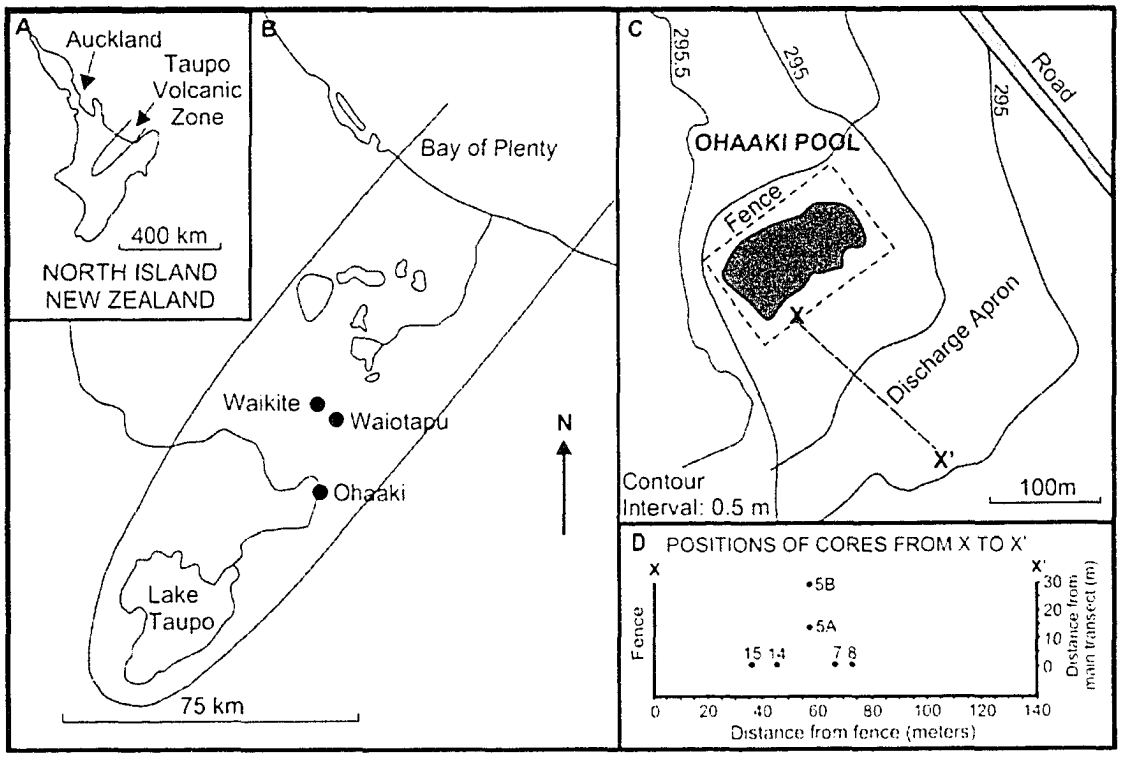

Figure 3-1 Map of (A) North Island, New Zealand, (B) the Lake Taupo region, (C) Ohaaki Pool, and (D) the transect along which the cores were collected. From Jones et al. (1998).

Chapter 4. Results

4.1 Introduction

In this chapter, the positions and intensities of the spectral features observed in the reflectance and absorbance spectra of opal-A between 0.5-25 μm are presented (Tables 4-1, 4-2, 4-3; Figs. 4-1, 4-2). A paper containing the results and discussions from the group A sample set and the crushed material was published in Geophysical Research Letters in December 2004, and it is provided in Appendix A. This chapter incorporates the findings that are presented in the paper with spectra collected from the group B sample set and the core. Reflectance spectra collected from the hand samples and cores are provided in Appendix B.

4.2 Reflectance results from hand samples and core

The main spectral features observed in the reflectance spectra between 0.5-2.5 μm are six troughs located at 1.40, 1.46, 1.90, 1.96, 2.21, and 2.26 μm; in addition, there are two weak troughs located at 0.96 and 1.15 μm (Table 4-1; Fig. 4-3A). The six troughs occur as three sequential pairs, with the first trough in each pair absorbing strongly and the second absorbing weakly.

In the wavelength range of 2.5-6.0 μm there are five troughs located at 2.73, 2.91, 4.68, 5.04, and 5.33 μm (Table 4-2; Fig. 4-3B). The strongest feature is located at 2.91 μm. Instrument noise does not permit separation of this feature from the feature at 2.73 μm in the spectra from the group B samples and core; instead, a broad trough is observed between 2.72-3.01 μm. Two troughs of medium intensities are

located at 5.04 and 5.33 μm, and a weak feature is detected at 4.68 μm in the group A sample set. In the wavelength range of 0.5-6.0 μm, the amplitude of the spectra vary, but the positions and intensities of the spectral features do not change.

In the wavelength range of 6-20 μm, there are six peaks located at 6.38, 8.00, 9.00, 10.00-10.28, 11.17-11.60, and 12.70-13.46 μm; and, there are three troughs located at 6.13, 7.35-7.71, and 12.03-12.46 μm (Table 4-3; Fig. 4-3C). In some spectra the peaks at 8.00 and 9.00 μm are the most intense spectral features; in other spectra, however, the five peaks at 6.38, 8.00, 9.00, 10.00-10.28, and 11.17-11.60 μm have comparable moderate intensities.

4.3 Reflectance results from crushed material

Reflectance spectra were collected between the wavelengths of 0.5-25.0 μm from crushed material of three different grain sizes (0-74 μm, 74-250 μm, and 250-500 μm). Similar to those observed in the spectra from the hand samples and core, the main spectral features for the crushed material between 0.5-2.5 μm are six troughs located at 1.40, 1.46, 1.90, 1.96, 2.21, and 2.26 μm; there are also three weakly absorbing features at 0.96, 1.15, and 1.20 μm (Table 4-1; Fig. 4-4). The six troughs occur in three sequential pairs, with the first trough in each pair absorbing strongly and the second absorbing weakly.

In the 2.5-6.0 μm wavelength range there are five troughs located at 2.74, 2.90, 4.69, 5.01, and 5.32 μm (Table 4-2; Fig. 4-5). The strongest feature is located at

2.91 μm, and it is clearly separated from the feature at 2.73 μm. The trough at 4.69 μm is very weak, whereas the features at 5.01 and 5.32 μm have medium intensities.

Between 6-25 μm, there are seven peaks located at 6.37, 7.95, 8.99, 10.15, 11.34-11.60, 12.86-13.09, and 20.90 μm, and, three troughs at 6.13, 7.34-7.71, and 12.05-12.31 μm (Table 4-3; Figs. 4-6, 4-7). The largest peaks are located at 7.95 and 8.99 μm, and this observation is consistent with the spectra collected from the hand samples and core.

4.4 Absorbance results from crushed material

Absorbance spectra were collected from NZ152 and NZ313 between 2.5-15 μm. In the range of 2.5-6.0 μm, there are four peaks located at 2.76, 2.94, 5.03, and 5.34 μm (Table 4-2; Fig. 4-8). The spectral feature at 2.94 μm has a moderate intensity, whereas the spectral features at 2.76, 5.03, and 5.34 μm have weak intensities.

Between the wavelengths of 6-14 μm, there are seven peaks at 6.11, 8.41, 8.99, 10.46, 12.51, 14.38, and 14.94 μm. There are also two troughs at 10.24 and 11.65 μm. The most intense spectral feature in the absorbance spectra is located at 8.99 μm, and this spectral feature has a shoulder feature located at 8.41 μm. Spectral feature having moderate intensity are located at 6.11, 10.46, and 12.51 μm, and the spectral features at 14.38 and 14.94 μm have weak intensities.

Generally, there is a good correlation between the position of the spectral features in the reflectance and absorbance spectra (Table 4-2); there are, however, four exceptions:

(1) There is no feature in the absorbance spectra that correlates with the weak spectral feature at 4.67-4.69 μm observed in the reflectance spectra from the group A hand samples.

(2) There is an offset between the largest reflectance spectral feature at ~8 μm and the largest absorbance spectral feature at 8.41 μm.

(3) There is only one spectral feature in the absorbance spectra at 10.46 μm, however there are two spectral peaks observed in the reflectance spectra between 10-12 μm.

(4) There are no spectral features in the reflectance data that can be correlated with the absorbance spectral features at 14.38 and 14.94 μm.

4.5 Variations in the reflectance spectra

4.5.1 Amplitude

In the range of 0.5-6.0 μm the amplitude of the spectra change as a function of grain size, with smaller grain sizes producing spectra with higher amplitudes (Fig. 4-5). Large variations in amplitude are observed between 6-13 μm (Fig. 4-6). The positions and/or relative intensities of some spectral features between 6-13 μm change as amplitude increases or decreases. In the spectra from the hand samples and core it is observed that when the spectral features at ~8 and ~9 μm have higher

intensities, the spectrum has a higher amplitude; conversely, when these features have lower intensities, the spectrum has a lower amplitude.

4.5.2 Relative band intensities

The relative intensities of the spectral features between 0.5-6.0 μm do not change. In the wavelength range of 6-25 μm, however, the relative band intensities do change, and the spectral features at ~8 and ~9 μm have a large impact on the intensity of the other spectral features between 6-25 μm. When the spectral features at ~8 and ~9 μm have high intensities, the bands between 10-12 μm are masked. As the bands at ~8 and ~9 μm decrease in intensity, the intensities of the bands at 6.13, 6.37, 10.00-10.28, and 11.17-11.60 μm increase.

4.5.3 Shifting of band positions

When the features at ~8 and ~9 μm have lower intensities, they occur at smaller wavelengths than when they have higher intensities. In general, the feature at ~8 μm shifts approximately 3-5 hundredths of a micrometer, whereas the feature at ~9 μm shifts approximately 0-2 hundredths of a micrometer. Systematic shifting of the spectral features is not observed between 0.5-6.0 μm.

The positions of the bands at 12.03-12.46 and 12.70-13.46 μm change systematically depending on the intensity of the bands at ~8 and ~9 μm: they shift to smaller wavelengths when the bands at ~8 and ~9 μm have high reflectance, compared to when they have low reflectance.

4.5.4 The effect of grain size on reflectance spectra

In the wavelength range of 0.5-6.0 μm, materials having smaller grain sizes produced spectra with higher amplitudes. In the wavelength range of 6-13 μm, both the amplitude of the spectrum and the positions and relative intensities of some spectral features changed as a function of grain size. In general, larger grain sizes produced spectra with higher intensity bands at ~8 and ~9 μm (Fig. 4-6). In these spectra, the bands between 10-12 μm are masked, the reflectance at 6.13 and 6.37 μm is low, and the bands at 12.25 and 12.96 μm are shifted to smaller wavelengths. In the spectra collected from the finest particle sizes, the bands at ~8 and ~9 μm have lower intensities and are shifted to shorter wavelengths; in addition, higher reflectance is observed for the bands at 6.13, 6.37, 10.15, and 11.34-11.60 μm.

In general, the spectral features at ~8 and ~9 μm are shifted a few hundredths of a micron, and the spectral features at 12.05-12.31 and 12.86-13.09 μm shifted a few tenths of a micron.

4.6 The two classes of spectra

Two distinct classes of spectra are observed in reflectance spectra between the wavelengths of 6-13 μm. The classes, called Class-1 and Class2/2A are distinguished by the relative intensities of the spectral features at 6.37, ~8, ~9, 10.00-10.28, and 11.17-11.60 μm. In the wavelength range of 0.5-6.0 μm, the two classes of spectra are not observed.

Class-1 spectra have a weak peak at 6.37 μm, strong peaks at ~8 and ~9 μm, and absent or very weak peaks between 10-12 μm (e.g. Appendix B Figs. 3, 16, 18). Class-2/2A spectra have a strong peak at 6.37 μm, weaker peaks at ~8 and ~9 μm, and two moderate peaks between 10-12 μm (e.g. Appendix B Figs. 6, 9). When the peaks between 10-12 μm have a higher intensity than the peaks at ~8 and ~9 μm, the spectrum is classified as a Class-2A spectrum. Some samples produced spectra belonged to both Class-1 and Class2/2A (e.g. Appendix B Figs. 12, 14, 16, 26).

Of the 293 reflectance spectra that were collected between 6-13 μm, 71% belong to Class-1, 37% belong to Class-2 and 8% belong to Class-2A (Tables 4-4, 4-5 A-D). The largest proportion of Class-1 spectra were collected from the core (92%), and the smallest proportion were collected from the group A sample set (37%).

4.6.1 The relationship between spectral class and grain size

Samples NZ152 and OP7 produced Class-1 spectra, and samples NZ313 and NZ341 produced Class-2/2A spectra. When crushed to grain sizes between 74-500 μm, samples NZ152 and OP7 continued to produce Class-1 spectra, and NZ341 continued to produce Class-2/2A spectra. When the grains were < 74 μm, all samples produce a Class-2 spectrum, with NZ313 and OP7 producing a Class-2A spectrum.

The spectra collected from hand sample NZ313 belonged to Class 2/2A, however the spectra collected from the crushed material at grain sizes 74-500 μm were Class-1. The crushed material from NZ313 that was sent to RELAB was not the same material from which the hand sample reflectance measurements were collected.

Heterogeneity within the samples is the cause of this discrepancy, and unfortunately the differences in the texture of the materials were not observed visually before the crushed materials were sent for analysis.

4.6.2 Band ratioing

In some cases, rough and uneven surfaces cause dissimilar amounts of light to be returned to the detector causing spectral differences. By ratioing the reflectance of spectral features, these effects can be mitigated. Band ratioing removes the effects of scattering observed in the spectra collected from natural materials.

Within each spectral class, there is a linear relationship between the intensities of the spectral features located at 7.95, 9.00, 10.12, and 11.47 μm (Figs. 4-9 to 4-11). These spectral features were used in the calculation of the band ratios because they are the primary features examined in the classification of opal-A spectra. For each spectral class, the following band ratios were calculated: 9.00 μm/7.95 μm, 10.12 μm/11.47 μm, 10.12 μm/9.00 μm, and 11.47 μm/9.00 μm.

For the ratio of 9.00 μm/7.95 μm, the slopes of the regression lines for Class-1 and Class-2 spectra (including Class-2A) are 3.29 and 1.50, respectively. For the ratio of 10.12 μm /11.47 μm, the slopes of the regression lines for Class-1 and Class-2 (including Class-2A) are 0.59 and 1.04, respectively. The ratio of 10.12 μm/9.00 μm for the Class-1 spectra is 0.34, for Class-2 is 0.76, and for class-2A is 1.49. The band ratio of 10.12 μm/9.00 μm is different for each spectral class, and can be used to distinguish between them.

The band ratios of the crushed material fall near the regression lines of the respective spectral class calculated from the hand samples and core spectra (Fig. 4-12). One exception is the band ratio of 9.00 μm/7.95 μm (Fig. 4-12A). For this ratio, the results from the crushed spectra fall below the regression lines of all classes.

4.7 Summary of results

With some exceptions, the features observed in the absorbance spectra have comparable positions and intensities to those observed in the reflectance spectra. The reflectance spectra show the presence of two classes of opal-A spectra that are distinguished by differences in the relative intensities of the reflectance spectral feature between 6-13 μm.

Class-1 spectra have a weak peak at 6.37 μm, strong peaks at ~8 and ~9 μm, and absent or very weak peaks between 10-12 μm. Class-2/2A spectra have a strong peak at 6.37 μm, weaker peaks at ~8 and ~9 μm, and two moderate peaks between 10-12 μm. When the peaks between 10-12 μm have a higher intensity than the peaks at ~8 and ~9 μm, the spectrum is classified as a Class-2A spectrum. For hand samples that produced Class-1 spectra, crushing of material to grain sizes < 74 μm resulted in the production of a Class-2 or 2A spectrum. For hand samples that produced Class-2 or 2A spectra, these materials produced these classes of spectra at every grain size. The classes of spectra were analyzed by a method called band ratioing. From this, it was determined that the spectral classes of opal-A are distinct.

4.8 Tables

Table 4-1 The positions of the reflectance spectral features of opal-A between 0.5-2.5 μm. These are the values of the band centers. In the text, when the range of wavelengths of a spectral feature's band center is smaller than 0.15 μm, the largest and smallest values are averaged. When the range is larger than 0.15 μm, then that range is provided.

Reflectance	
Group A (0.5-2.5 μm)	Crushed (0.5-2.5 μm)
0.96	0.95-0.96
1.15	1.13-1.15
---[1]	1.20
1.40	1.34-1.40
1.46	1.45-1.46
1.90	1.90
1.96	1.95-1.96
2.21	2.20-2.21
2.26	2.25-2.26

[1] No feature observed

Table 4-2 The positions of the reflectance and absorbance spectral features of opal-A between 2.5-6 μm. See caption for table 4-1.

Reflectance				Absorbance
Group A (2.5-19 μm)	Group B (2.5-14 μm)	Cores (2.5-14 μm)	Crushed (2.5-25 μm)	Crushed (2.5-14 μm)
2.72-2.74	2.72-3.01[1]	2.74-2.99[1]	2.72-2.74	2.76
2.90-2.92			2.90-2.92	2.93-2.94
4.67-4.69	---[2]	---[2]	4.69	---[2]
5.01-5.06	5.00-5.01	5.01-5.03	5.01	5.02-5.04
5.32-5.33	5.32-5.33	5.32-5.33	5.32	5.33-5.34

[1] Two separate features unresolvable due to instrument noise

[2] No feature observed

Table 4-3 The position of the reflectance and absorbance spectral features of opal-A between 6-25 μm. See caption for table 4-1.

Reflectance				Absorbance
Group A (2.5-19 μm)	Group B (2.5-14 μm)	Cores (2.5-14 μm)	Crushed (2.5-25 μm)	Crushed (2.5-15 μm)
6.11-6.14	6.11-6.12	6.11-6.14	6.12-6.13	6.11
6.32-6.44	6.35-6.36	6.35-6.49	6.35-6.39	---[1]
7.40-7.71	7.35-7.40	7.42-7.51	7.34-7.41	---[1]
7.95-8.10	7.91-8.06	7.97-8.02	7.89-7.95	8.41
9.00-9.12	8.97-9.08	8.97-9.03	8.97-9.02	8.99
10.04-10.28	10.08-10.14	10.00-10.04	10.10-10.20	10.21-10.27
11.17-11.60	11.22	11.32-11.42	11.34-11.60	11.60-11.74
12.11-12.46	12.03-12.34	12.05-12.33	12.05-12.31	12.45-12.51
12.70-13.46	12.80-13.09	12.89-13.02	12.86-13.09	---[1]
---[1]	---[1]	---[1]	---[1]	14.38
---[1]	---[1]	---[1]	---[1]	14.97
---[2]	---[2]	---[2]	20.9	---[2]

[1] No feature observed

[2] Beyond the spectral range of the instrument

Table 4-4 The distribution of spectral classes based on the reflectance spectra between the wavelengths range of 6-13 μm. Percentages many not add up to 100% due to rounding.

	Group A		Group B		Cores		Crushed		Total	
Total Spectra	98		85		98		12		293	
Class-1	36	37%	75	88%	92	94%	6	50%	209	71%
Class-2	45	46%	6	7%	6	7%	4	33%	61	31%
Class-2A	17	17%	4	5%	0	0%	2	17%	23	8%

Table 4-5 (A) A list showing which class of spectra the hand samples from the group A sample set produced. The numbers in the brackets refer to the name of the spectra.

Class-1	Class-2	Class-2A
NZ152B (1-11)	NZ313UL1 (1-10)	NZ313-D (1-13)
NZ152E (1-2)	NZ313UL2 (1-9)	NZ341D (1-4)
NZ152G (1-12)	NZ341UL2 (1-12)	
NZ341UL1 (1-3)	NZ341UL1 (4-10)	
NZ413I (1-8)	NZ413O (1-7)	

Table 4-5 (B) A list showing which class of spectra the hand samples from the group B sample set produced. The numbers in the brackets refer to the name of the spectra.

Class-1	Class-2	Class-2A
NZ507E (1-4)	NZ509W (1-6)	NZ507W (1-4)
NZ507G (1-7)		
NZ509E (1-5)		
NZ509G (1-9)		
NZ518E (1-5)		
NZ518G (1-8)		
NZ518W (1-9)		
NZ530E (1-4)		
NZ530G (1-11)		
NZ530W (1-13)		

Table 4-5 (C) A list showing which class of spectra the core sample set produced. The numbers in the brackets refer to the name of the spectra.

Class-1	Class-2
OP5-A (1-11)	OP5B-A (8-10)
OP5A-A (1-14)	OP14-B (11-13)
OP5B-A (1-7)	
OP5B-C (1-11)	
OP7-A (1-8)	
OP8-C (1-14)	
OP14-B (1-18)	
OP15-E (1-9)	

Table 4-5 (D) A list showing which class of spectra the crushed sample produced. The numbers in the brackets refer to the name of the spectra.

Class-1	Class-2	Class-2A
NZ152 (74-250 μm)	NZ152 (0-74 μm)	NZ341 (0-74 μm)
NZ152 (250-500 μm)	NZ313 (0-74 μm)	OP7 (0-74 μm)
NZ313 (74-250 μm)	NZ341 (74-250 μm)	
NZ313 (250-500 μm)	NZ341 (250-500 μm)	
OP7 (74-250 μm)		
OP7 (250-500 μm)		

4.9 Figures

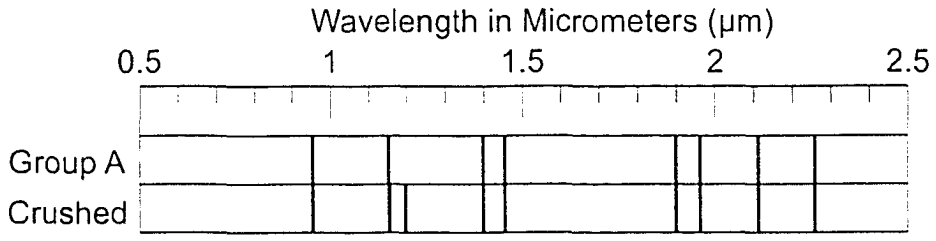

Figure 4-1 The spectral signature diagram for opal-A between 0.5-2.5 µm. The black bars indicate the location and the range of values observed for each spectral feature.

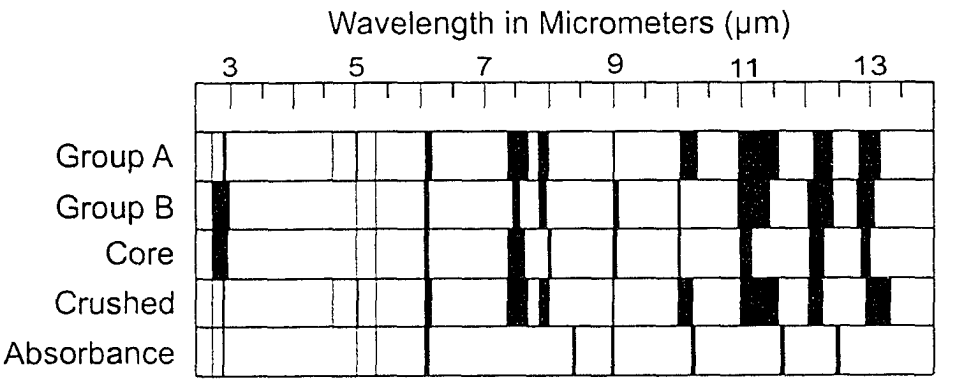

Figure 4-2 The spectral signature diagram for opal-A between 2.5-14 μm. The width of the black bars indicate the location and the range of values observed for each spectral feature. An additional spectral feature was observed in the spectra from crushed materials at 20.9 μm.

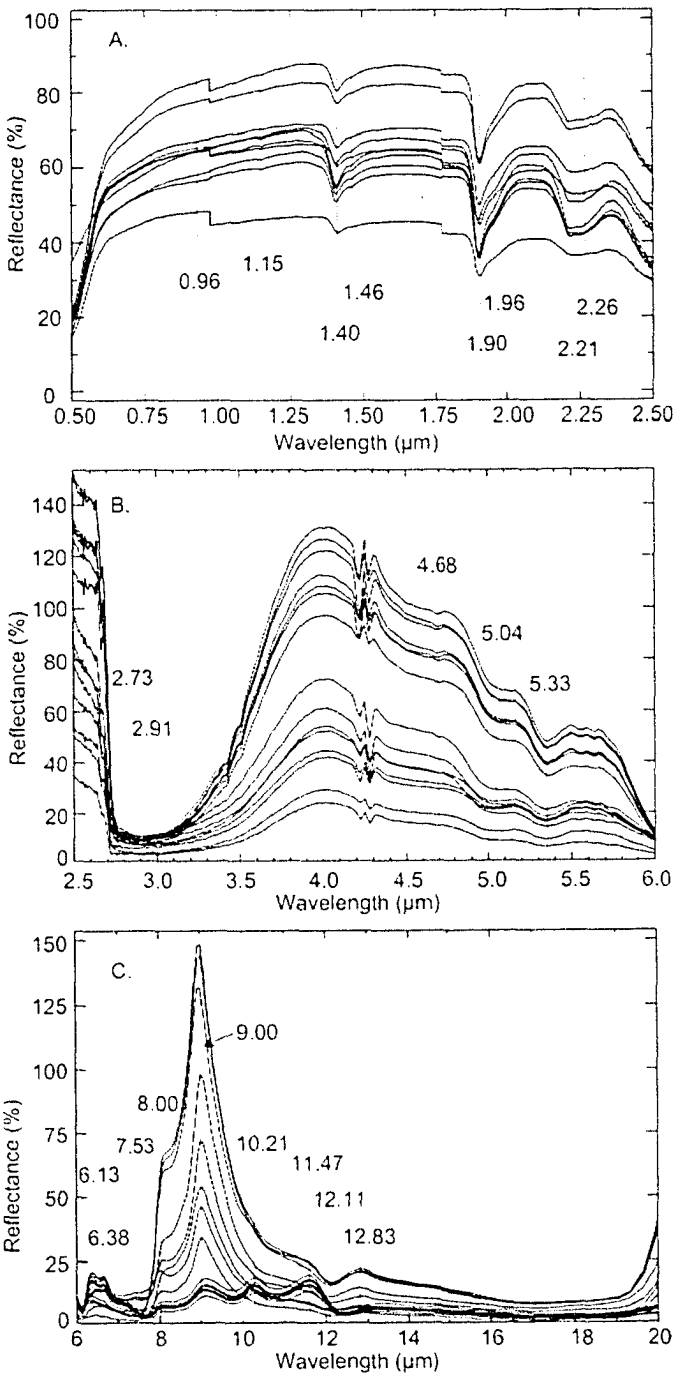

Figure 4-3 The reflectance spectra collected from NZ413 from 0.5-2.5 μm (A), 2.5-6.0 μm (B) and 6-20 μm (C). Measurements were collected using an ASD-Field Spec (A) and a Bomen MB 102 FTIR (B and C).

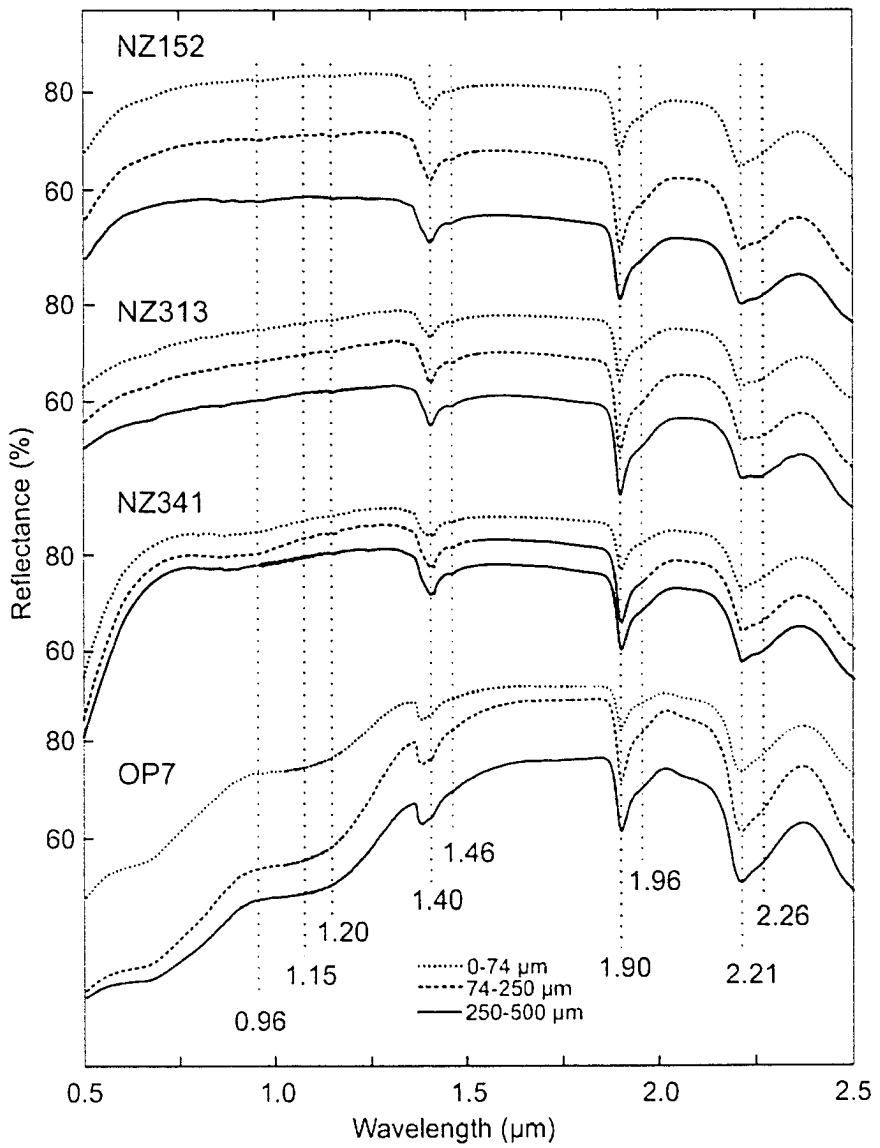

Figure 4-4 The reflectance spectra collected from the crushed material of NZ152, NZ313, NZ341 and OP7 between the wavelengths of 0.5-2.5 μm at grain sizes 0-74, 74-250, and 250-500 μm. Measurements were collected using a UV-VIS-NIR Bidirectional Spectrometer (RELAB).

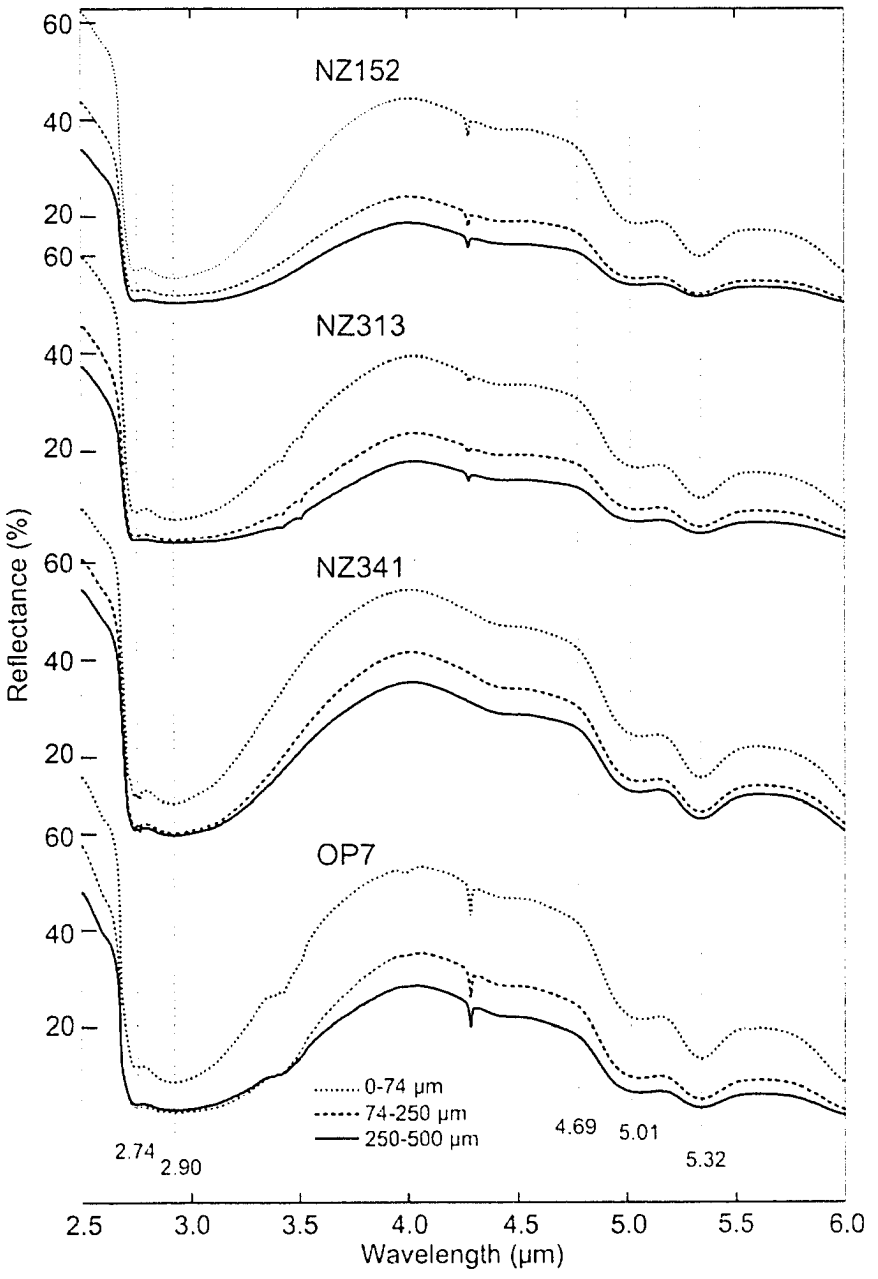

Figure 4-5 The reflectance spectra collected from the crushed material of NZ152, NZ313, NZ341, and OP7 between the wavelengths of 2.5-6.0 μm at grain sizes 0-74, 74-250, and 250-500 μm. Measurements were collected using a Nicolet Nexus 870 FT-IR Spectrometer (RELAB).

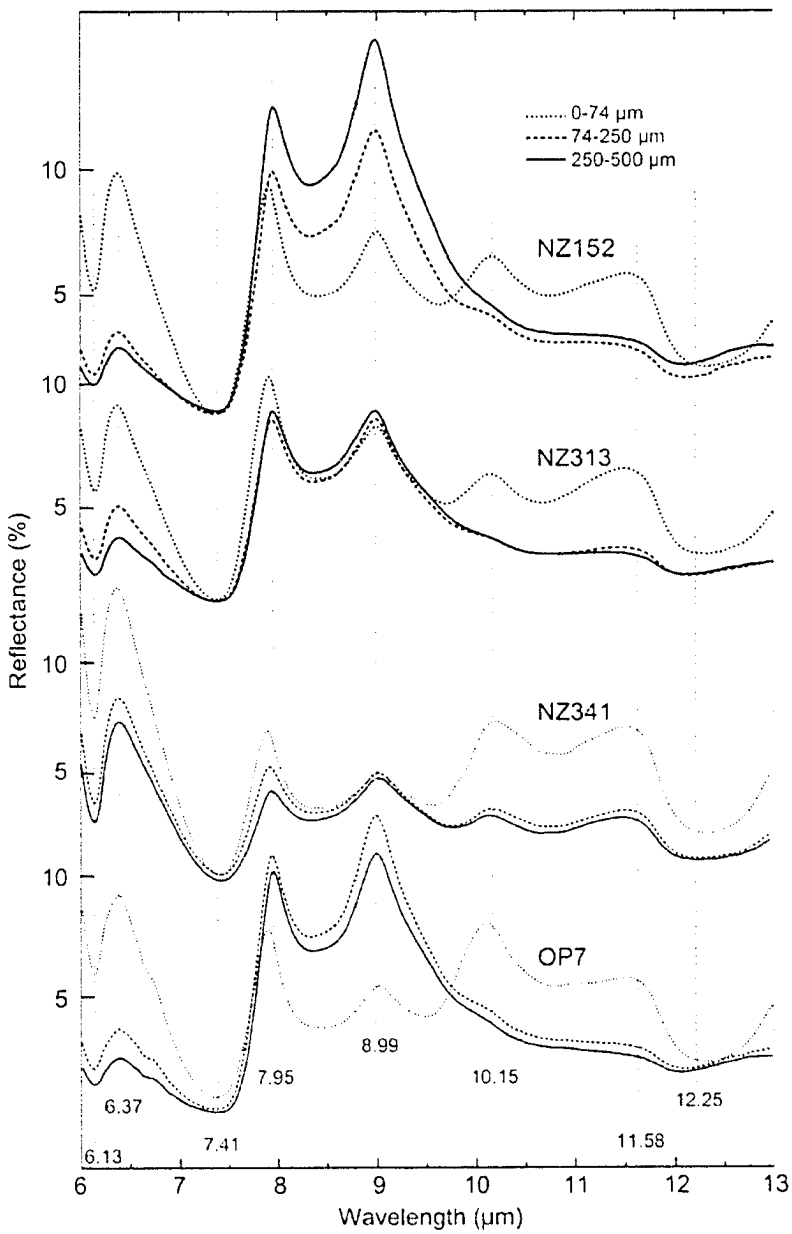

Figure 4-6 The reflectance spectra collected from the crushed material of NZ152, NZ313, NZ341, and OP7 between the wavelengths of 6-13 µm at grain sizes 0-74, 74-250, and 250-500 µm. Measurements were collected using a Nicolet Nexus 870 FT-IR Spectrometer (RELAB).

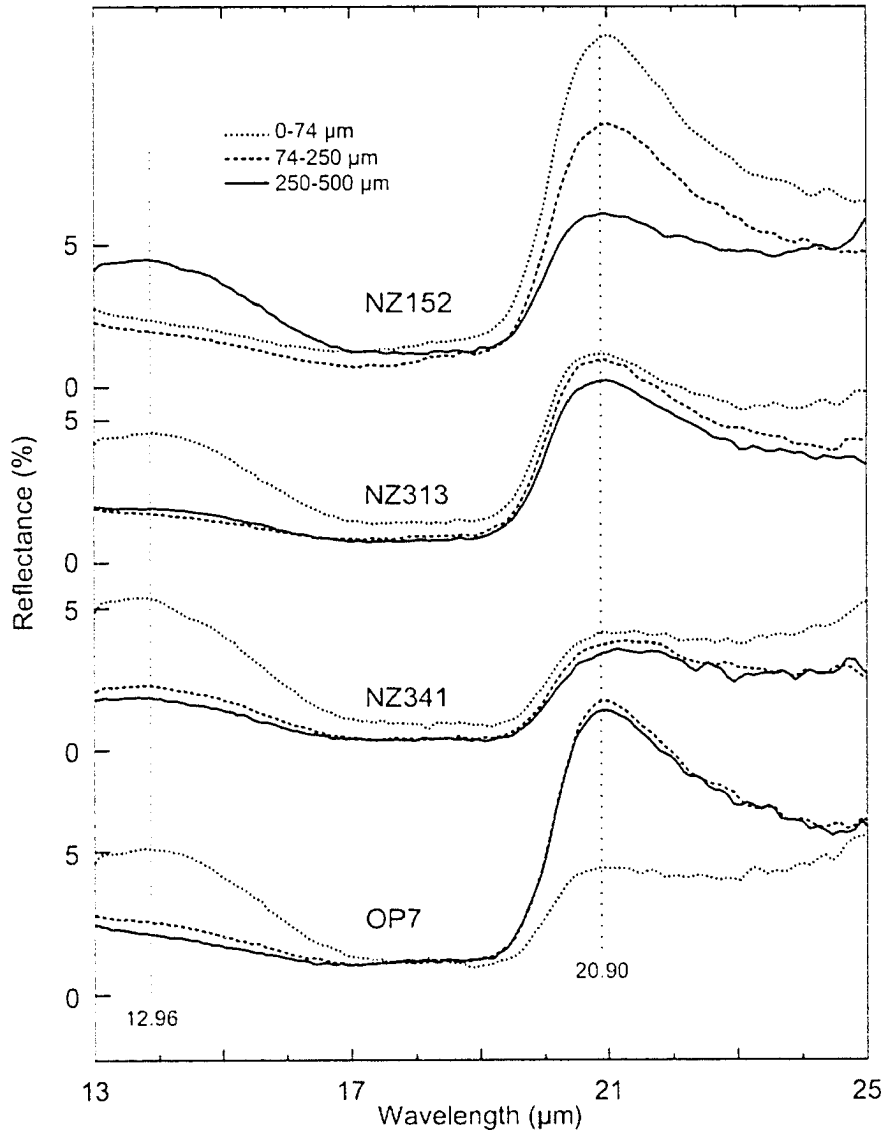

Figure 4-7 The reflectance spectra collected from the crushed material of NZ152, NZ313, NZ341, and OP7 between the wavelengths of 13-25 µm at grain sizes 0-74, 74-250, and 250-500 µm. Measurements were collected using a Nicolet Nexus 870 FT-IR Spectrometer (RELAB).

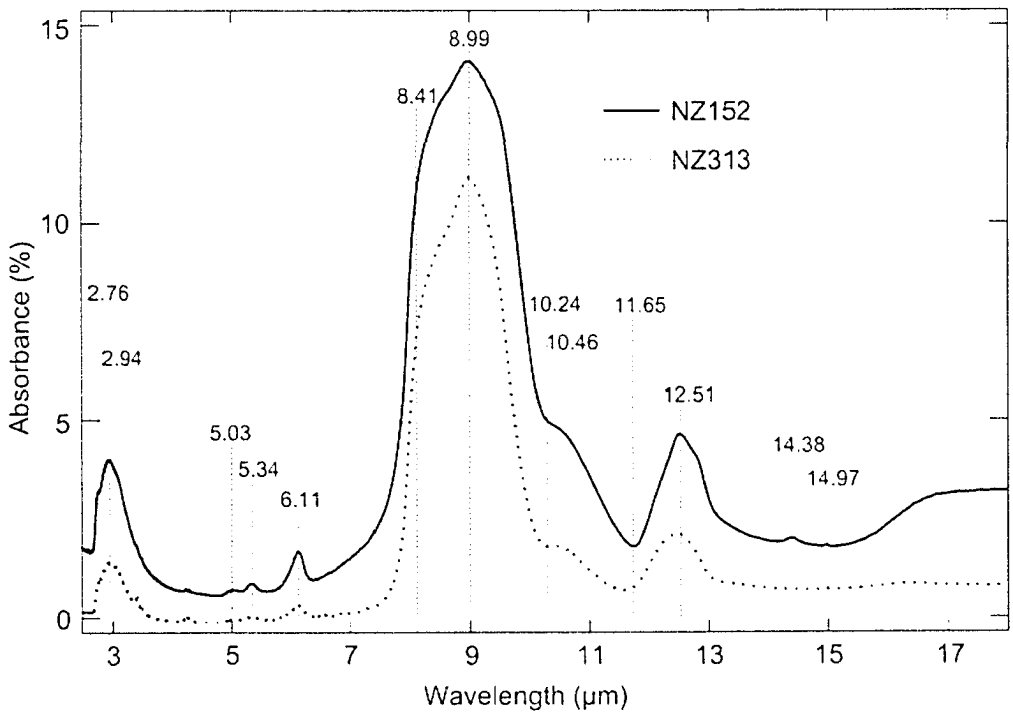

Figure 4-8 The absorbance spectra collected from the crushed material of NZ152 and NZ313 between 2.5-14 μm. Measurements were collected using a Nicolet Magna 750 FTIR.

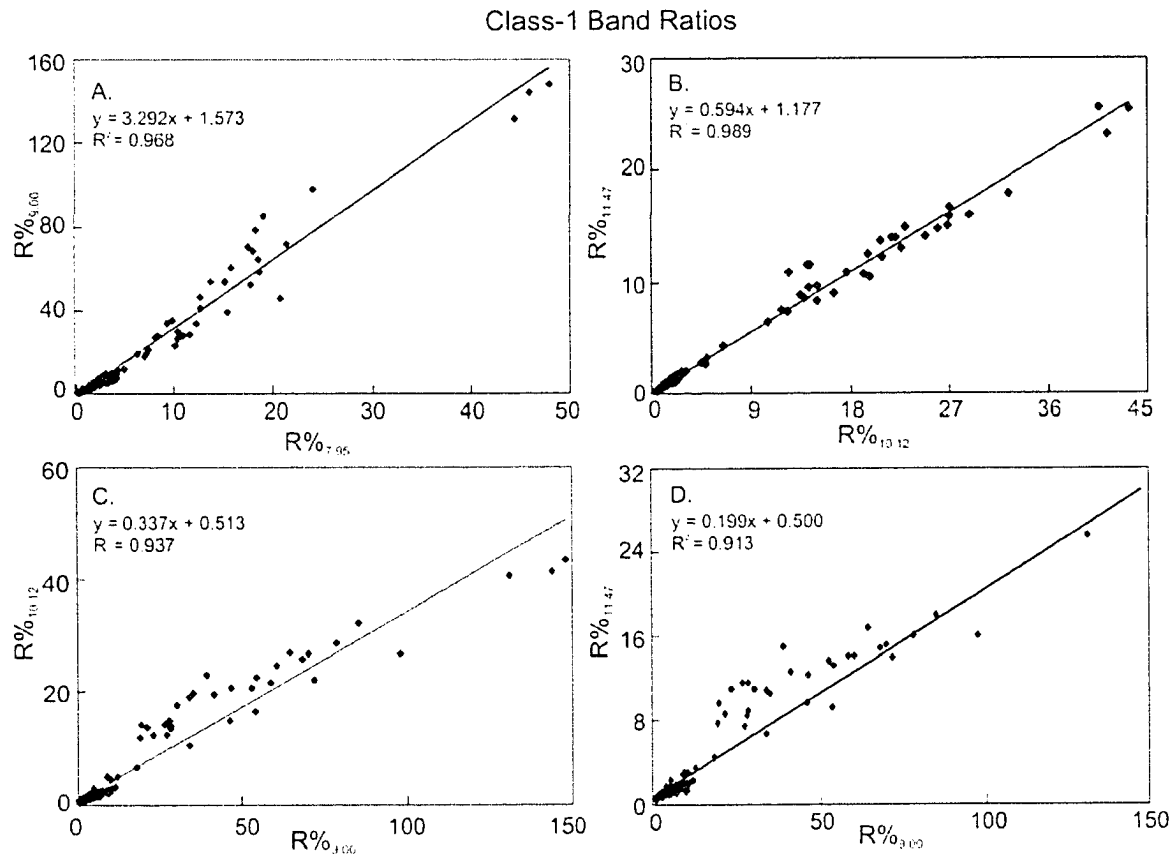

Figure 4-9 (A-D) The band ratios for all Class-1 spectra with the equation of the regression line and the r-squared value (N = 203).

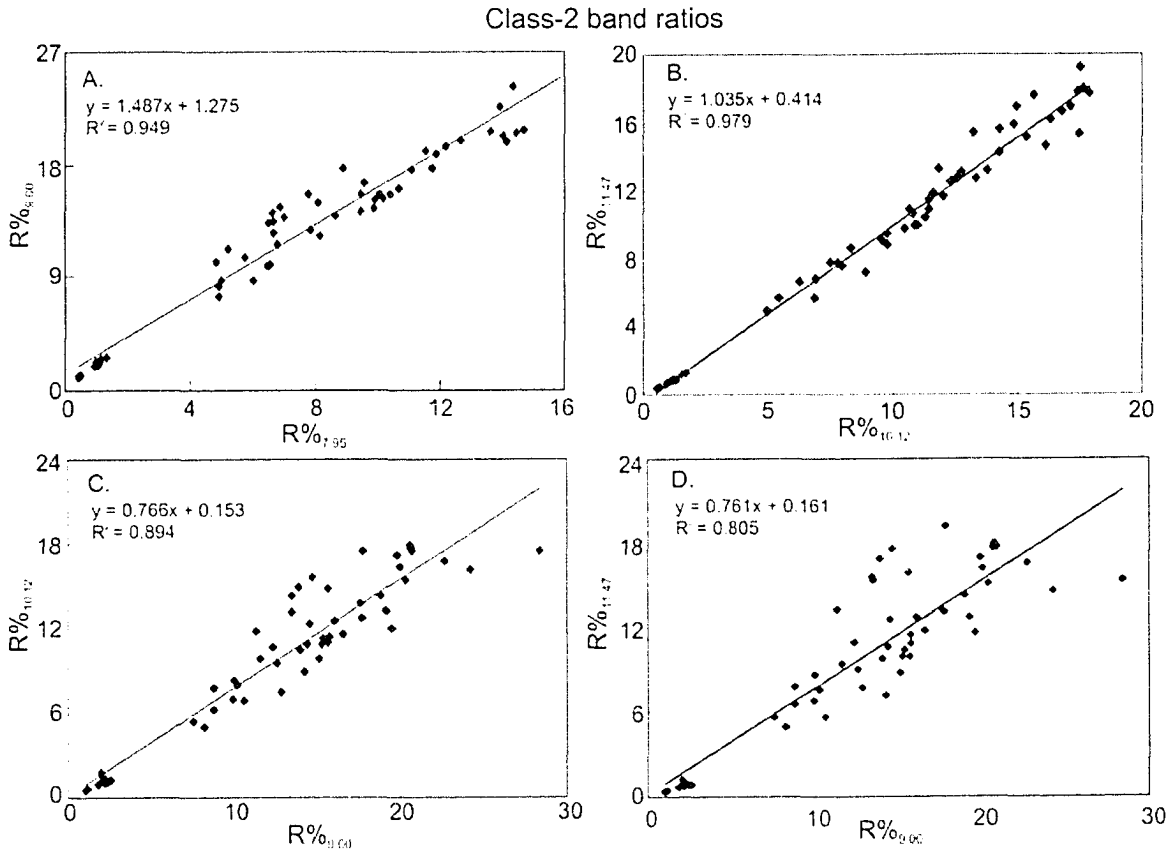

Figure 4-10 (A-D) The band ratios for all Class-2 spectra with the equation of the regression line and the r-squared value (N = 57).

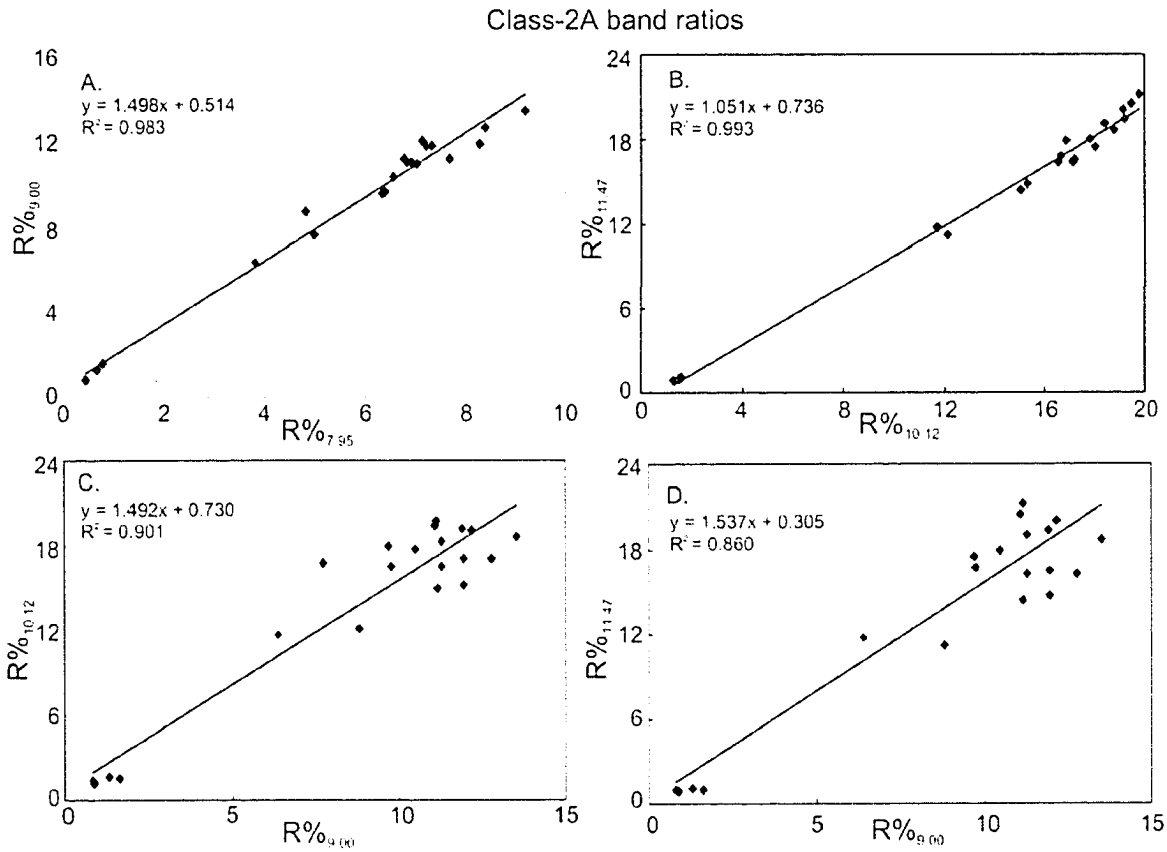

Figure 4-11 (A-D) The band ratios for all Class-2A spectra with the equation of the regression line and the r-squared value (N = 21).

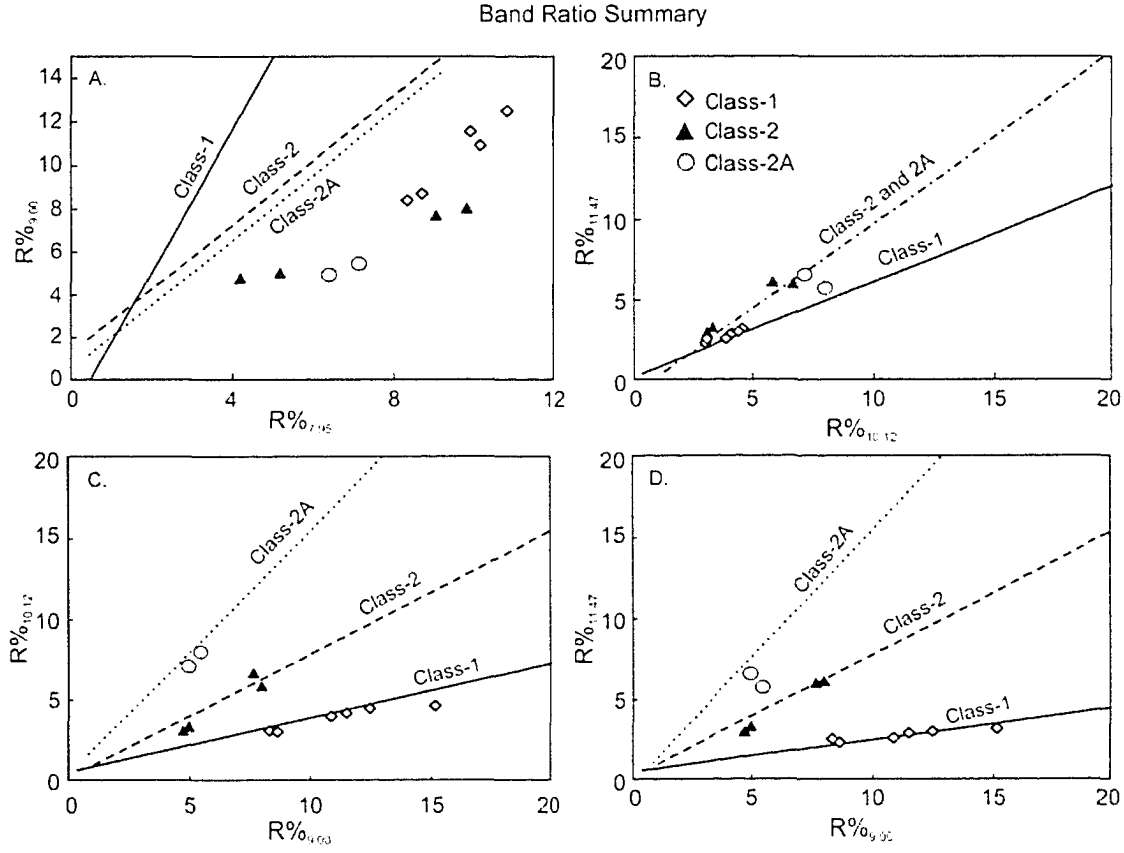

Figure 4-12 (A-D) Comparison of the band ratios of the crushed samples with those of the different classes of hand sample and core spectra (regression lines). Diamonds: Class-1 spectra from crushed material, Triangles: Class-2 spectra from crushed material, Circles: Class-2A spectra from crushed material.

Chapter 5. Discussion

5.1 The spectral features of water and hydroxyl

Spectral features in the reflectance and absorbance spectra from opal-A can be correlated with the vibrational frequencies of water, hydroxyl, and silanol (Tables 5-1, 5-2, 5-3, 5-4). The fundamental vibrational modes of water and hydroxyl, and the corresponding overtone and combination bands, are observed as distinct spectral features between the wavelengths of 0.5-3.1 μm.

Overtones of the –OH stretch of hydroxyl give rise to the pair of spectral features located at 1.40 and 1.46 μm. The cation bound to hydroxyl cannot be identified, however, it is assumed that hydroxyl is bound to hydrogen or silicon to form water or silanol, respectively. The feature at 1.40 μm is related to water or silanol not hydrogen-bound (isolated), whereas the feature at 1.46 μm is related to water or silanol that is hydrogen-bound (cf. Aines and Rossman, 1984). Additional overtones of the –OH stretch are located at 0.96, 1.15, and 1.20 μm (e.g. Hunt, 1977).

Overtones of the –OH stretch and HOH bend of water are present at 1.90 and 1.96 μm. These spectral feature are attributed solely to the presence of water. The feature at 1.90 μm is due to water that is not hydrogen bound (isolated), whereas the feature at 1.96 μm is due to water that is hydrogen-bound (Langer and Flörke, 1974).

The combination band involving the –OH fundamental stretch of hydroxyl produces spectral features at 2.21 and 2.26 μm. The position of the combination band varies between 2.2-2.3 μm depending on which cation is bound to hydroxyl. For example, hydroxyl bound to aluminum and silicon produce a spectral feature at 2.2

μm whereas, hydroxyl bound to magnesium produce a spectral feature at 2.3 μm (Hunt et al., 1973). In studies by Hunt and Salisbury (1970) and Langer and Flörke (1974) the spectral features at 2.21 and 2.26 μm were allocated to molecules of isolated and hydrogen-bound silanol, respectively.

The fundamental mode of the hydroxyl stretch of the isolated silanol group is observed in the reflectance spectra at 2.73 μm and in the absorbance spectra at 2.76 μm (cf. Keller and Pickett, 1949; McDonald, 1958; Dijkstra et al., 2002). The broad spectral feature observed in the reflectance spectra at 2.91 μm and in the absorbance spectra at 2.94 μm is the result of hydrogen-bound silanol (cf. Keller and Pickett, 1949; McDonald, 1958; Dijkstra et al., 2002). The broadening of the reflectance feature at 2.91 μm is due to the overlapping of the fundamental –OH stretch of the hydroxyl group and the asymmetric –OH stretch of water which occurs between the wavelengths of 2.9-3.1 μm (Dijkstra et al., 2002).

The spectral feature relating to the HOH bend of molecular water in an extended network is observed in the reflectance and absorbance data at 6.13 μm (Hunt, 1977; Aines and Rossman, 1984). Located at 6.37 μm in the reflectance data is a peak that varies in intensity directly with the trough at 6.13 μm. The presence or significance of this peak at 6.37 μm was not found in the literature. Based on the close proximity of this peak to the trough relating to the HOH bend of molecular water and that these features have related intensities, the peak at 6.37 μm is likely related to the HOH bend of molecular water.

5.1.1 The structure of water and hydroxyl in opal-A

The shape of the spectral features between 0.5-3.1 μm reveal information about the molecular environment that water and silanol inhabit. Each of the reflectance spectral features at 1.40, 1.46, 1.90, 1.96, 2.21, 2.26, and 2.73 μm have narrow shapes, which is consistent with what is expected for molecules that exist in regular and ordered positions in the lattice (McDonald, 1958; Hunt, 1977; Aines and Rossman, 1984). Conversely, broad spectral features at these locations would indicate that water and silanol exist in random orientations in the material. In summary, the hydrated components of opal-A are integrated into the Si-O network in an ordered manner, although the Si-O network itself does not possess a crystalline structure.

Based on the positions of the spectral features observed in the opal-A spectra between 0.5-3.1 μm, it can be interpreted that there are two forms of water and silanol present: isolated and hydrogen-bound. Langer and Flörke (1974) proposed a model for incorporating isolated and hydrogen-bound water and silanol into opal-A. In this model, silanol and water exist in the primary silica spheres and are not in the vicinity of other silanol or water molecules; therefore, these molecules would not be hydrogen-bound. Outside of the primary silica spheres there is water and silanol existing in a larger hydrated network, which would explain the presence of hydrogen-bound water and hydrogen-bound silanol.

5.2 The spectral features of silica

5.2.1 The Christensen feature

The Christensen feature is a transmission maximum in the opal-A reflectance spectra that is located between 7.35-7.71 μm. Conel (1969) noted that for non-crystalline silica polymorphs the Christensen features can be located between 7.1-7.4 μm. For crystalline silicates, however, the Christensen feature is typically located between 7.5-9.0 μm (Salisbury et al., 1991; Cooper et al., 2002).

The position of the Christensen feature has been associated with the degree of Si-O polymerization (Logan et al., 1973). A material with a high degree of silica polymerization is expected to display a Christensen feature at low wavelengths. Non-crystalline silica polymorphs, however, can produce Christensen features at lower wavelengths than quartz (Fig. 5-1). Considering that non-crystalline silica polymorphs are less polymerized than quartz, the low-wavelength position of the Christensen feature can not be solely controlled by the degree of silica polymerization. Since the Christensen feature is located adjacent to the fundamental Si-O assymetrical stretch, it is likely that a displacement of the Si-O asymmetrical stretch to lower wavelengths is also responsible for displacing the Christensen feature in the spectra of non-crystalline silica phases.

5.2.2 The Si-O stretch and bend

The fundamental vibrational modes of the Si-O asymmetrical stretch for opal-A are located in the reflectance spectra at ~8 and ~9 μm. The first fundamental

vibration band at ~8 μm is located at a lower wavelength than the first fundamental vibration band of quartz.

In the absorbance spectra of opal-A, it is observed that the first fundamental vibration band of the Si-O asymmetrical stretch is located at 8.41 μm. When compared to the position of the corresponding band in reflectance, there is a shift of approximately 0.41 μm. A shift in the reflectance and absorbance bands relating to the fundamental Si-O assymetrical stretch has been observed by Clark and Roush (1984) and Salisbury et al. (1987). Salisbury et al. (1987) did not quantify the shift, but attributed it to a sharp change in the real part of the refractive index, which is concurrent with a maximum increase in the imaginary part of the refractive index. This occurs on the shorter wavelength side of a strong absorption band, causing a shift in the reflectance peak to a shorter wavelength. It was also noted by Salisbury et al. (1987) that not only had the peak shifted, but its shape had also changed. Since the position of the first fundamental band determines the position of the Christensen feature, shifting the first fundamental vibrational mode to lower wavelengths would also cause the Christensen feature to shift.

The fundamental vibrational mode of the Si-O bend is located at 20.90 μm in the reflectance spectra. The position of this spectral feature is in the range of 18-25 μm, which was noted by Salisbury et al. (1991) as being the range in which the Si-O bending mode of silicates could be found. Since the absorbance data was limited to 2.5-15 μm, no corresponding absorption feature could be observed.

5.2.3 The Si-OH bend

Spectral features relating to the fundamental mode of the Si-OH bend of silanol are observed in the reflectance data between 10-12 μm (Bellamy, 1975; Ryskin, 1974; Socrates, 1980). These reflectance features were observed in the spectra collected from poorly consolidated samples and fine grained material (e.g. Fig.4-3, 4-6). It was also noted that as grain size decreased, the intensity of the feature between 10-12 μm increased. Although these peaks are allocated to the fundamental mode of the Si-OH bend, they behave in a manner similar to that of transparency features as defined by Salisbury et al. (1991).

Two peaks are observed in the reflectance spectra relating to the fundamental mode of the Si-OH bend, but only one is observed in the absorbance spectra (Fig. 4-8). The two reflectance peaks may be the expression of a single fundamental vibrational mode of the silanol group. In this case, the center of the band is saturated, as shown by the trough in reflectance at 10.46 μm, and light is reflected solely in the wings. Reflection in the wings increases with a decrease in grain size, as the band center becomes saturated. This effect has been observed for the spectral features related to the fundamental OH vibrations (Salisbury et al., 1991).

5.2.4 The transmission feature

A transmission maximum, which is here referred to as a transmission feature, is located in the reflectance spectra between 12.03-12.46 μm; the corresponding absorbance feature is located between 12.45-12.51 μm. The transmission feature is similar in nature to the Christensen feature, and both are related to the Christensen

frequency (Lyon, 1967). The significance of the transmission maximum is not known, and it is not observed in the spectra of quartz.

5.2.5 The transparency feature

Commonly located between 10.5-12 μm, transparency features are observed solely in the reflectance spectra of material with grain sizes < 74 μm (Salisbury et al., 1991). When present in the spectra of opal-A, the transparency feature was located between 12.70-13.46 μm, and its intensity increased with a decrease in grain size.

5.2.6 The overtones and combinations of Si-O

Additional overtones of the Si-O stretch are located at 4.68, 5.04, and 5.33 μm (Salisbury et al., 1987; Salisbury et al., 1991). In Goryniuk et al. (2004) (Appendix A), the spectral features between 4-6 μm were identified as overtone and combination modes of water and hydroxyl. Upon further examination, it was realized that this initial assessment was incorrect. These features have subsequently been interpreted as being overtones and combination modes of the internal and lattice modes of silicates (Salisbury et al., 1987; Salisbury et al., 1991).

In absorbance spectra there are overtones and combination modes of the Si-O stretch located at 5.03 and 5.34 μm. There is no corresponding spectral feature observed in absorbance for the reflectance spectral feature at 4.68 μm. The presence of additional weak overtone and combination modes in reflectance spectra is

explained in Salisbury et al. (1987) as being the combined effect of surface and volume scattering by particles, which is minimized in absorption measurements.

5.3 Spectral classes and their relationship to opal-A formation

The fabrics of the siliceous sinters formed in hydrothermal deposits are controlled by the growth patterns and composition of the microbial community (Jones et al., 1998). As a result, materials can be compositionally similar, but they can vary dramatically in texture. These textural differences are observable in the hand samples from the Taupo Volcanic Zone, and can also be identified using infrared spectroscopy.

The classes of opal-A spectra (Class-1 and Class-2/2A) observed in the hand samples and core from Taupo Volcanic Zone relate to the amount of silica precipitation that has occurred in the pore spaces between the "primary" silica sphere. Opal-A is comprised of "primary" silica spheres, which are randomly cemented together to form "secondary" silica spheres. The pore spaces between these "secondary" spheres can be filled to varying degrees by additional silica precipitation.

5.3.1 Class-1 spectra

The samples from which the Class-1 spectra were collected are well-consolidated samples having silica that has either nearly or completely filled the pore spaces. Spectrally, these samples behave like a cohesive polished surface, and this effect for quartz was noted by Conel (1969), Salisbury and Eastes (1985), and was expanded on in Salisbury et al. (1991).

5.3.2 Class-2/2A spectra

The Class-2/2A spectra were collected from hand samples and cores which were poorly consolidated and had high porosity. Unlike the Class-1 spectra, the fundamental Si-O assymetrical stretch of the Class-2/2A spectra are attenuated and transparency features are present. These observations are consistent with the spectral behavior of fine-grained material.

It is possible that samples producing Class-2/2A spectra may be comprised of small clusters of silica spheres having numerous pore spaces between them that are only partially filled by secondary silica precipitation. If the silica spheres were smaller than 74 μm, a Class-2/2A spectrum would be produced. Alternately, these samples may be formed by poorly cemented larger clusters of silica that have fine grains (< 74 μm) clinging to their surfaces. In this case, the shape of the spectrum would be dominated by the spectral behavior of these fine particles (Salisbury and Wald, 1992).

5.4 Implications for remote sensing

Infrared spectroscopy can be used to remotely identify silica phases and investigate their diagenetic history. Michalski et al. (2003) used emission spectra to differentiate between opal, coesite, cristobalite, and tridymite, although distinguishing between opal-A and opal-CT was not possible because the spectra were too similar. When the opal-A spectra from the Taupo Volcanic Zone are compared to the spectra

presented in Michalski et al. (2003), the Class-1 spectra are equivalent to the opal-A/opal-CT spectrum (Fig 5-1). The Class-2/2A spectrum, however, is unique. Until now, a Class-2/2A spectrum has not been available in literature. It is sufficiently distinct from the other silica phases to enable its definitive identification. The discovery of this second type of opal-A spectrum enables a distinction between the silica phases.

This identification of the Class-2/2A opal-A spectrum may also be useful for identifying opal-A on other planets. Based on the spectra collected from crushed material, the Class-2/2A spectrum is produced when the opal-A grains have a diameter of < 74 μm. Particles < 50 μm in size dominate many planetary surfaces (Mustard and Hays, 1997), and the particle size range for dust on Mars is estimated to be ~0.1-10 μm (e.g., Christensen and Moore, 1992). Additionally, many of the larger "particles" in a mature soil on planetary surfaces have been interpreted to be agglomerates of finer particles (Salisbury and Walter, 1989). Until now, spectra from fine grained opal-A material have not been available. Furthermore, since the two bands between 10-12 μm in the Class-2/2A spectrum are due to the bend of the Si-OH bond, this spectral type is indicative of hydrated materials.

5.4.1 The usefulness of band ratios

Perhaps the most intriguing aspect about the reflectance spectra of opal-A is the intensity relationships between the spectral feature located at 8.0, 9.0, 10.12, and 11.37 μm. Within a spectral classes (as defined in section 4.6), there is a linear relationship between the relative intensities of these four spectral features, and

between the classes this relationships changes (Figs. 4-9 to 4-11). As a result, distinction between classes can be accomplished with band ratios. The most useful band ratio is that of the 10.12 μm/11.47 μm pair, which is unique for each class and sub-class.

With the exception of the 9.00 μm/8.00 μm ratio, there was good agreement between the band ratios from the crushed samples and the hand samples and core (Fig. 4-12). At the present time there is no explanation as to why the 9.00 μm/8.00 μm ratio from the crushed material does not fit on the regression line of the hand sample and core data, but the remaining band ratios can be used to identify the physical form of opal-A.

5.5 Tables

Table 5-1 The position of reflectance spectral features between 0.5-2.5 μm correlated with the vibrational movement of the active group.

Reflectance		
Group A (0.5-2.5 μm)	Crushed (0.5-2.5 μm)	Description
0.96	0.95-0.96	H_2O and OH^-
1.15	1.13-1.15	H_2O and OH^-
---[1]	1.20	H_2O and OH^-
1.40	1.34-1.40	OH^- (Isolated)
1.46	1.45-1.46	OH^- (H-Bound)
1.90	1.90	H_2O (Isolated)
1.96	1.95-1.96	H_2O (H-Bound)
2.21	2.20-2.21	Si-OH (Isolated)
2.26	2.25-2.26	Si-OH (H-Bound)

[1] No feature observed

Table 5-2 The position of reflectance spectral features between 2.5-6.0 μm correlated with the vibrational movement of the active group.

Reflectance				
Group A (2.5-19 μm)	Group B (2.5-14 μm)	Cores (2.5-14 μm)	Crushed (2.5-25 μm)	Description
2.72-2.74	2.72-3.01[1]	2.74-2.99[1]	2.72-2.74	Si-OH (Isolated)
2.90-2.92			2.90-2.92	Si-OH (H-Bound)
4.67-4.69	---[2]	---[2]	4.69	Si-O (Ovt./Comb.)
5.01-5.06	5.00-5.01	5.01-5.03	5.01	Si-O (Ovt./Comb.)
5.32-5.33	5.32-5.33	5.32-5.33	5.32	Si-O (Ovt./Comb.)

[1] Two separate features unresolvable due to instrument noise

[2] No feature observed

Table 5-3 The position of reflectance spectral features between 6-25 μm correlated with the vibrational movement of the active group.

Reflectance				
Group A (2.5-19 μm)	Group B (2.5-14 μm)	Cores (2.5-14 μm)	Crushed (2.5-25 μm)	Description
6.11-6.14	6.11-6.12	6.11-6.14	6.12-6.13	Molecular H_2O
6.32-6.44	6.35-6.36	6.35-6.49	6.35-6.39	Molecular H_2O
7.40-7.71	7.35-7.40	7.42-7.51	7.34-7.41	Christensen Freq.
7.95-8.10	7.91-8.06	7.97-8.02	7.89-7.95	Si-O Asy. Stretch
9.00-9.12	8.97-9.08	8.97-9.03	8.97-9.02	Si-O Asy. Stretch
10.04-10.28	10.08-10.14	10.00-10.04	10.10-10.20	Si-OH Bend
11.17-11.60	11.22	11.32-11.42	11.34-11.60	Si-OH SBend
12.11-12.46	12.03-12.34	12.05-12.33	12.05-12.31	Transmission Feat.
12.70-13.46	12.80-13.09	12.89-13.02	12.86-13.09	Transparency Feat.
---[1]	---[1]	---[1]	20.90	Si-O Bend

[1] Outside the spectral range of the instrument

Table 5-4 The position of absorbance spectral features between 2.5-15 μm correlated with the vibrational movement of the active group.

Absorbance	
Crushed (0.5-2.5 μm)	Description
2.76	Si-OH (Isolated)
2.93-2.94	Si-OH (H-Bound)
5.02-5.04	Si-O (Ovt./Comb.)
5.33-5.34	Si-O (Ovt./Comb.)
6.11	Molecular H_2O
8.41	Si-O Stretch
8.99	Si-O Stretch
10.21-10.27	Si-OH Bend (Trough)
10.46	Si-OH Bend (Peak)
11.60-11.74	Si-OH Bend (Trough)
12.45-12.51	Transmission Feat.
14.38	Si-O
14.97	Si-O

5.6 Figures

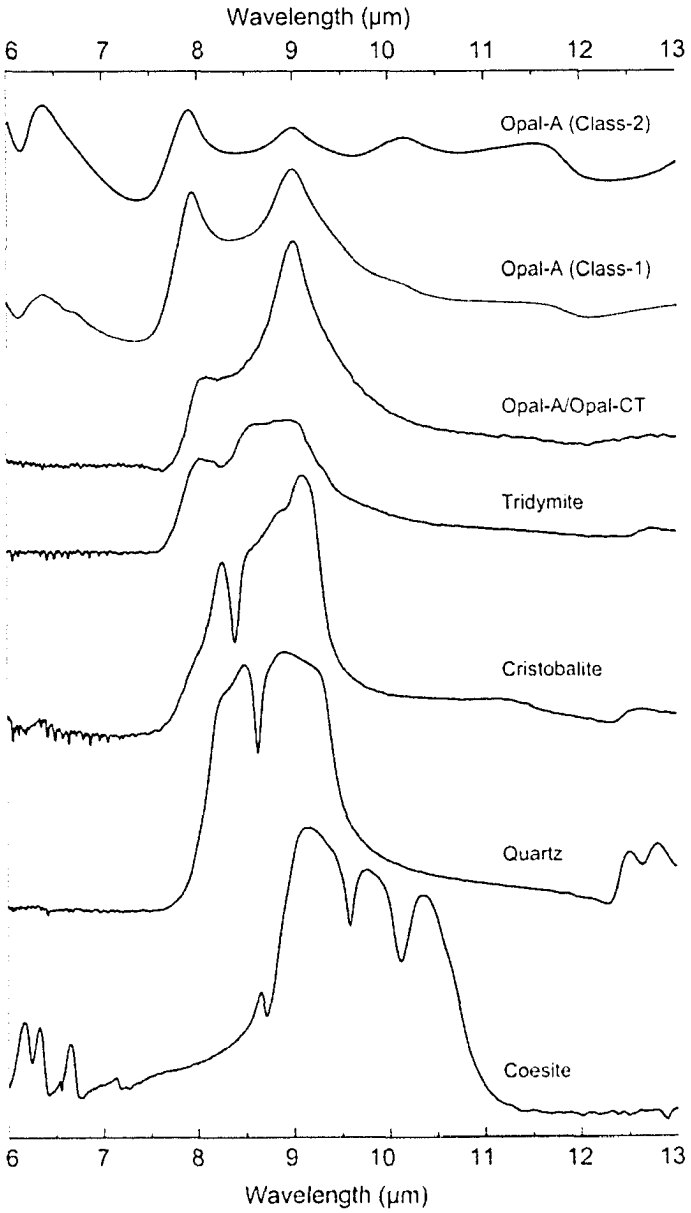

Figure 5-1 Reflectance and emittance spectra from various silica phases. Spectra of coesite, quartz, cristobalite, tridymite and opal-A/opal-CT are from Michalski et al. (2003), and were collected in emission. The Class-1 and Class-2 opal-A spectra are from NZ152 (250-500 μm and 0-74 μm grain fractions, respectively), and were collected in reflectance.

Chapter 6. Conclusion

6.1 The nature of opal-A infrared spectra

Opal-A is an amorphous silica phase that is formed in hydrothermal settings through biological and abiotic means. In a dilute solution, fully hydroxylated SiO_4^{4-} molecules exist in the form of free silanol $Si(OH)_4$, but at higher silica concentrations, polymerization occurs and siloxane bonds (Si-O-Si) form (Coradin and Lopez, 2003). Water that is supersaturated with respect to silica can precipitate amorphous silica directly from hydrothermal fluids abiotically. Alternately, microbes can actively precipitate amorphous silica and produce fabrics that act as templates for additional silica precipitation (Jones et al., 1998).

The reflectance and absorbance spectra of opal-A confirm that opal-A is a hydrated material, consisting of silica that is interspersed with well-ordered, isolated and hydrogen-bound water and hydroxyl. Furthermore, two classes of reflectance spectra (Class-1 and Class-2/2A) were observed for opal-A. The classes are observed between 6-13 μm, and classification was accomplished by examining the features at 6.37, ~8, ~9, 10.00-10.20, and 11.17-11.60 μm. Band ratioing the spectral features at 7.95, 8.00, 10.12, and 11.47 μm shows that the classes are distinct and that there are no intermediate classes. Furthermore, the band ratios can be used for class identification.

Since the spectral classes are essentially identical between 0.5-6.0 μm, the classes relate to the formational and diagenetic history of the samples and not compositional differences. Class-1 spectra were produced by well-consolidated samples with low porosity, whereas the Class-2/2A spectra were produced by poorly-

consolidated materials with high porosity. This suggests that the Class-1 and Class-2/2A spectra identify the degree of secondary silica precipitation that has occurred.

Samples producing Class-1 spectra are composed of fine-grained amorphous silica spheres. These samples are spectrally similar to coarse-grained materials because the pore spaces between the silica spheres have been filled by secondary silica. Samples that produce Class-2/2A spectra are composed of fine-grained amorphous silica spheres without secondary silica infilling. Particle size is one of the fundamental parameters that determines the optical properties of particulate materials and has a very significant effect on reflectance spectra between 6-25 μm (e.g. Lyon, 1964; Vincent and Hunt, 1968; Conel 1969; Logan et al., 1971; Salisbury et al., 1991). The above changes are systematic and are governed by the physical properties of the samples. It is well documented that physical properties such as grain size, porosity, and the degree of consolidation have a dramatic effect on reflectance spectra (e.g. Salisbury et al., 1991).

6.2 Implications for planetary research

Hydrothermal systems have been implicated as possible locations for the origin and evolution of early life, and purely amorphous opal-A and partially crystalline opal-CT are candidate forms of secondary silica on Mars (Michalski et al., 2003). The detection of a Class-2/2A opal-A spectrum on a planetary surface would identify an amorphous material that is poorly consolidated with high porosity. The addition of this spectrum might assist in the search for hot springs on planetary surfaces. Since opal-A can form in the presence of bacteria, it is one of the minerals

of interest in planetary investigations. Its detection on other planets could be consistent with the presence of water and possibly the presence of bacteria.

Bibliography

Aronson, J.R., Emslie, A.G. and McLinden, H.G., 1966. Infrared spectra from particulate surfaces. Science, 152: 345-346.

Aines, R.D. and Rossman, G.R., 1984. Water in minerals? A peak in the infrared. Journal of Geophysical Research, 89(B6): 4,059-4,071.

Bandfield, J.L., Hamilton, V.E. and Christensen, P.R., 2000. A global view of Martian surface compositions from MGS-TES. Science, 287: 1,626-1,630.

Basile, L. J., Ferraro, J. R., LaBonville, P. and Wall, M.C., 1973. A study of force fields for tetrahedral molecules and ions. Coordinated Chemistry Reviews, 11: 21-69.

Bellamy, L.J., 1975. The infra-red spectra of complex molecules. Chapman and Hall, London, 433 pp.

Brown, G.E. and Gibbs, G.V., 1969. Oxygen coordination and the Si-O bond. American Mineralogist, 54: 1,528-1,539.

Browne, P.R.L. and Ellis, A., 1970. The Ohaaki-Broadlands hydrothermal area, New Zealand: mineralogy and related geochemistry. American Journal of Science, 269: 97-131.

Christensen, P.R., Bandfield, J.L., Smith, M.D., Hamilton, V.E. and Clark, R.N., 2000. Identification of a basaltic component on the martian surface from Thermal Emission Spectrometer data. Journal of Geophysical Research, 105: 9,609-9,621.

Christensen, P.R. and Moore, H.J., 1992. The martian surface layer. In: Kieffer, H.H., Jakosky, B.M., Snyder, C.W., Matthews, M.S. (Eds.), Mars. University of

Arizona Press, Tucson, pp. 686–729.

Clark, R.N., 2004. Chapter 2: Spectroscopy of rocks and minerals, and principles of spectroscopy. M.S. Ramsey, P.L. King, G. A Swayze (Editors), In: Infrared Spectroscopy in Geochemistry, Exploration Geochemistry, and Remote Sensing. Mineralogical Association of Canada, London, Ontario, pp. 17-55.

Clark, R.N. and Roush, T.L., 1984. Reflectance spectroscopy: Quantitative analysis techniques for remote sensing applications. Journal of Geophysics Research, 89(B7): 6,329-6,340.

Conel, J.E., 1969. Infrared emissivities of silicates: Experimental results and a cloudy atmosphere model of spectral emission from condensed particulate mediums. Journal of Geophysical Research, 74: 1,614-1,623.

Cooper, B.L., Salisbury, J.W., Killen, R.M. and Potter, A.E., 2002. Mid-infrared spectral features of rocks and their powders. Journal of Geophysical Research, 107(E4): 1-19.

Coradin, T. and Lopez, P.J., 2003. Biogenic silica patterning: Simple chemistry or subtle biology? ChemBioChem, 3: 1-9.

Dijkstra, T.W., Duchateau, R., van Santen, R.A., Meetsma, A. and Yap, G.P.A., 2002. Silsesquioxane models for geminal silica surface silanol sites: A spectroscopic investigation of different types of silanols. Journal of American Chemical Society, 124: 9,856-9,864.

Feynman, 1963. The Feynman Lectures on Physics, Vol I, Addison Wesley, Reading MA.

Flörke, O.W., 1972. Transport and deposition of SiO_2 with H_2O under supercritical conditions. Kristal und Technik, 7: 159-166.

Flynn, G.J., Henning, T., Keller, L.P. and Mutschke, H., 2002. Infrared spectroscopy of cosmic dust. In: G. Videen & M. Kocifaj (Eds.). Optics of Cosmic Dust. Dordrecht, The Netherlands: Kluwer Academic Publishers, 37-56 pp.

Gibbs, G.V., 1982. Molecules as models for bonding in silicates. American Mineralogist, 67: 421-450.

Goryniuk, M.C., Rivard, B.A. and Jones, B., 2004. The reflectance spectra of opal-A (0.5–25 μm) from the Taupo Volcanic Zone: Spectra that may identify hydrothermal systems on planetary surfaces. Geophysical Research Letters, 31: L24701, doi:10.1029/2004GL021481

Hamilton, V.E, Wyatt, M.B., McSween, H.Y. and Christensen, P.R., 2001. Analysis of terrestrial and martian volcanic compositions using thermal emission spectroscopy: II. Applications to martian surface spectra from MGS TES. Journal of Geophysical Research, 106: 14,733-14,746.

Head, J.W., Hiesinger, H., Ivanov, M.A., Kreslavsky, M.A., Pratt, S. and Thomson, B.J., 1999. Possible ancient oceans on Mars: Evidence from Mars orbiter laser altimeter data. Science, 286: 2,134-2,137.

Hunt, G.R., 1977. Spectral signatures of particulate materials in the visible and near infrared. Geophysics, 42(3): 501-513.

Hunt, G.R. and Salisbury, J.W., 1970. Visible and near-infrared spectra of minerals and rocks: I. Silicate minerals. Modern Geology, 1: 283-300.

Hunt, G.R., Salisbury, J.W. and Lenhoff, C.J., 1973. Visible and near-infrared spectra of minerals and rocks: VI. Additional silicates. Modern Geology, 4: 85-106.

Jones, B. and Renaut, R.W., 2003. Petrography and genesis of spicular and columnar geyserite from the Whakarewarewa and Orakeikorako geothermal areas, North Island, New Zealand. Canadian Journal of Earth Science, 40: 1,585-1,610.

Jones, B. and Renaut, R.W., 2004. Water content of opal-A: Implications for the origin of laminae in geyserite and sinter. Journal of Sedimentary Research, 74(1): 117-128.

Jones, J.B. and Segnit, E.R., 1971. The nature of opal: Opal nomenclature and constituent phases. Geological Society of Australia, 8(1): 57-68.

Jones, B., Renaut, R.W. and Rosen, M.R., 1998. Microbial biofacies in hot-spring sinters: A model based on Ohaaki Pool, North Island, New Zealand. Journal of Sedimentary Research, 68(3): 413-434.

Jones, B., Renaut, R.W. and Rosen, M.R., 2001. Biogenicity of gold- and silver-bearing siliceous sinters forming in hot (75°C) anaerobic spring-waters of Champagne Pool, Waiotapu, North Island, New Zealand. Journal of the Geological Society, 158: 895-911.

Keller, W.D. and Pickett, E.E., 1949. Absorption of infrared radiation by powdered silica minerals. American Mineralogist, 34: 855-868.

Langer, K. and Flörke, O.W., 1974. Near infrared absorption spectra (4000-9000 cm^{-1}) of opals and the role of "water" in these SiO_2*nH_2O minerals. Fortschritte der Mineralogie, 52: 17-51.

Logan, L.M., Hunt, G.R., Salisbury, J.W. and Balsamo, S.R., 1973. Compositional implications of Christiansen frequency maximums for infrared remote sensing applications. Journal of Geophysical Research, 78(23): 4,983-5,003.

Lynne, B.Y. and Campbell, K.A., 2004. Morphologic and mineralogic transformations from opal-A to opal-CT in low-temperature siliceous sinter diagenesis, Taupo Volcanic Zone, New Zealand. Journal of Sedimentary Research, 74(4): 561-579.

Lyon, R.J.P., 1964. Evaluation of infrared spectrophotometry for compositional analysis of lunar and planetary soils. Part II: Rough and powdered surfaces. NASA-CF-100, Washington, D.C., 262 pp.

Lyon, R.J.P., 1967. Chapter 8: Infrared absorption spectra. In: J. Zussman (Editor), Physical methods in determinative mineralogy. Academic Press, London, England, pp. 371-403.

Mahon, W.A.J. and Finlayson, J.B., 1972. The chemistry of the Broadlands geothermal area New Zealand. American Journal of Science, 272: 48-68.

McDonald, R.S., 1958. Surface functionality of amorphous silica by infrared spectroscopy. Journal of Physical Chemistry, 62: 1,168-1,178.

McSween, H.Y.J., 2002. The rocks of Mars, from far and near. Meteoritics and Planetary Science, 37: 7-25.

Michalski, J.R., Kraft, M.D., Diedrich, T., Sharp, T.G. and Christensen, P.R., 2003. Thermal emission spectroscopy of the silica polymorphs and consideration for remote sensing of Mars. Geophysical Research Letters, 30(19): 2008, doi:10.1029/2003GL018354.

Milkey, R.G., 1960. Infrared spectra of some tectosilicates. American Mineralogist, 45: 990-1007.

Moenke, H.H.W., 1974. Chapter 16: Silica, the three dimensional silicates, borosilicates and beryllium silicates. In: V.C. Farmer (Editor), The infrared spectra of minerals. Mineralogical Society (Great Britain), London, pp. 365-382.

Mustard, J.F. and Hays, J.E., 1997. Effects of hyperfine particles on reflectance spectra from 0.3 to 25 μm. Icarus, 125: 145-163.

Nakamoto, K., 1970. Infrared spectra of inorganic and coordination compounds. John Wiley and Sons, New York, 448 pp.

Pauling, L., 1980. The nature of the silicon-oxygen bond. American Mineralogist, 65: 321-323.

Ryskin, Y.I., 1974. Chapter 9: The vibration of protons in minerals: hydroxyl, water and ammonium. In: V.C. Farmer (Editor), The infrared spectra of minerals. Mineralogical Society (Great Britain), London, pp. 137-181.

Salisbury J.W. and Eastes, J. W., 1985. The effect of particle size and porosity on spectral contrast in the Mid-Infrared. Icarus, 64: 586-588.

Salisbury, J.W. and Wald, A., 1992. The role of volume scattering in reducing spectral contrast of Reststrahlen bands in spectra of powdered materials. Icarus, 96: 121-128.

Salisbury, J.W. and Walter, L.S., 1989. Thermal infrared (2.5-13.5 μm) spectroscopic remote sensing of igneous rock types on particulate planetary surfaces. Journal of Geophysical Research, 98: 9,192-9,202.

Salisbury, J.W., Hapke, B. and Eastes, J. W., 1987. Usefulness of weak bands in midinfrared remote sensing of particulate planetary surfaces. Journal of Geophysical Research, 92(B1): 702-710.

Salisbury, J.W., Wald, A. and D'Aria, D.M., 1994. Thermal-infrared remote sensing and Kirchhoff's law: 1. Laboratory measurements. Journal of Geophysical Research, 99(B6): 11,897-11,911.

Salisbury, J.W., Walter, L.S., Vergo, N. and D'Aria, D.M., 1991. Infrared (2.1-25 micrometers) Spectra of Minerals. Johns Hopkins University Press, Baltimore, MD., 249 pp.

Socrates, G., 1980. Infrared characteristics of group frequencies. John Wiley & Sons, Ltd., Bristol, 153 pp.

Walter, L.S. and Salisbury, J.W., 1989. Spectral Characterization of igneous rocks in the 9- to 12-μm region. Journal of Geophysical Research, 94(B7): 9,203-9,213.

White, R.B. and Minser, D.G., 1984. Ramen spectra and structure of natural glasses. Journal of Non-Crystalline Solids, 67: 45-59.

Wyatt, M.B. and McSween, H.Y., 2001. An alternative hypothesis for basalt and andesite on Mars: Global surface compositions from MGS-TES. Meteoritics and Planetary Science, 36(Supplement): A226.

Appendix A:

The reflectance spectra of opal-A (0.5–25 μm) from the Taupo Volcanic Zone: Spectra that may identify hydrothermal systems on planetary surfaces

The reflectance spectra of opal-A (0.5–25 μm) from the Taupo Volcanic Zone: Spectra that may identify hydrothermal systems on planetary surfaces

Michelle C. Goryniuk, Benoit A. Rivard, and Brian Jones

Department of Earth and Atmospheric Sciences, University of Alberta, Edmonton, Alberta, Canada

Received 13 September 2004; accepted 26 October 2004; published 16 December 2004.

[1] Opal-A, the main component of siliceous sinters in many terrestrial hydrothermal systems, is a hydrated silicate that commonly incorporates silicified microorganisms. The detection of opal-A on the surface of Mars, therefore, may carry important implications in the search for extraterrestrial life. Sinters from the discharge apron of Ohaaki Pool (North Island, New Zealand) yielded reflectance spectra (wavelengths between 0.5–25 μm) that indicate the presence of absorbed water, trapped water, and silanol in opal-A. Two classes (1 and 2) of reflectance spectra were detected between the wavelengths of 6–13 μm. The Class-1 spectrum is similar to existing opal spectra, and was collected from well-consolidated samples that had low porosity. The Class-2 spectrum is unique when compared to the spectra of other silica polymorphs, and was collected from poorly consolidated samples that had high porosity. *INDEX TERMS:* 3934 Mineral Physics: Optical, infrared, and Raman spectroscopy; 5460 Planetology: Solid Surface Planets: Physical properties of materials; 5464 Planetology: Solid Surface Planets: Remote sensing; 6225 Planetology: Solar System Objects: Mars. **Citation:** Goryniuk, M. C., B. A. Rivard, and B. Jones (2004), The reflectance spectra of opal-A (0.5–25 μm) from the Taupo Volcanic Zone: Spectra that may identify hydrothermal systems on planetary surfaces, *Geophys. Res. Lett.*, *31*, L24701, doi:10.1029/2004GL021481.

1. Introduction

[2] Opal-A ($SiO_2.nH_2O$), which is composed of silica spheres 1500–3000 Å in diameter [*Rodgers et al.*, 2004], is a hydrated silica (1–15.6 wt. % H_2O) characterized by silanol (OH attached to Si), absorbed water attached to silanol, and/or water that is trapped between the silica beads [*Jones and Renaut*, 2004]. Opal-A is the dominant component of siliceous sinters that are found on the discharge aprons around modern geysers and hot springs. Such sinters commonly contain numerous microorganisms that have been replaced and encrusted by opal-A [*Jones et al.*, 1998]. Thus, detection of opal-A on any planetary surface, including Mars, may carry important implications in the search for extraterrestrial life.

[3] *Michalski et al.* [2003] showed that silica polymorphs (opal, tridymite, cristobalite, quartz and coesite) are spectrally distinguishable at high resolutions. It is difficult, however, to differentiate between the opaline phases (opal-A, opal-CT, opal-C) because they are spectrally similar. The main theme of this paper is the discovery of two classes of opal-A spectral signatures, one that resembles the opal-A spectrum presented by *Michalski et al.* [2003], and another spectrum that is distinct from other silica polymorphs, which has not been previously documented. The discovery of this new opal-A spectrum is significant because it came from opal-A deposits that have high porosity. If identified on the surface of Mars, the spectrum would indicate the presence of opal-A that has not been exposed to extensive secondary silica precipitation.

0094-8276/04/2004GL021481$05.00

2. Materials and Methods

2.1. Site Description

[4] Samples of siliceous sinter were collected from the discharge apron around Ohaaki Pool (~45 m long and ~15 wide), which is located in the Taupo Volcanic Zone on the North Island of New Zealand [*Jones et al.*, 1998]. The sinters were precipitated from discharged alkaline Na-HCO_3-Cl dilute spring waters at 95°C [*Mahon and Finlayson*, 1972]. Mineralogy was confirmed by x-ray diffraction of powdered cavity mounts using a Rigaku rotating anode-diffractometer, and by SEM analysis of the morphology of the precipitates [*Jones et al.*, 1998].

2.2. Description of Samples

[5] Four hand samples (NZ152, NZ313, NZ341, and NZ413) and 10 cores were examined. NZ313 and NZ341 were poorly consolidated and characterized by visible porosity. NZ152 was a more consolidated sample and showed no visible porosity. The basal part of NZ413 was consolidated, whereas the upper part was formed of less consolidated and more porous material. The cores are characterized by thin horizontal laminations (1–5 mm thick), which are the result of biotic and abiotic processes [*Jones et al.*, 1998; *Jones and Renaut*, 2004].

2.3. Instrumentation Setup

[6] Bidirectional reflectance measurements from the wavelengths between 2.5–22 μm were collected from cut and natural surfaces of hand samples using a Bomen MB102 Fourier transform infrared (FTIR) spectrometer. Using a globar light source, and a viewing angle of 35°, measurements were collected at a resolution of 16 cm^{-1}, with a field of view of approximately 4 × 4 mm. The measurements were collected from flat surfaces along continuous linear transects. Thirty-two scans (for one spectrum) were made in each location, then the sample was moved ~5 mm and another measurement was taken. The same samples were also analyzed using the ASD field spec FR, which collected reflectance spectra from 0.4–2.5 μm.

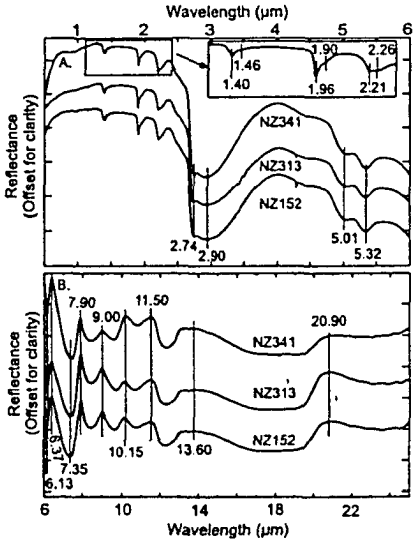

Figure 1. The spectral features of opal-A documented between the wavelengths of 0.5–6 μm (a), and 6–25 μm (b), collected from samples NZ152, NZ313, and NZ341, grain size faction <74 μm. Measurements were collected using a UV-VIS-NIR Bidirectional Spectrometer (0.32–1.8 μm) and a Nicolet Nexus 870 FT-IR Spectrometer (1.8–26 μm).

[7] Analyses of loose crushed material were carried out at the Reflectance Experiment Laboratory (RELAB) at Brown University, Rhode Island, using a UV-VIS-NIR Bidirectional Spectrometer (0.32–1.8 μm, incidence/emergence angles at 30° and 0°) and a Nicolet Nexus 870 FT-IR Spectrometer (1.8–26 μm).

3. Results and Discussion

3.1. Band Assignment

3.1.1. Spectral Features in the Range of 0.5–7.0 μm

[8] The major spectral features of opal-A, related to the presence of OH and H_2O, are located at 1.40, 1.46, 1.90, 1.96, 2.21, 2.26, 2.74, 2.90, 5.01, 5.32, 6.13, and 6.37 μm (Figure 1a and Table 1) [*Langer and Florke*, 1974; *Hunt*, 1977; *Salisbury et al.*, 1991a, 1991b; *Dijkstra et al.*, 2002].

[9] Sharp troughs at 1.40 and 1.90 μm are consistent with isolated H_2O and OH that exist in similar positions in the crystalline environment. Troughs at 1.46 and 1.96 μm are assigned to H-bound H_2O and OH. At 2.21 and 2.74 μm, and at 2.26 and 2.90 μm, are the stretching and bending modes of isolated and H-bound silanol, respectively. Troughs at 5.01 and 5.32 μm are assigned to the overtones of H_2O and OH whereas the trough at 6.13 μm and the peak at 6.37 μm are due to isolated molecular H_2O.

[10] These observations are consistent with the model of *Langer and Florke* [1974] and *Adams et al.* [1991] where H_2O is found trapped as isolated molecules free from H-bonding and as liquid water in which the molecules are hydrogen bonded to other H_2O molecules. This model also includes the presence of –OH bonded to silicon either interacting with water on the surface, or protected from interaction with water [*Frondel*, 1982].

3.1.2. Spectral Features in the Range of 7–25 μm

[11] For opal-A, the major spectral features at 7.90, 9.00, 10.15, 11.50, 13.60, and 20.90 μm (Figure 1b and Table 1), are related to the fundamental vibrational frequencies of the Si-O stretch and bend [*McDonald*, 1958; *Lyon*, 1967; *Salisbury and Walter*, 1989].

[12] The Christiansen Feature (CF) for opal-A is located at 7.35 μm. The CF for silicates commonly falls between 7.5–9 μm [*Salisbury et al.*, 1991b], but can go as low as 7.35 for the silica polymorphs [*Michalski et al.*, 2003]. The Reststrahlen band at 7.90 μm, which is positioned at a shorter wavelength than any Reststrahlen band observed in other silica phases [*Hunt and Salisbury*, 1970; *Hunt et al.*, 1973], could be the result of a shorter Si-O bond length, and a larger Si-O-Si angle than that of quartz [*Gibbs*, 1982; *Pauling*, 1980; *Smith and Bailey*, 1963]. The Reststrahlen band at 9.00 μm is characteristic of the major bands for tectosilicates, which typically occur at wavelengths close to 9.1 μm.

[13] Two peaks at 10.15 and 11.50 μm are attributed to the Si-O stretch of the Si-O bond of the terminal oxygens of silanol [*Moenke*, 1974], and the peak at 10.15 μm is a common feature in spectra for diatoms and other types of opaline silica [*Sun*, 1962; *Chester and Elderfield*, 1968; *Moenke*, 1974]. The amplitude of the peak at 11.50 μm varies directly with the amplitude of the band at 10.15 μm, and therefore can also be attributed to silanol. Although these two features have been observed in the spectra of silicates that have been subjected to vigorous grinding [*Takamura et al.*, 1964], we know of no other study describing the presence of these two features in spectra from natural surfaces.

[14] The transparency feature at 13.60 μm, and a single Si-O-Si bending vibration is located at 20.90 μm, with the

Table 1. The Position of Spectral Features for NZ152 Between 0.5–25 μm (Grain Size 0–74 μm), Correlated With the Vibrational Movement of the Active Molecule

λ (μm)	Vibrational Movement	Active Molecule
1.40	Overtone of–OH stretch	H_2O and OH^-[a,b,c]
1.46	Overtone of–OH stretch	OH^-[d]
1.90	–OH stretch, H-O-H bend	Isolated H_2O[a,b,c]
1.96	–OH stretch	H-Bound H_2O[d]
2.21	–OH stretch, Si–OH bend	Isolated Si-OH[a,c]
2.26	–OH stretch, Si–OH bend	H-bound Si-OH[a,c]
2.74	–OH stretch (sym.)	Isolated Si-OH[e]
2.90	–OH stretch (asym.)	H-bound Si-OH[e]
5.01	Overtone (H_2O, OH^-)	H_2O, OH^-[f]
5.32	Overtone (H_2O, OH^-)	H_2O, OH^-[f]
6.13	H-O-H bend	H_2O[a]
7.35	Christensen Frequency	—[f]
7.90	Si-O stretch (asym.)	Si-O-Si[f,g]
9.00	Si-O stretch (asym.)	Si-O-Si[h]
10.15	Si-O stretch	Isolated Si-OH[h]
11.50	Si-O stretch	H-Bound Si-OH[h]
13.60	Transparency Features	—[g]
20.90	Si-O-Si bend (asym.)	Si-O-Si[i]

[a] *Aines and Rossman* [1984].
[b] *Hunt* [1977].
[c] *McDonald* [1958].
[d] *Langer and Florke* [1974].
[e] *Dijkstra et al.* [2002].
[f] *Salisbury et al.* [1991b].
[g] *Salisbury and Walter* [1989].
[h] *Moenke* [1974].
[i] *Milkey* [1960].

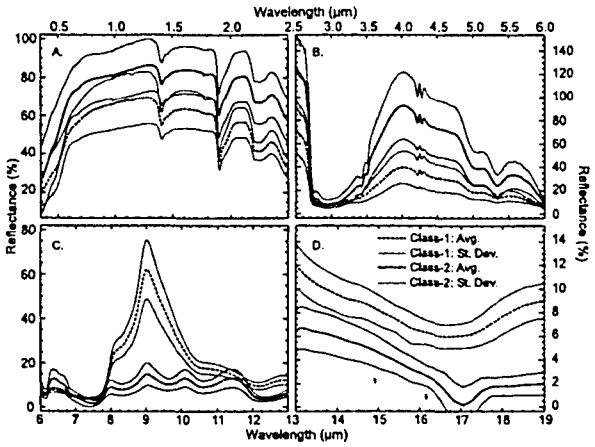

Figure 2. The average Class-1 and Class-2 spectra from NZ152, NZ313, NZ341, and NZ413, between 0.5–2.5 μm (a), 2.5–6.0 μm (b), 6.0–13.0 μm (c), 13.0–19.0 μm (d). Spectra were manually placed into a class, and then an average and standard deviation were calculated for each of the classes. Measurements were collected using an ASD Fieldspec (0.1–2.5 μm), and a Bomen MB102 FTIR (2.5–22 μm).

shape of this last feature being consistent with poorly ordered material [*Milkey*, 1960].

3.2. Two Spectral Classes

[15] Between the wavelengths of 6–13 μm, two classes of spectra (Class 1 and 2) were observed in hand samples, cores, and crushed materials (Figure 2c). The two classes were characterized by changes in the relative intensities of the bands at 6.37, 7.90, 9.00, 10.15, and 11.37 μm, and by the amplitude of the entire spectrum between 6–13 μm. The two classes were not distinguishable below 6 μm, however Class-1 spectra, on average, had lower amplitudes than Class-2 (Figures 2a and 2b).

[16] Class-1 spectra have a weak peak at 6.37 μm, strong peaks at 7.90 and 9.00 μm, absent or very weak peaks between 10–12 μm, and a spectrum with large amplitude. Class-2 spectra have a strong peak at 6.37 μm, weaker peaks at 7.90 and 9.00 μm, two moderate peaks between 10–12 μm, and a spectrum with low amplitude. Among 77 spectra that were collected from four hand samples, 12 were Class-1 spectra, and 65 were Class-2.

3.3. Effect of Physical Properties on Reflectance Spectra

[17] The two classes of opal-A spectra, first collected from whole and uncrushed hands samples, probably reflect differences in physical properties, such as grain size and porosity, relating to the amount of silica cement precipitated in the pore spaces. To test this, three hand samples (NZ152, NZ313, NZ341) and one core sample (OP7) were crushed to three different grain sizes (0–74 μm, 74–250 μm, and 250–500 μm). *Hunt* [1977] and *Salisbury et al.* [1991a] have extensively documented the effects that grain size and porosity have on reflectance spectra.

[18] Uncrushed hand samples of well consolidated material with low porosity (NZ152 and OP7) produced Class-1 spectra. These samples were well consolidated and had low porosity because silica cement had filled the pore spaces between the silica spheres. After crushing, grain size factions >74 μm yielded Class-1 spectra, whereas grain size factions <74 μm produced Class-2 spectra (Figure 3).

[19] Uncrushed hand samples of poorly consolidated material with high porosity (NZ313 and NZ341) produced Class-2 spectra. These samples were poorly consolidated and had high porosity because there was only a small amount of silica cement holding the spheres together but not filling the pore spaces. These samples continued to produce Class-2 spectra when crushed, irrespective of grain size.

[20] Crushing of the well consolidated samples had no effect on the spectra until the grains were <74 μm, when they became optically thin, whereas the poorly consolidated samples consisted of poorly cemented silica spheres (smaller than <74 μm), and crushing had little effect on the bulk of the material. *Conel* [1969] and *Salisbury and Eastes* [1985] argued that attenuation of the Reststrahlen bands for fine-grained material was due to particle size and only indirectly (but critically) to porosity. The comparison of the peaks at 7.90 and 9.00 μm in Class-1 (Figure 2c), compared to those in Class-2 show this attenuation.

4. Relevance for Mars Exploration

[21] The thermal emission spectrum of opal-A presented by *Michalski et al.* [2003] corresponds to the Class-1 opal-A spectrum presented herein. The Class-2 opal-A spectrum, which has been collected from natural surfaces and relates to poorly consolidated opal-A, is currently not included in the deconvolution of Martian surface spectra. Because distinguishing between the opaline phases is difficult spectrally, the addition of the Class-2 opal-A spectrum, which is distinct and unique, may assist in the identification of hydrothermal systems on the surface of Mars.

5. Conclusions

[22] A detailed study of the spectral properties of opal-A from the Ohaaki Pool spring system has provided the following conclusions:

[23] • "OH" exists as isolated and H-bonded H_2O molecules, and as isolated or H-bonded silanol.

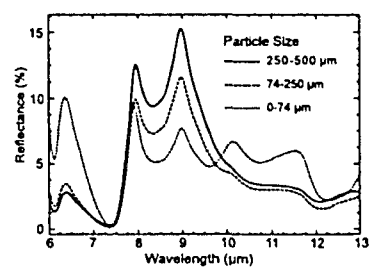

Figure 3. Three spectra from NZ152 between the wavelengths of 6–13 μm, from three grain size factions (0–74 μm, 74–250 μm, and 250–500 μm). Measurements were collected using a Nicolet Nexus 870 FT-IR Spectrometer (1.8–26 μm).

Appendix B:

The reflectance spectra from the hand samples and cores

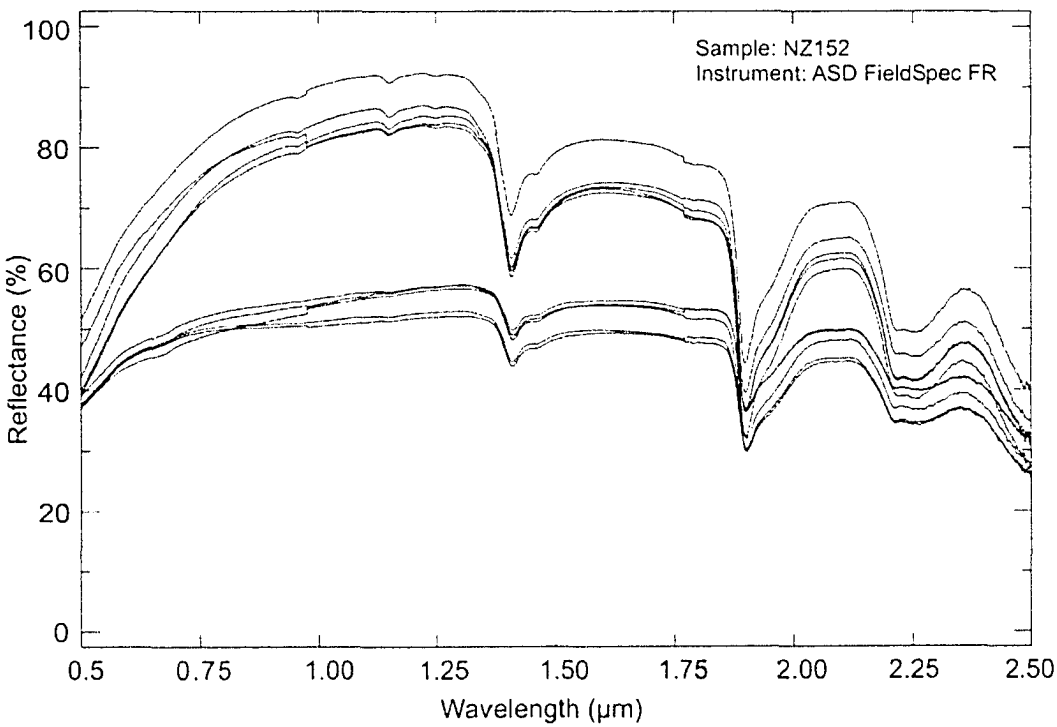

Figure 1. Reflectance spectra from NZ152 between 0.5-2.5 μm.

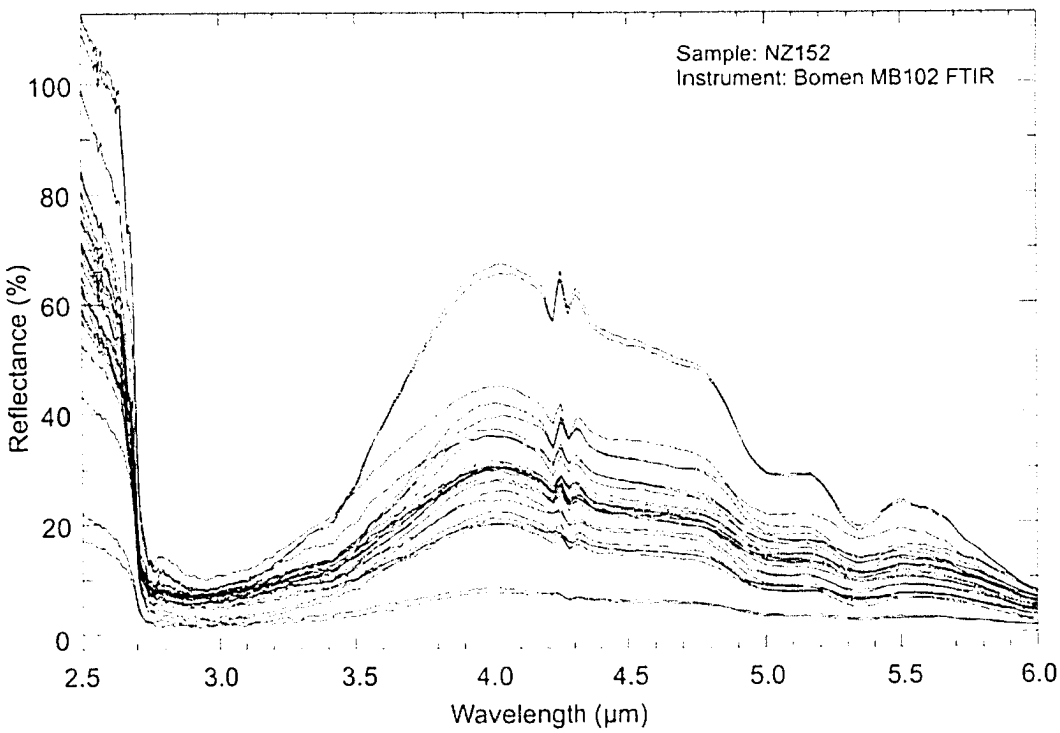

Figure 2. Reflectance spectra from NZ152 between 2.5-6.0 μm.

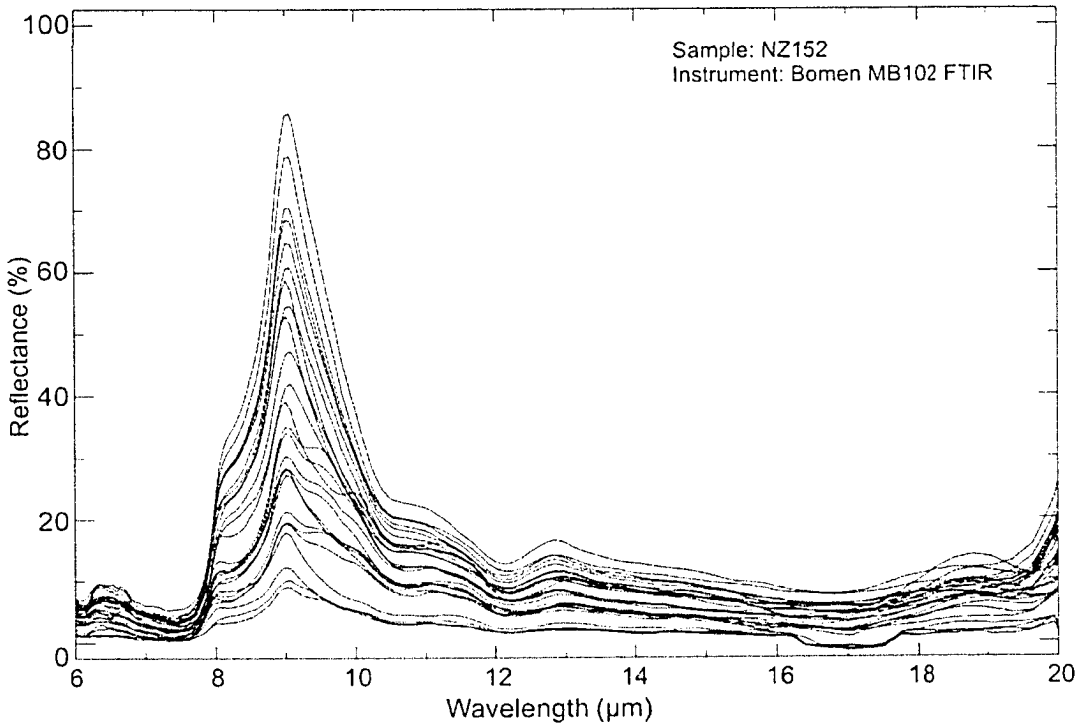

Figure 3. Reflectance spectra from NZ152 between 6-20 μm.

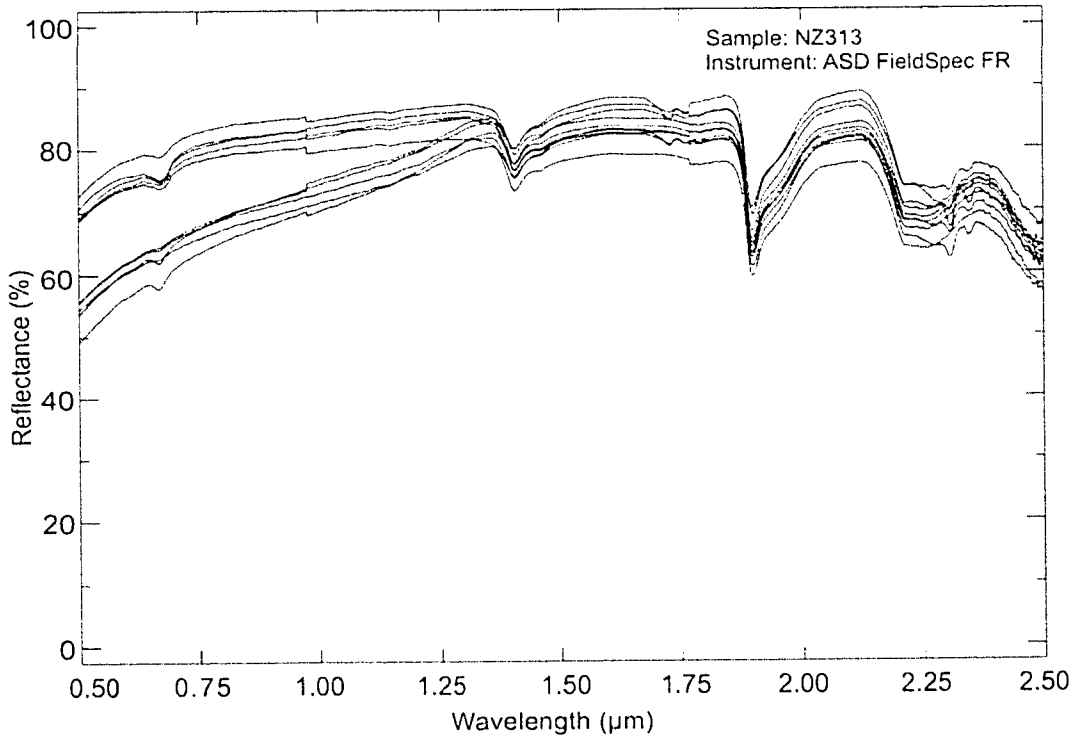

Figure 4. Reflectance spectra from NZ313 between 0.5-2.5 μm.

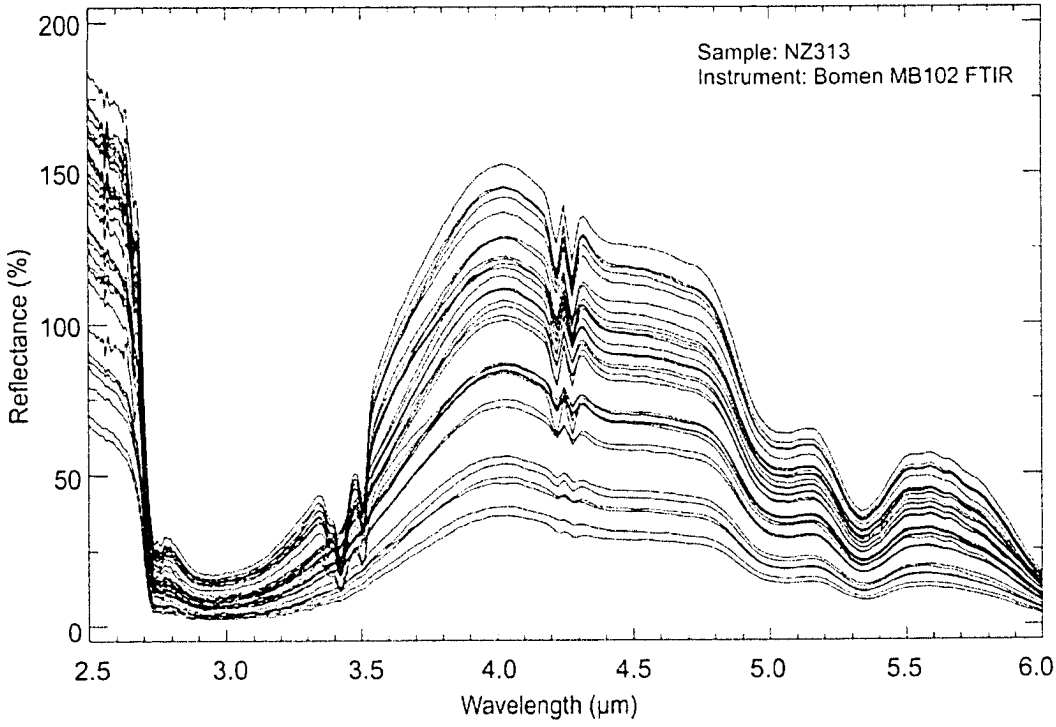

Figure 5. Reflectance spectra from NZ313 between 2.5-6.0 µm.

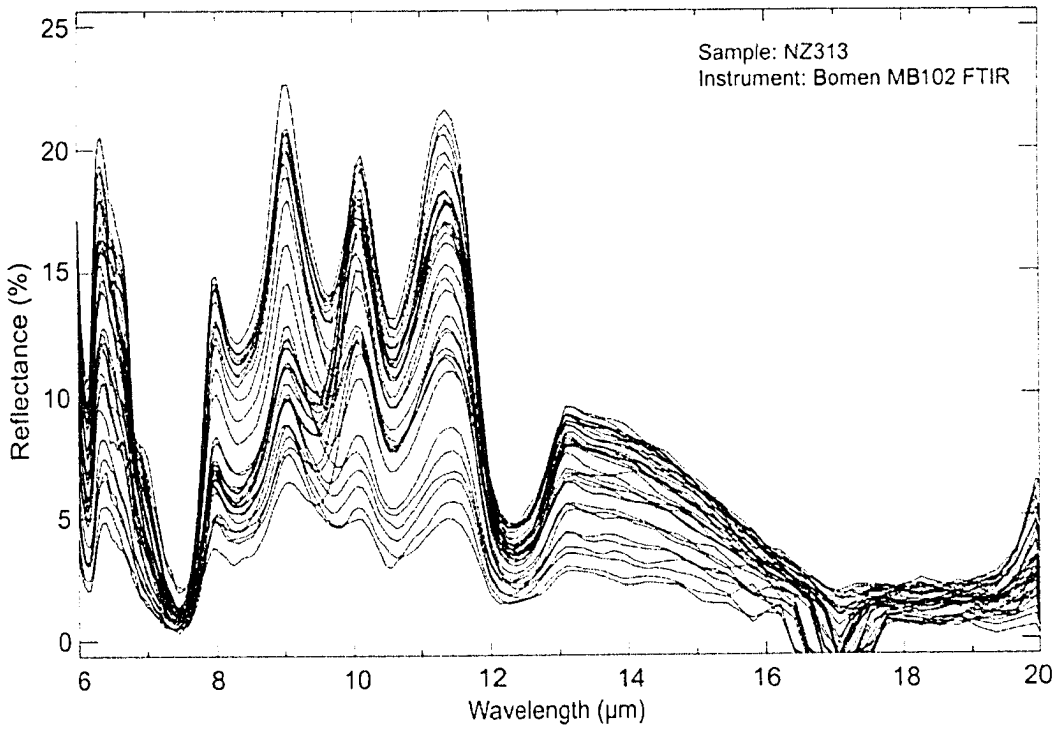

Figure 6. Reflectance spectra from NZ313 between 6-20 μm.

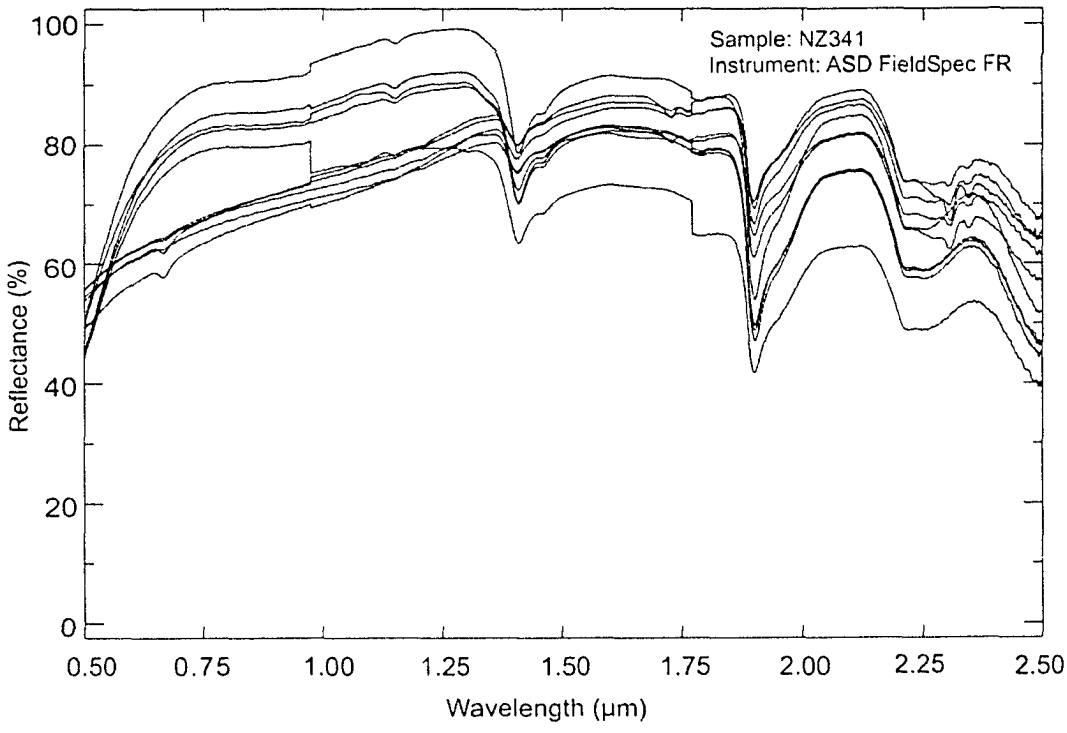

Figure 7. Reflectance spectra from NZ341 between 0.5-2.5 μm.

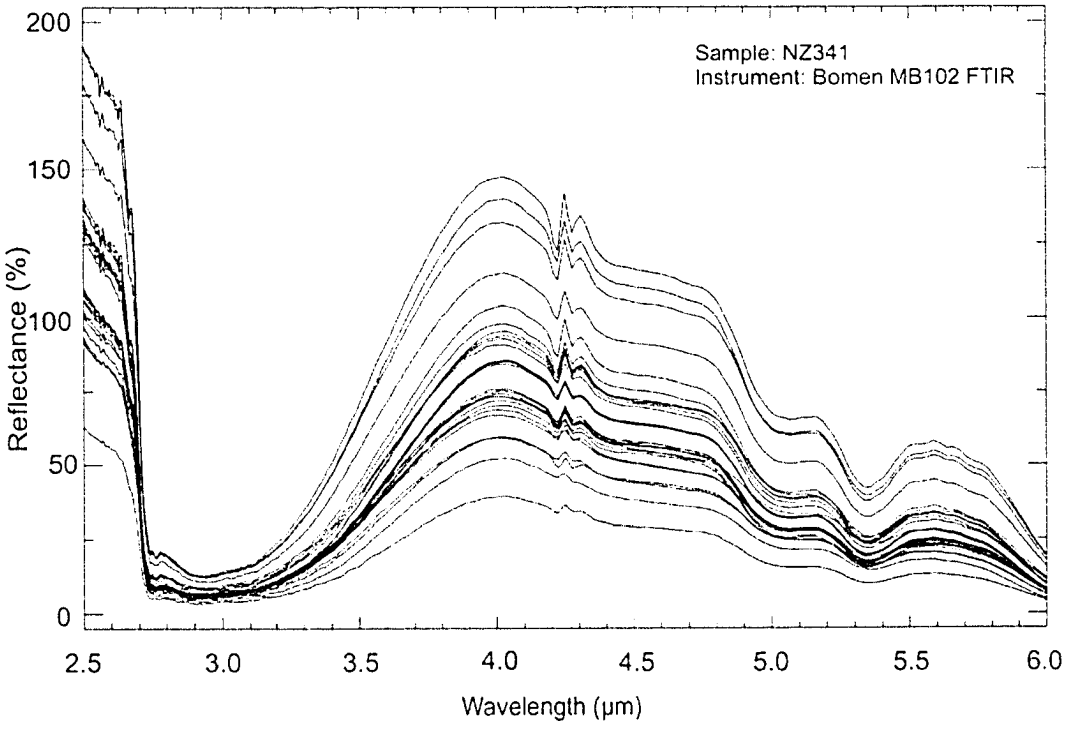

Figure 8. Reflectance spectra from NZ341 between 2.5-6.0 µm.

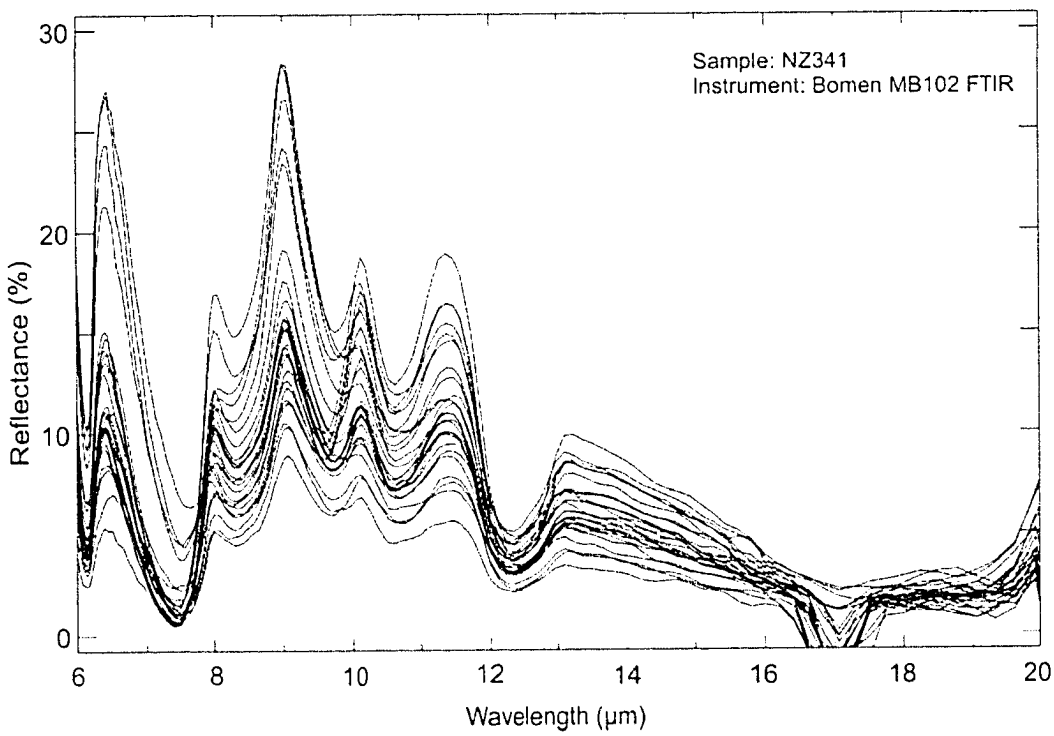

Figure 9. Reflectance spectra from NZ341 between 6-20 μm.

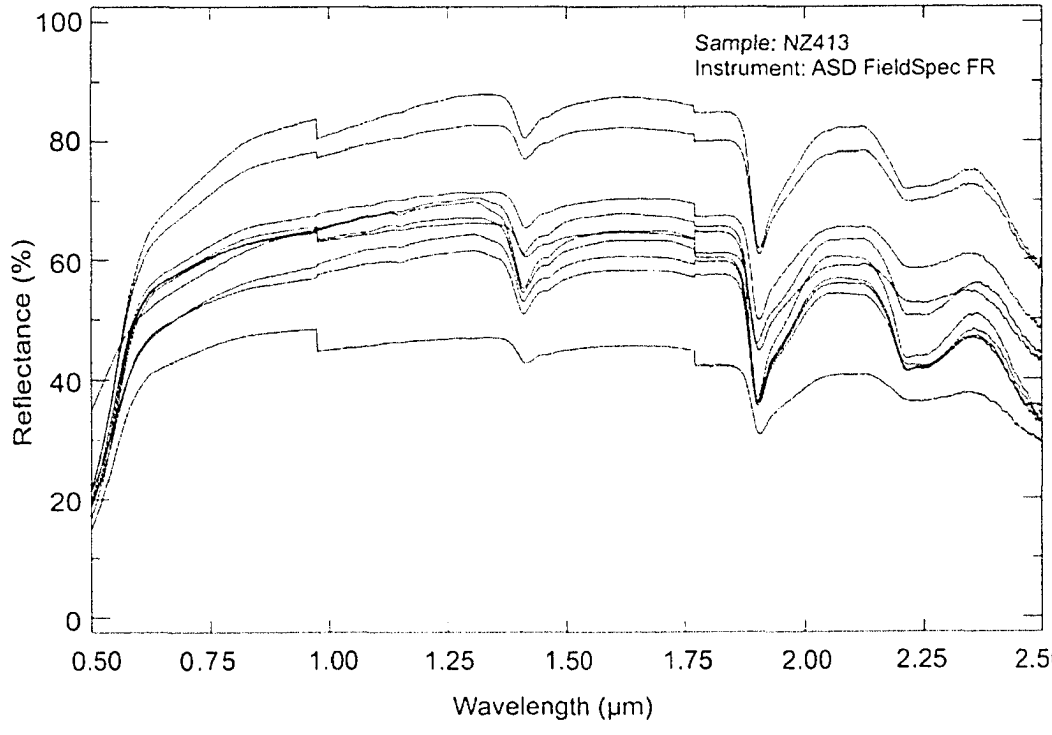

Figure 10. Reflectance spectra from NZ413 between 0.5-2.5 μm.

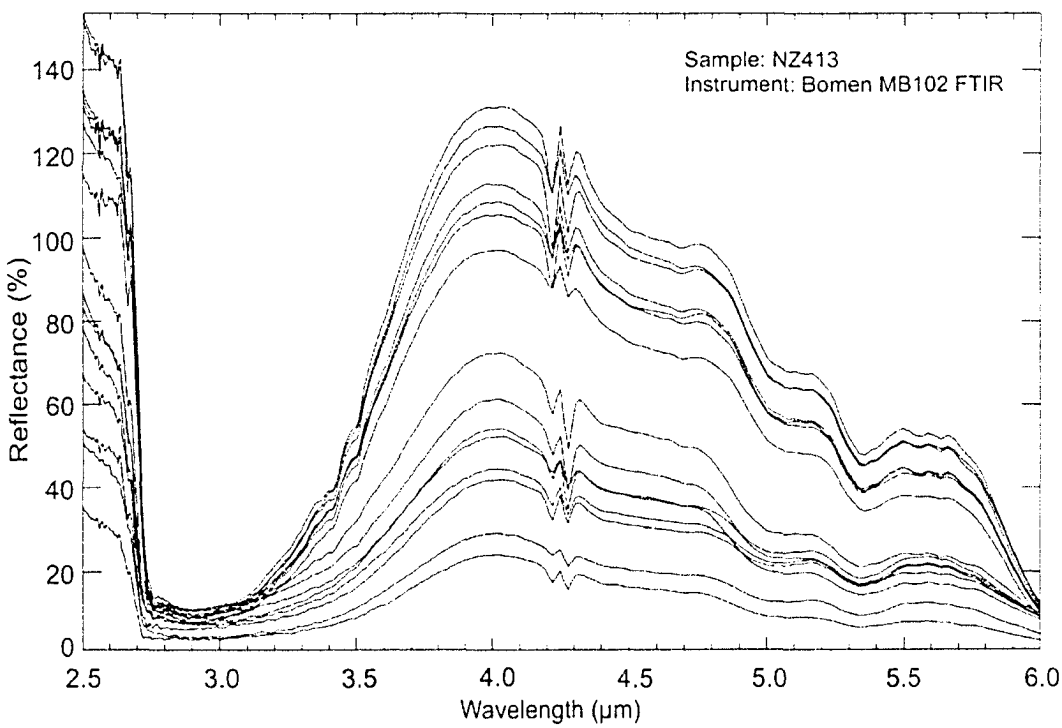

Figure 11. Reflectance spectra from NZ413 between 2.5-6.0 µm.

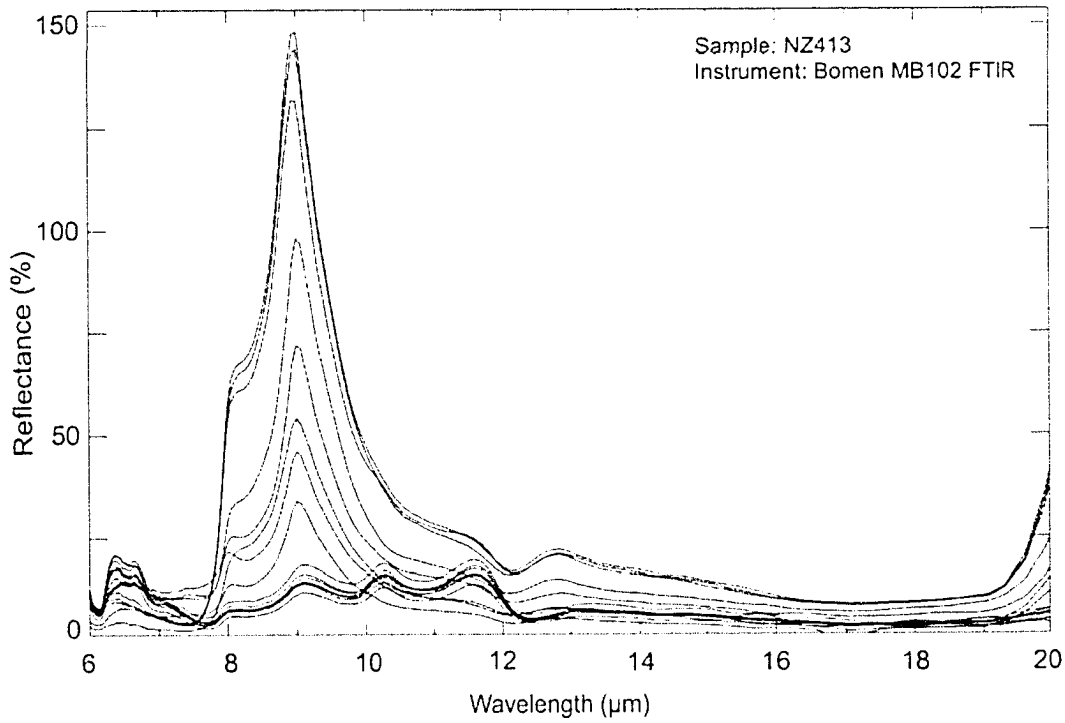

Figure 12. Reflectance spectra from NZ413 between 6-20 μm.

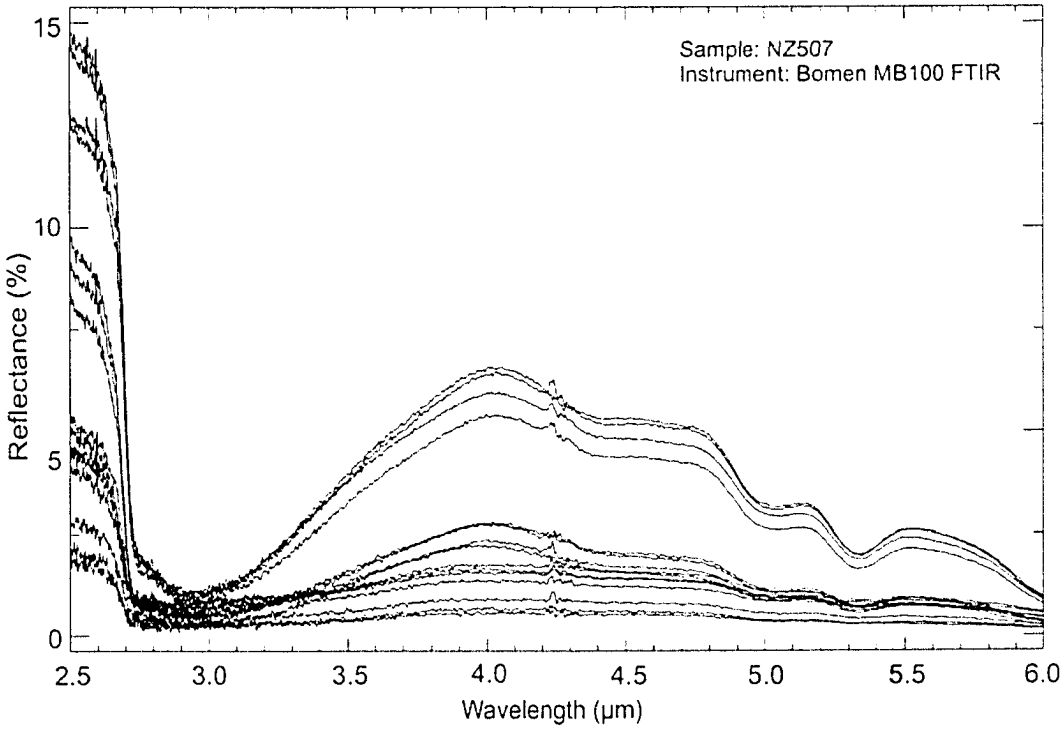

Figure 13. Reflectance spectra from NZ507 between 2.5-6.0 μm.

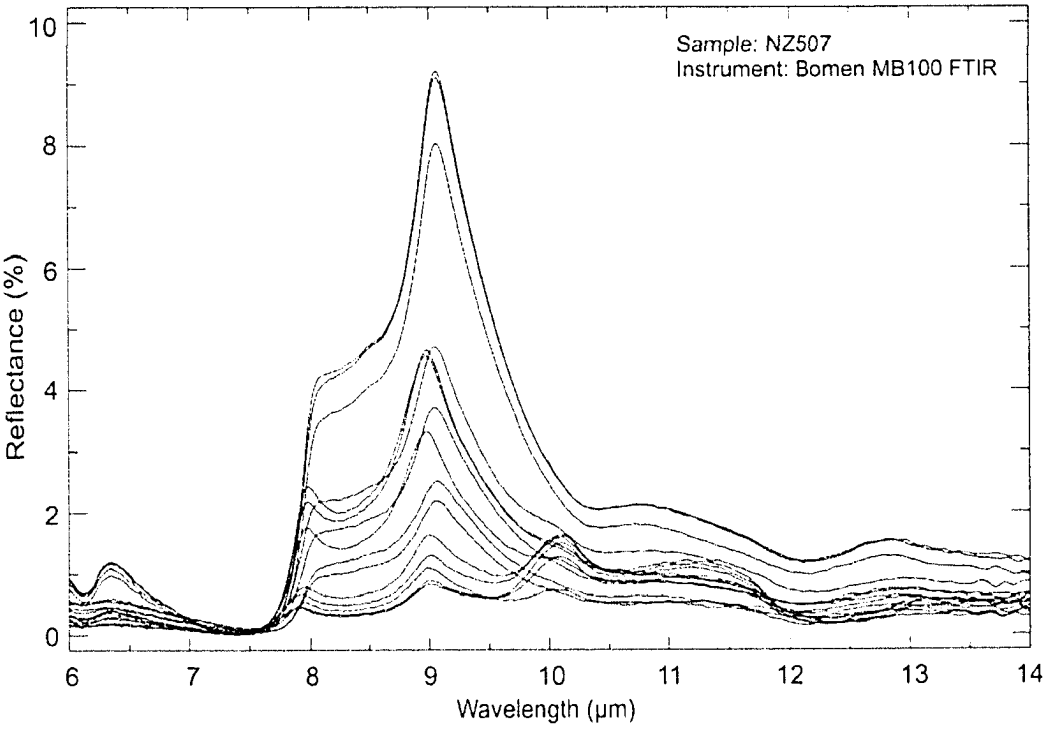

Figure 14. Reflectance spectra from NZ507 between 6-14 μm.

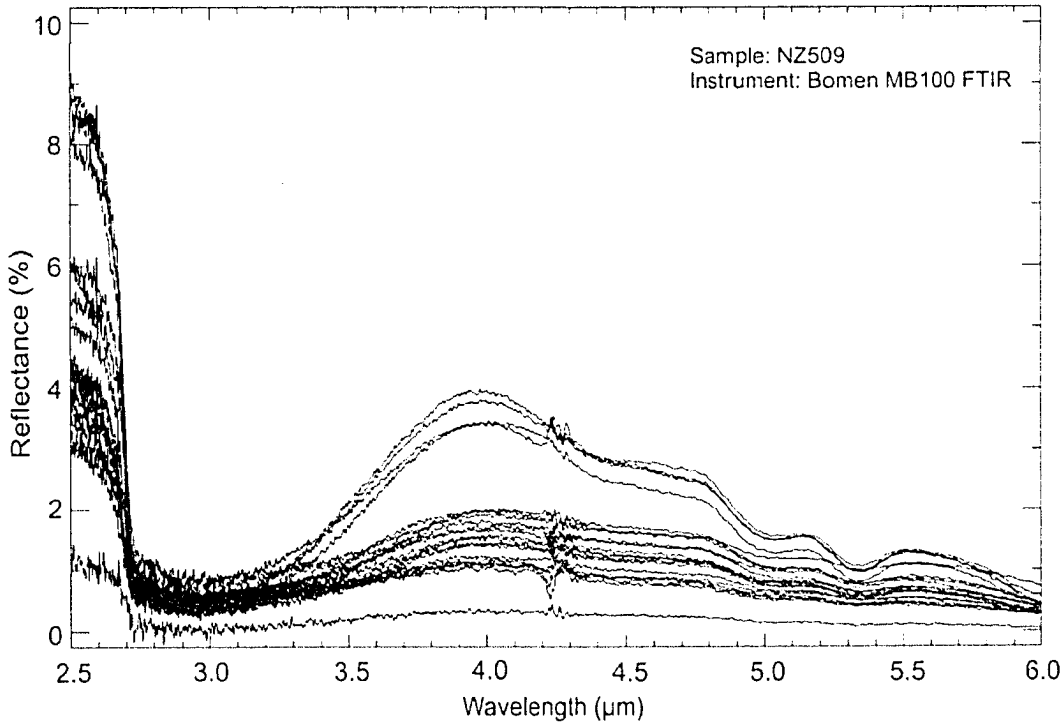

Figure 15. Reflectance spectra from NZ509 between 2.5-6.0 μm.

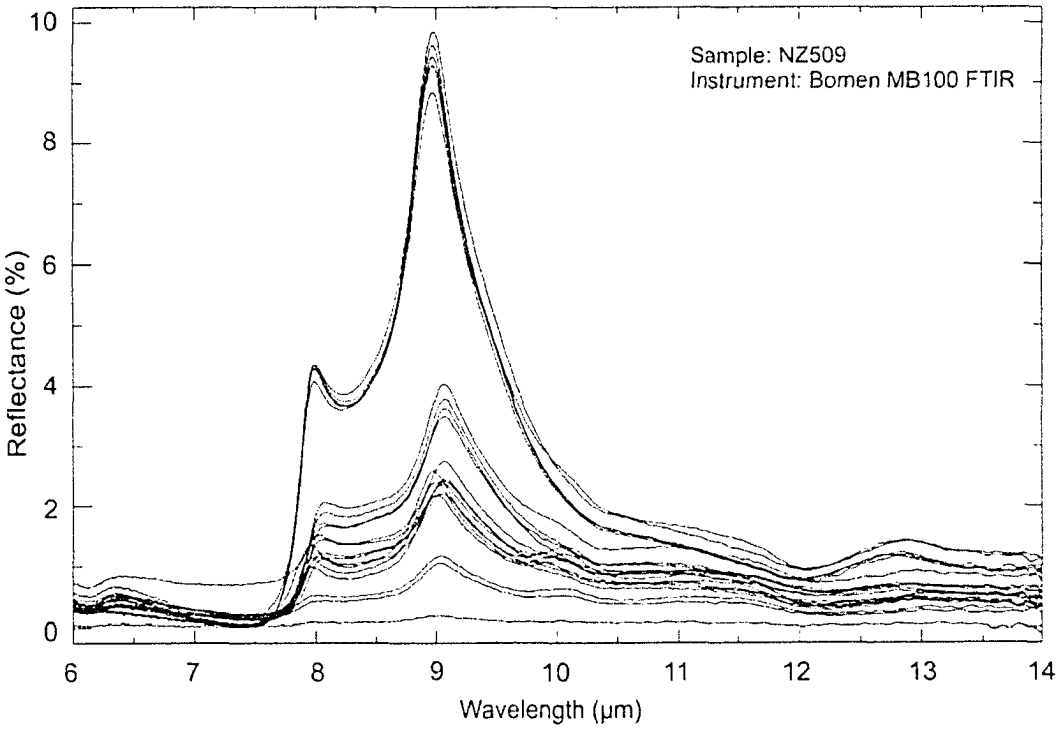

Figure 16. Reflectance spectra from NZ509 between 6-14 μm.

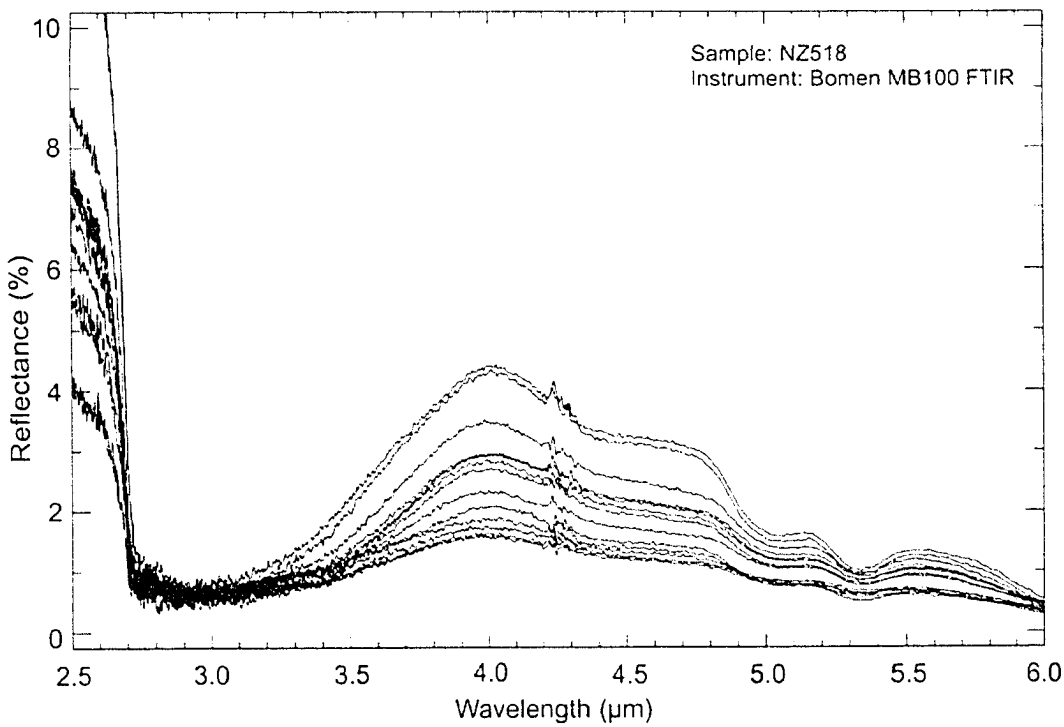

Figure 17. Reflectance spectra from NZ518 between 2.5-6.0 μm.

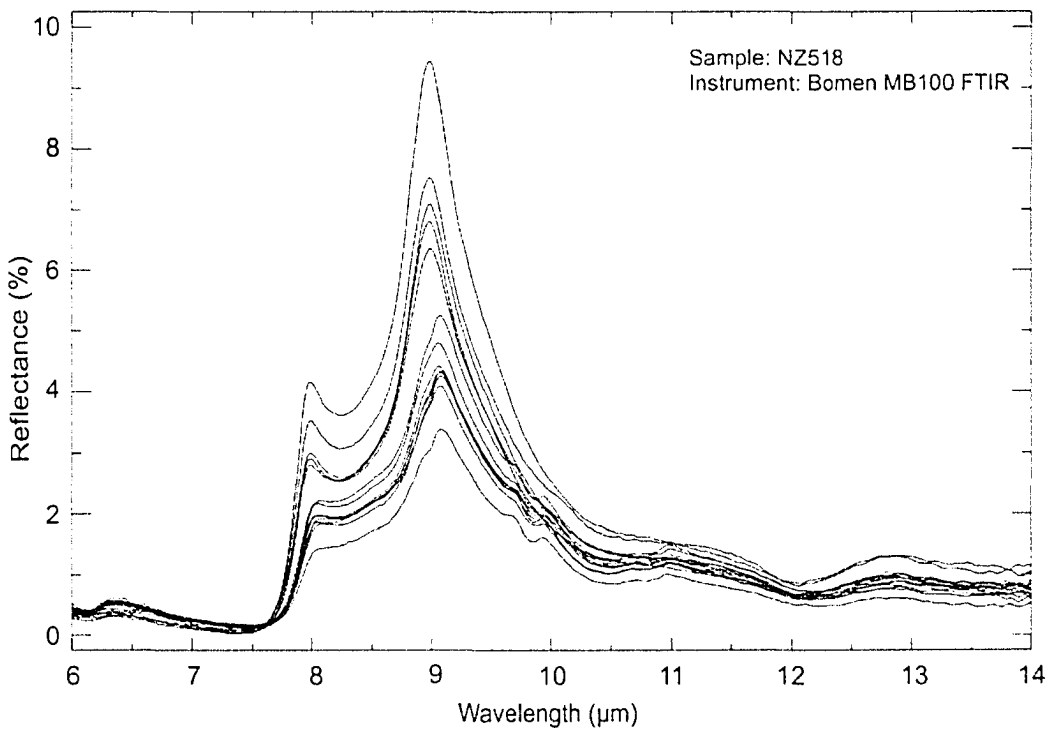

Figure 18. Reflectance spectra from NZ518 between 6-14 μm.

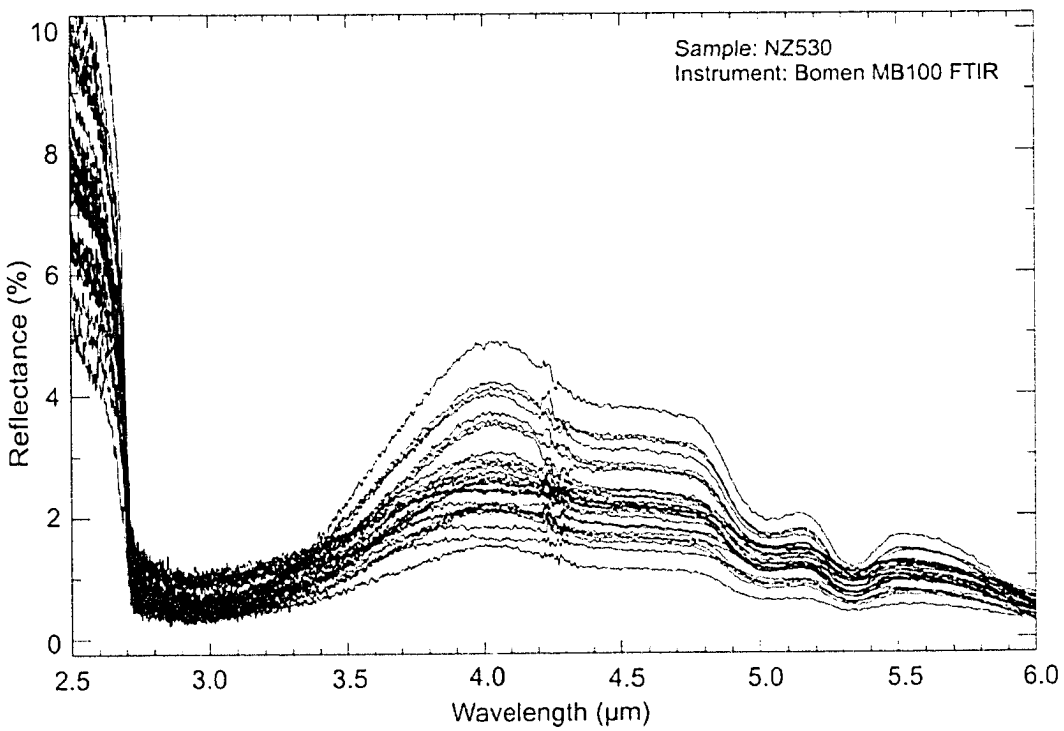

Figure 19. Reflectance spectra from NZ530 between 2.5-6.0 μm.

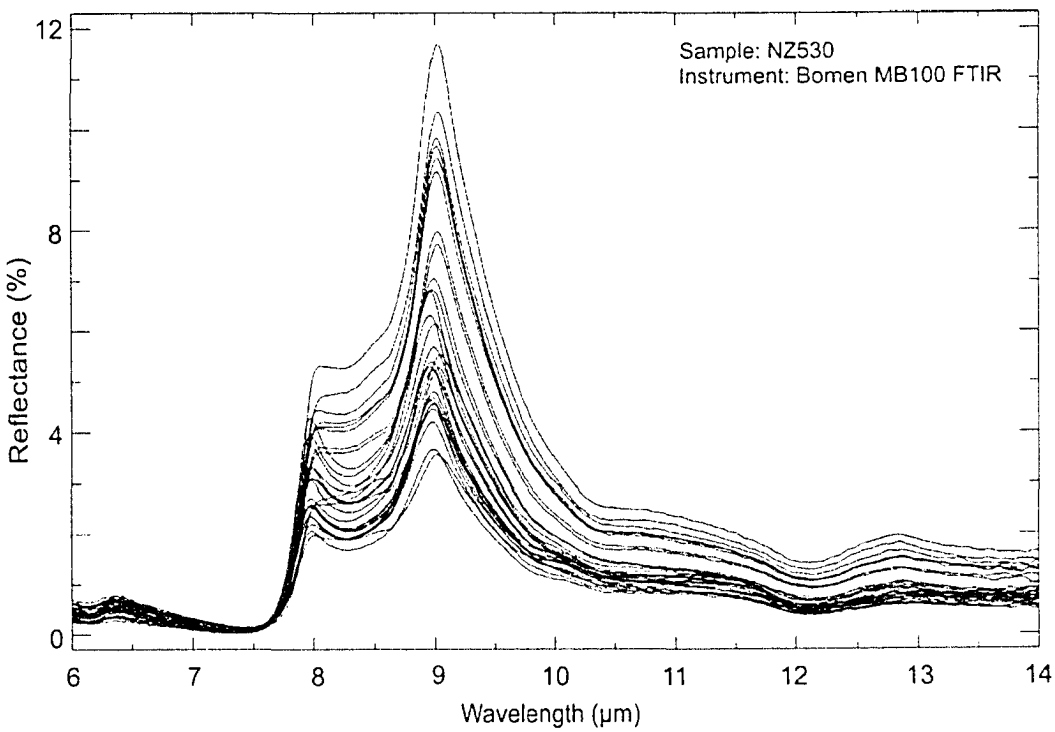

Figure 20. Reflectance spectra from NZ530 between 6-14 µm.

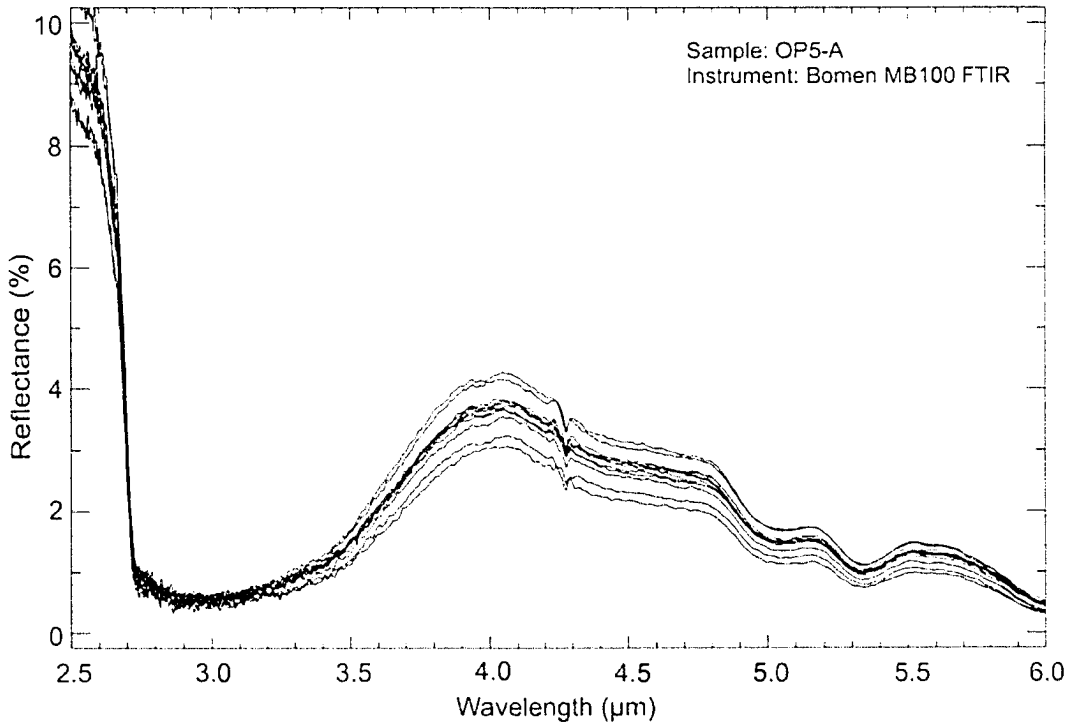

Figure 21. Reflectance spectra from OP5-A between 2.5-6.0 μm.

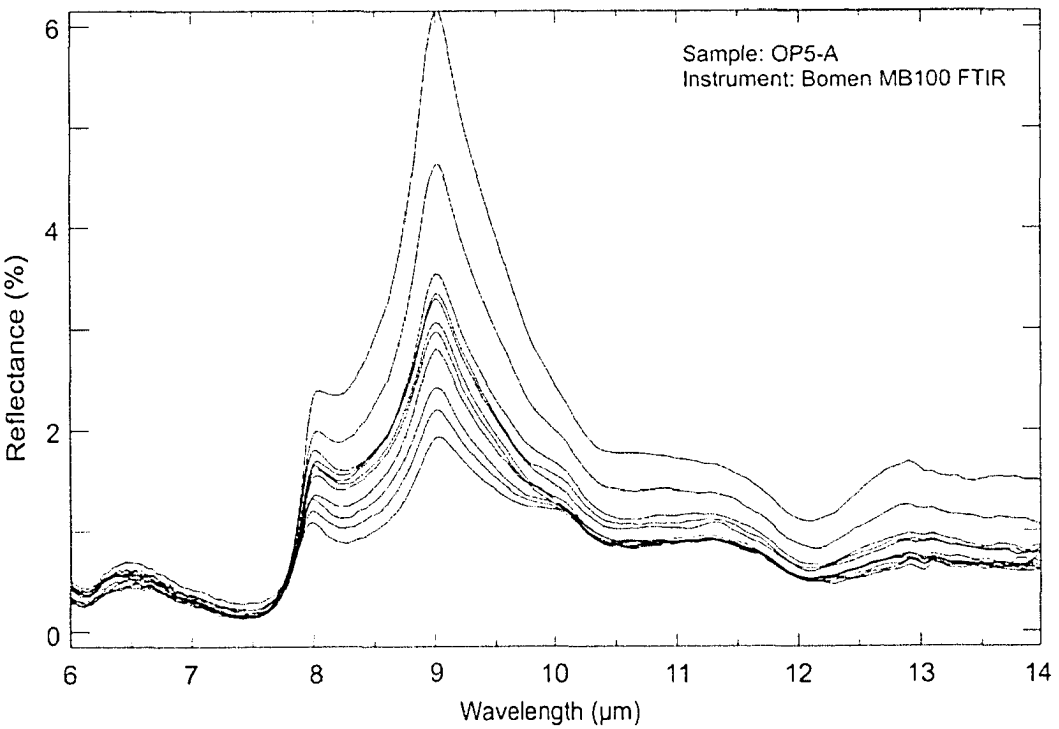

Figure 22. Reflectance spectra from OP5-A between 6-14 μm.

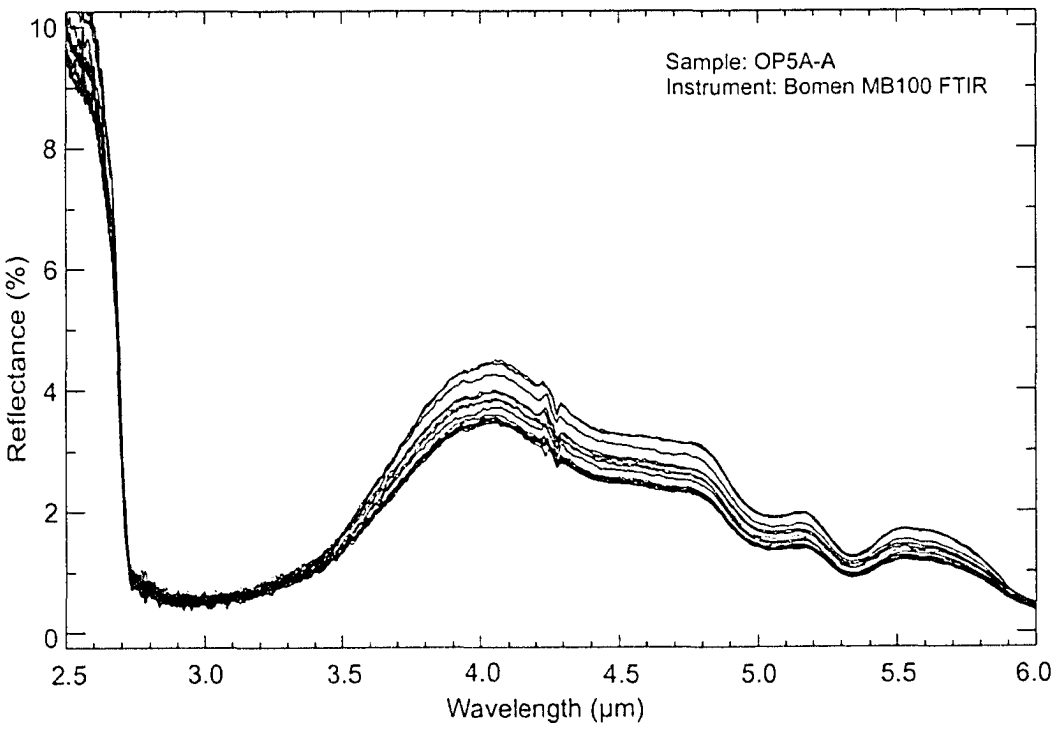

Figure 23. Reflectance spectra from OP5A-A between 2.5-6.0 μm

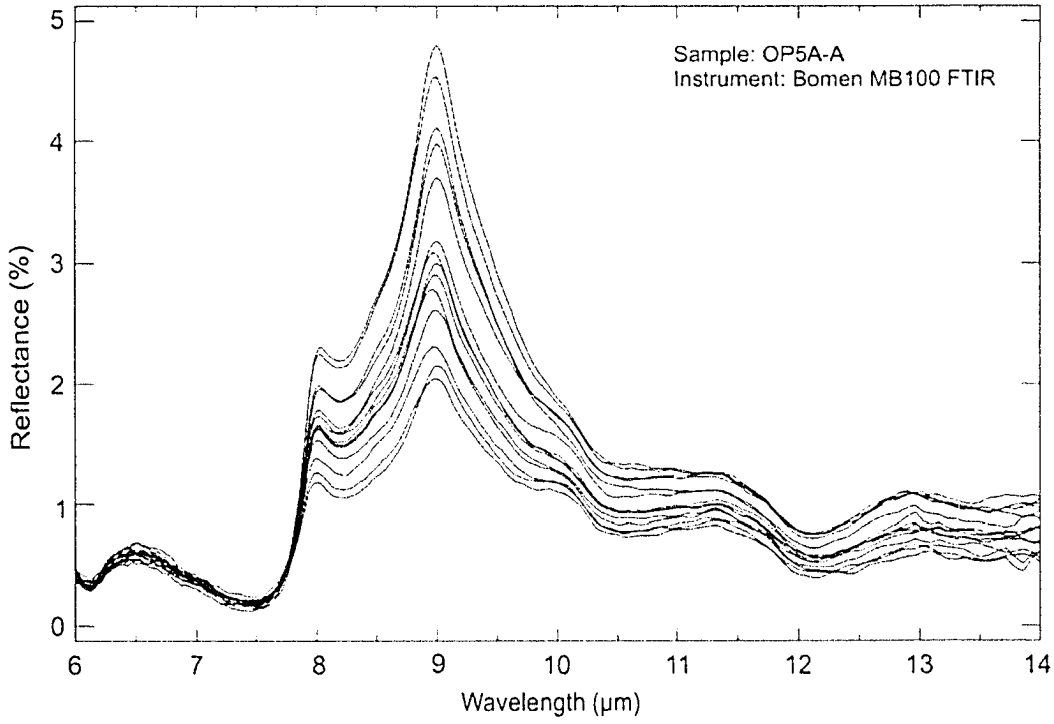

Figure 24. Reflectance spectra from OP5A-A between 6-14 μm.

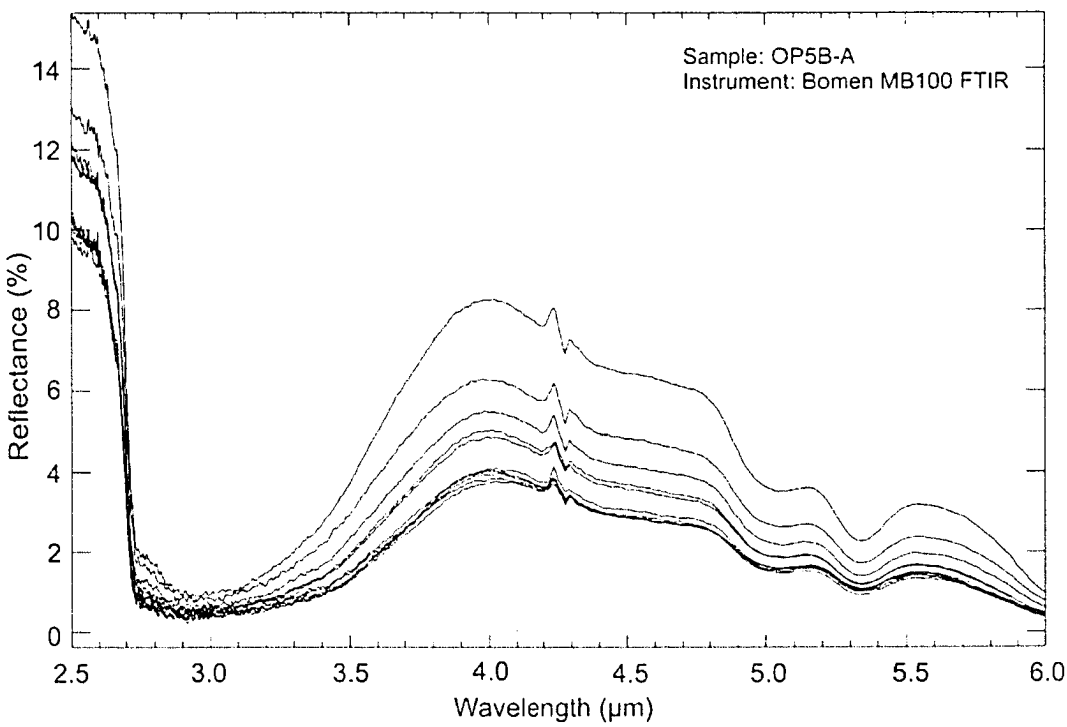

Figure 25. Reflectance spectra from OP5B-A between 2.5-6.0 μm.

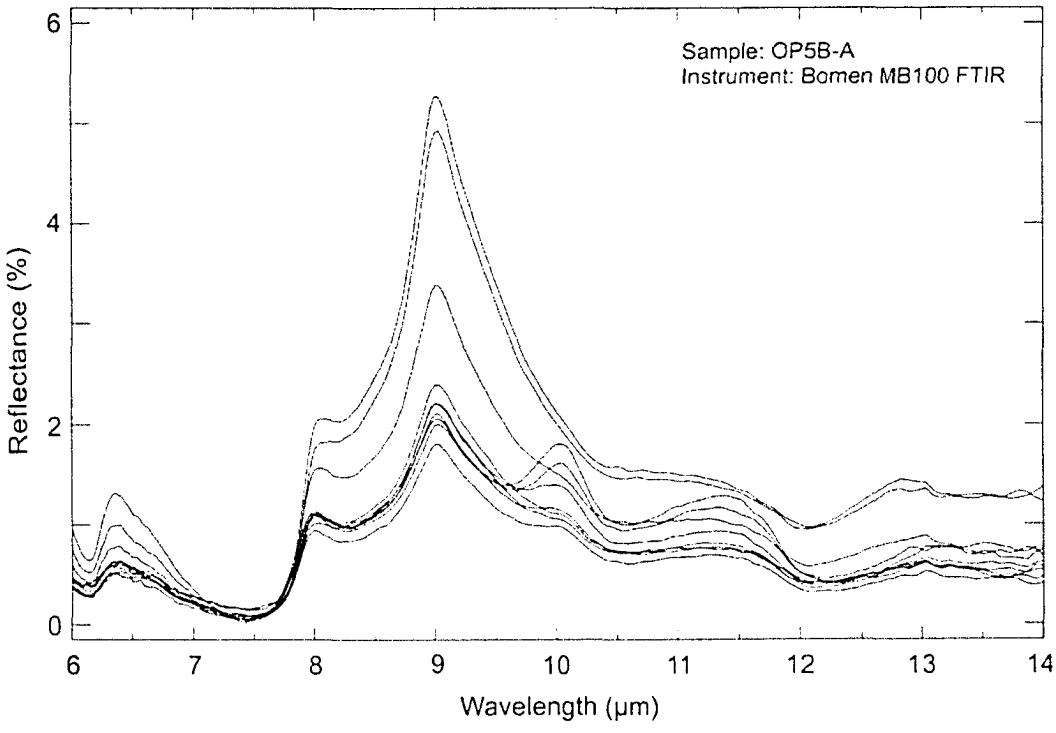

Figure 26. Reflectance spectra from OP5B-A between 6-14 μm.

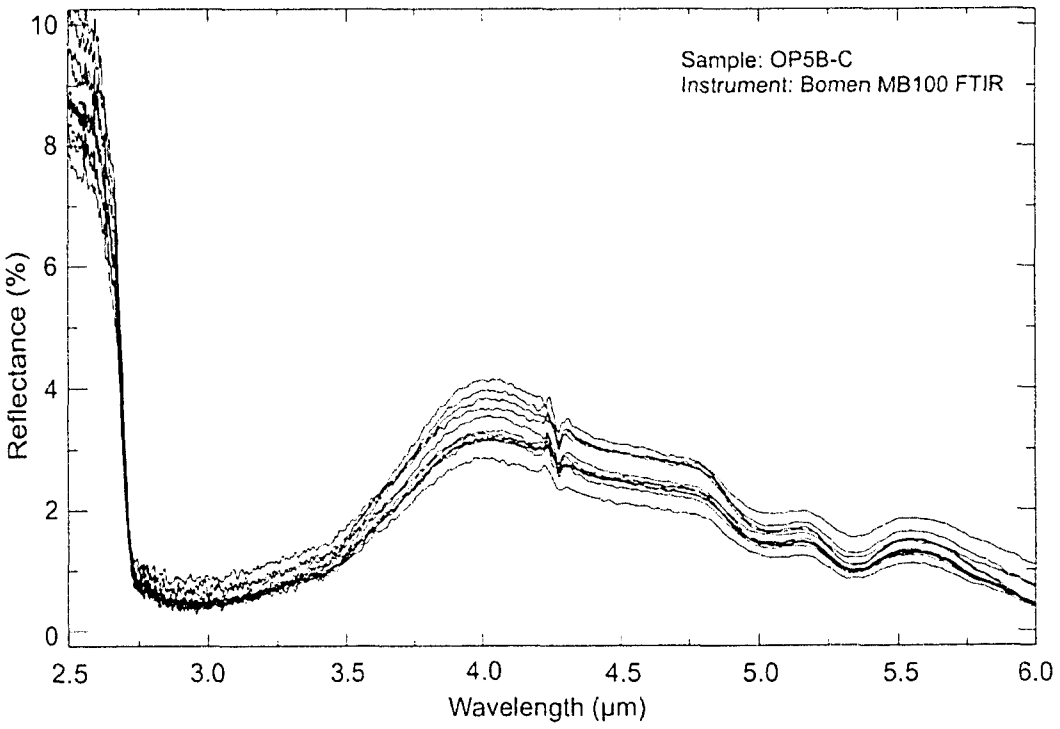

Figure 27. Reflectance spectra from OP5B-C between 2.5-6.0 μm.

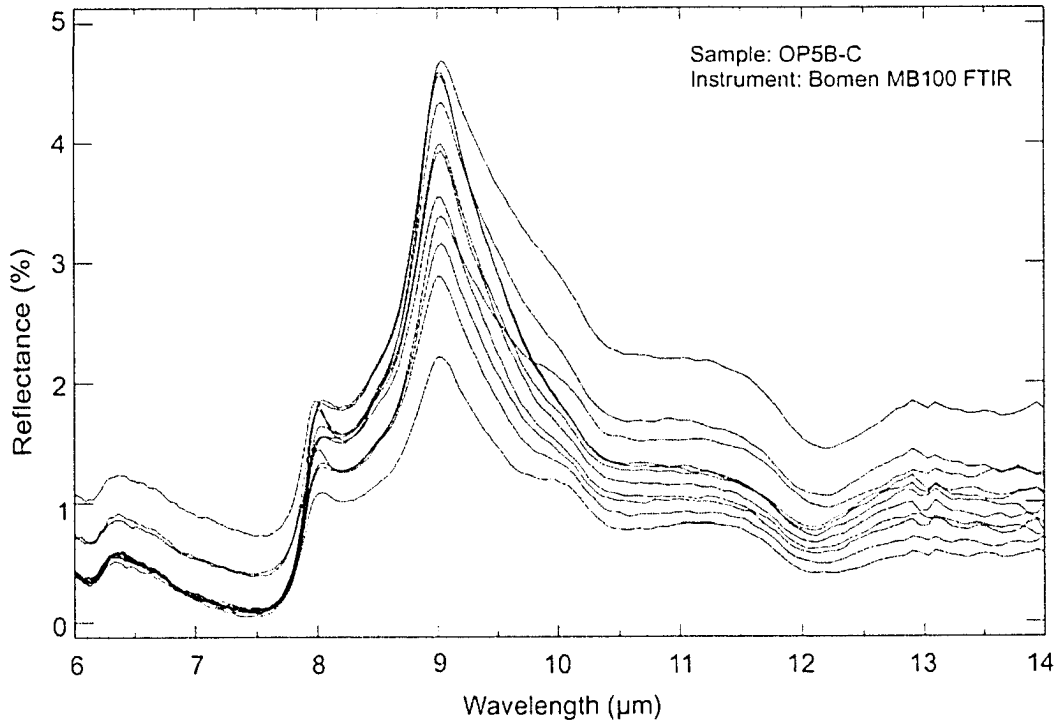

Figure 28. Reflectance spectra from OP5B-C between 6-14 μm.

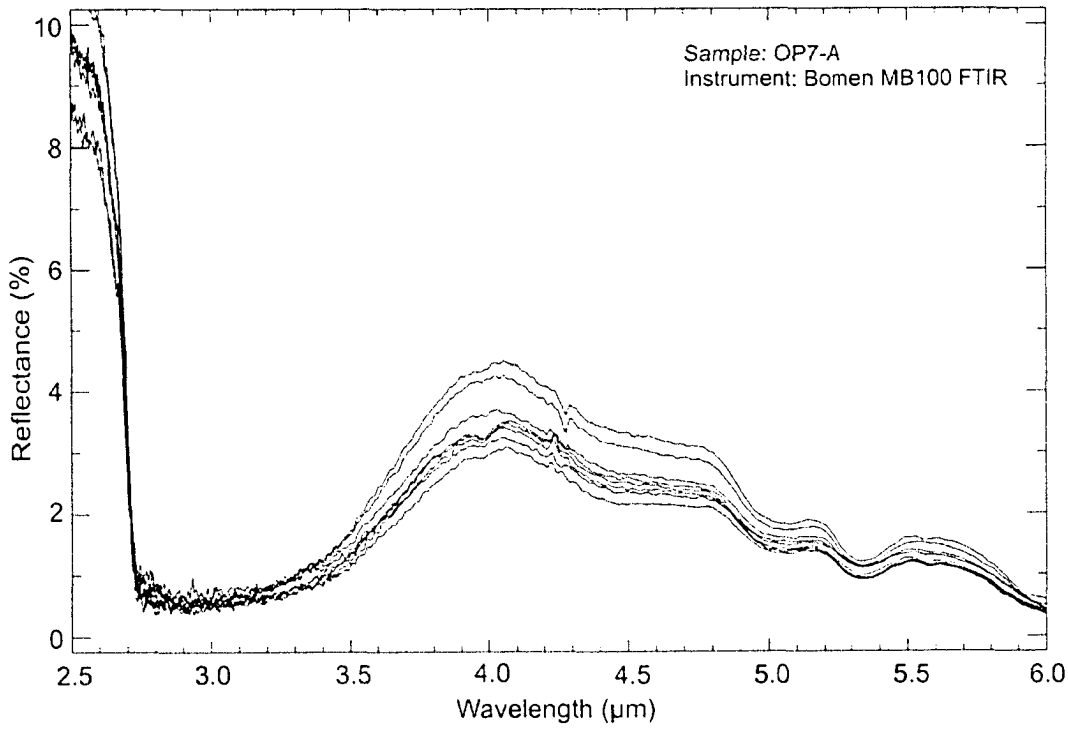

Figure 29. Reflectance spectra from OP7-A between 2.5-6.0 µm.

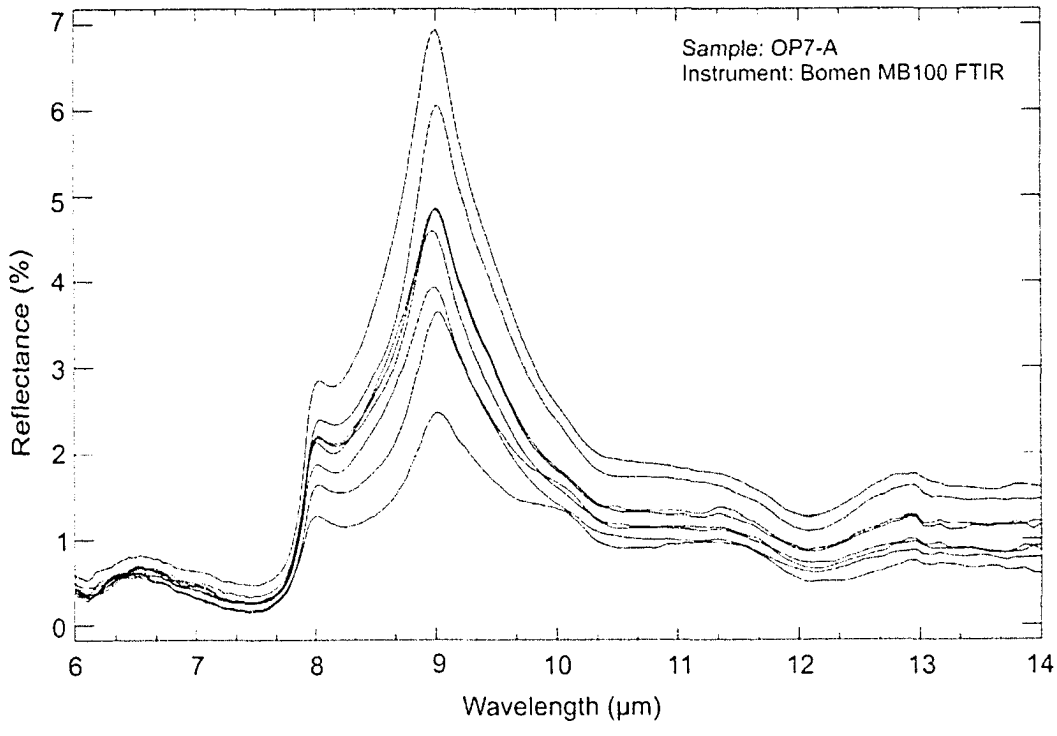

Figure 30. Reflectance spectra from OP7-A between 6-14 μm.

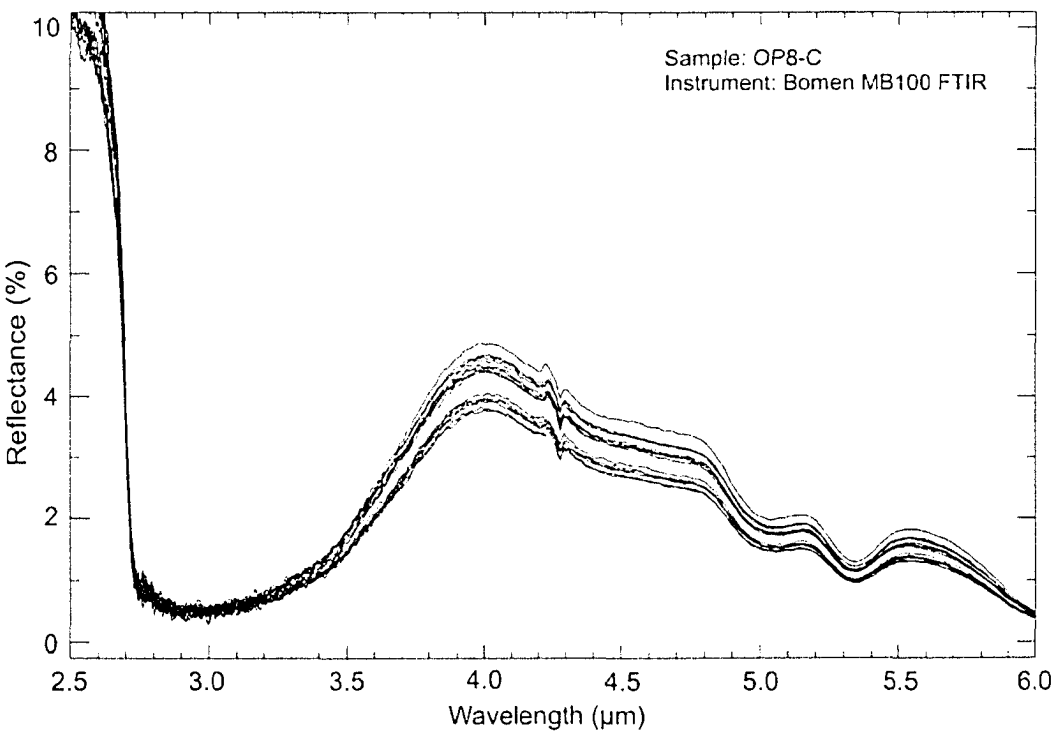

Figure 31. Reflectance spectra from OP8-C between 2.5-6.0 μm.

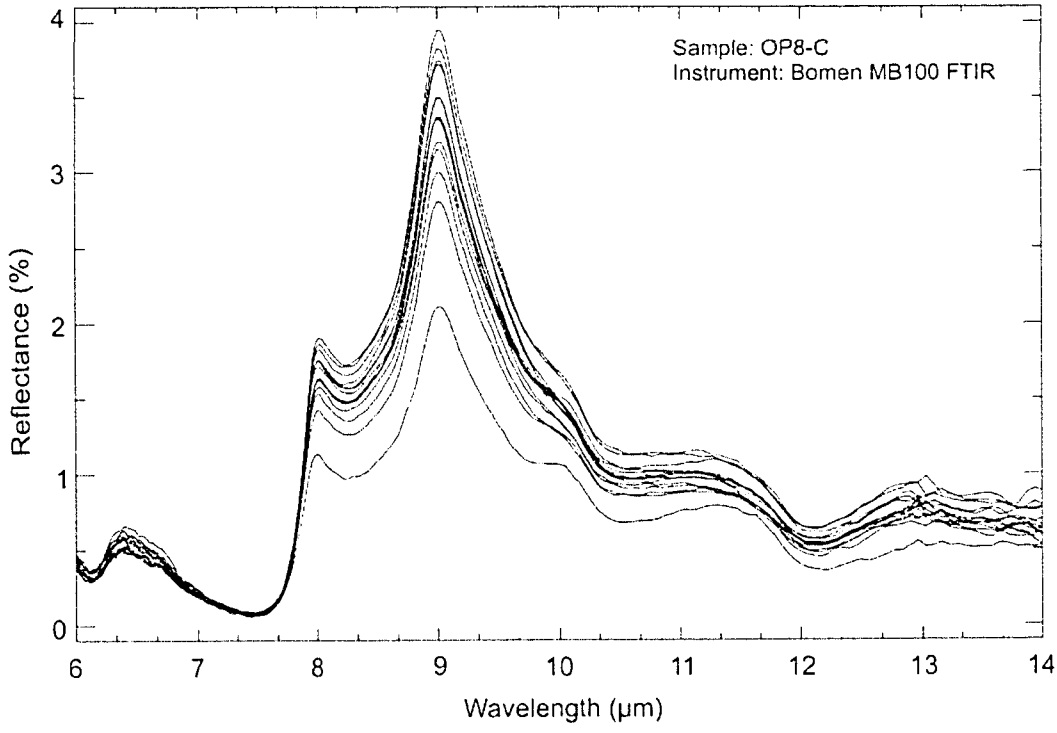

Figure 32. Reflectance spectra from OP8-C between 6-14 μm.

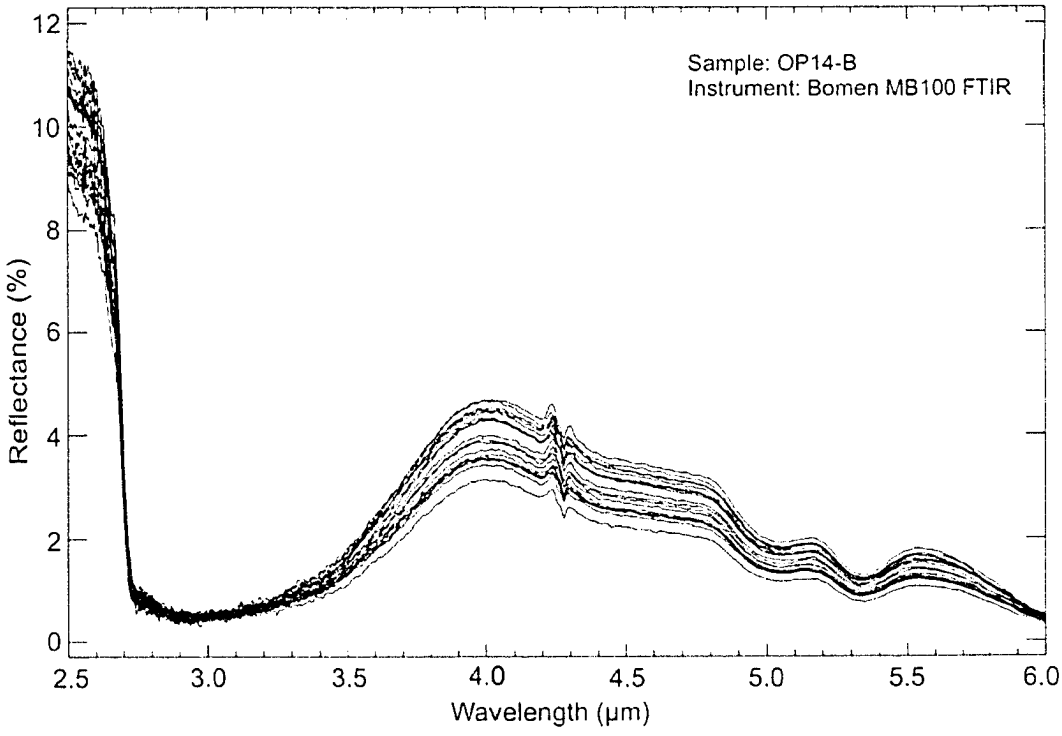

Figure 33. Reflectance spectra from OP14-B between 2.5-6.0 μm.

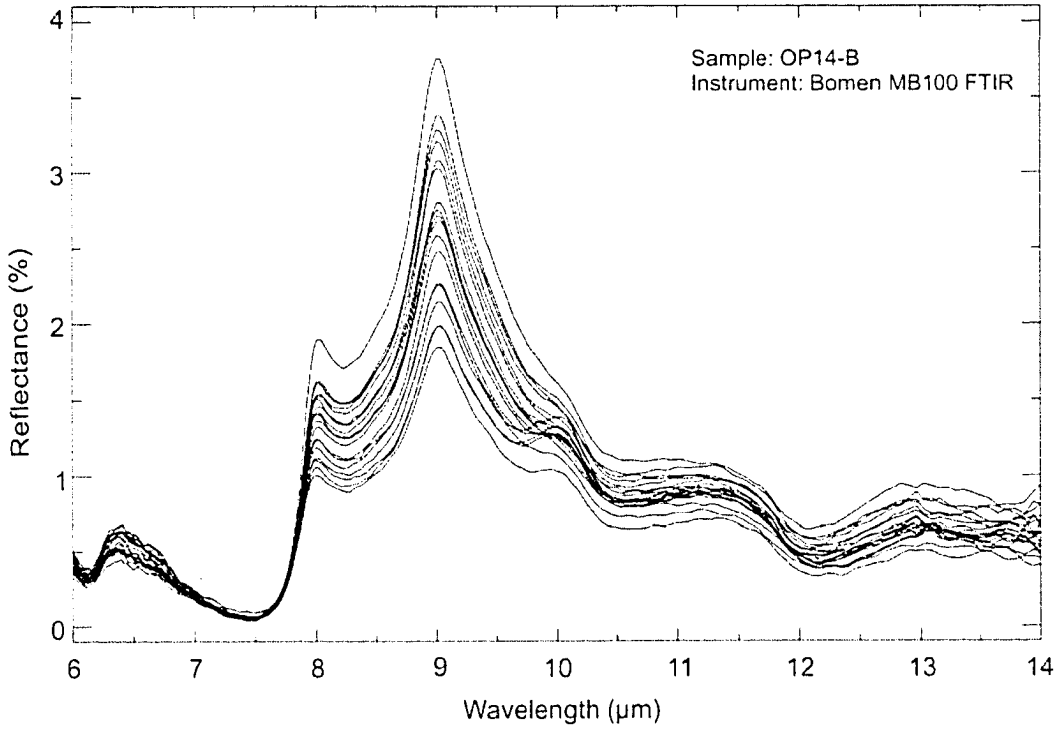

Figure 34. Reflectance spectra from OP14-B between 6-14 μm.

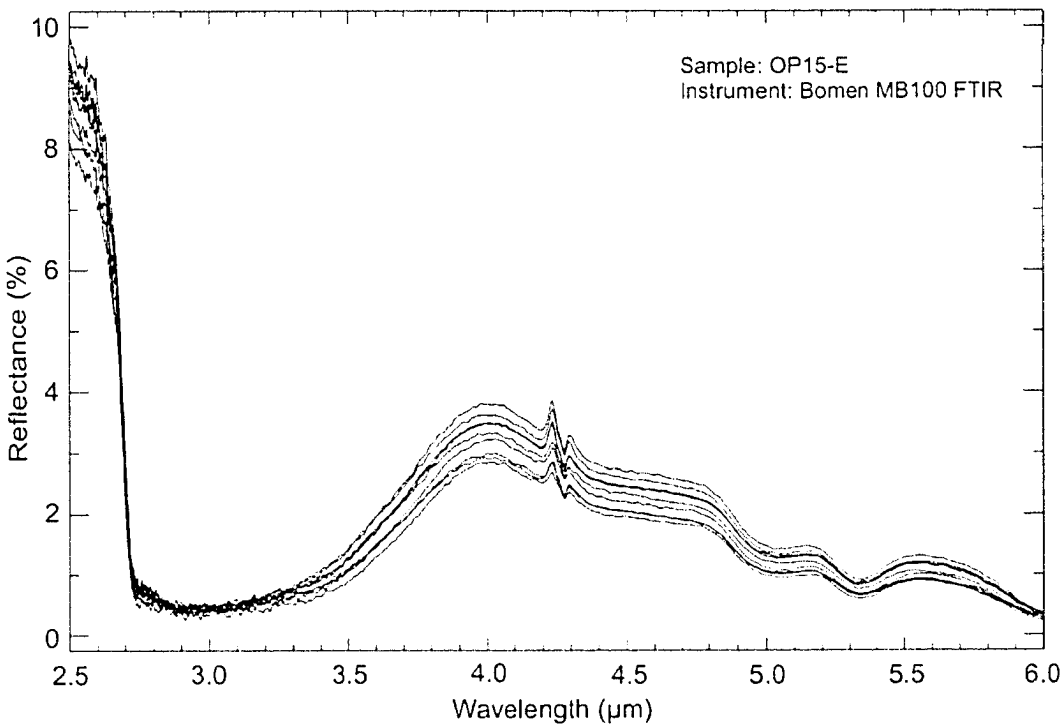

Figure 35. Reflectance spectra from OP15-E between 2.5-6.0 μm.

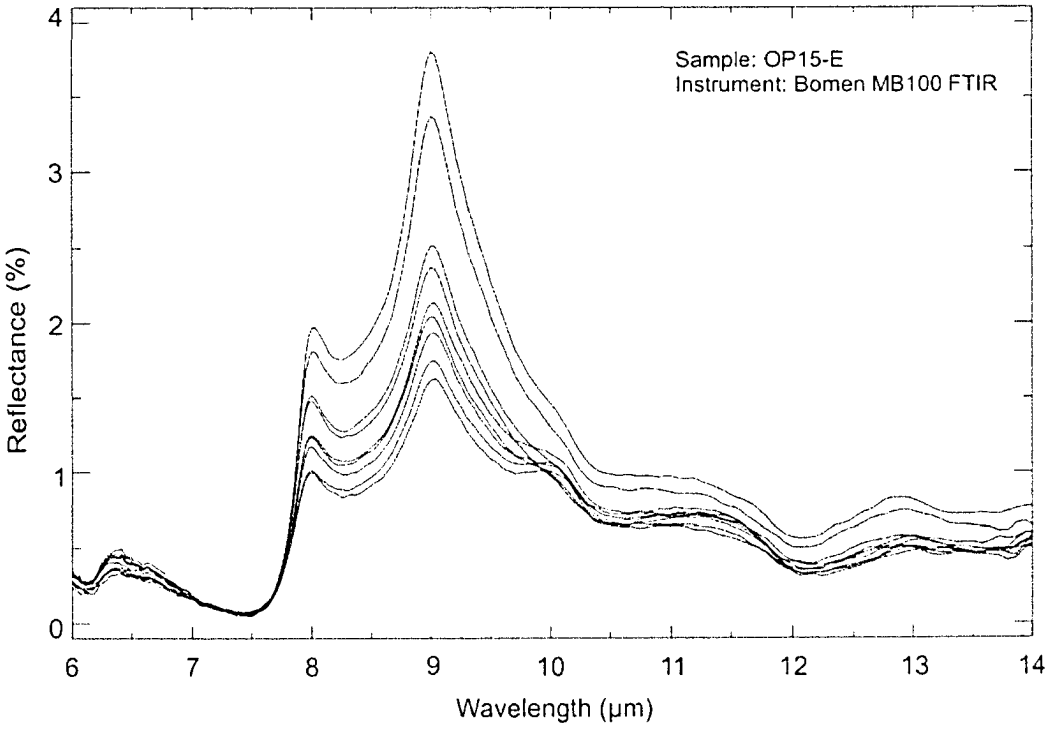

Figure 36. Reflectance spectra from OP15-E between 6-14 μm.